Physics Library
QC
.P5812
V.56
no. 12

THE PHYSICAL REVIEW

VOLUME 56 | *Second Series* | NUMBER 12

DECEMBER 15, 1939

Published for the

AMERICAN PHYSICAL SOCIETY

by the

AMERICAN INSTITUTE OF PHYSICS
Incorporated

LANCASTER, PA., AND NEW YORK, N. Y.

UNIVERSITY OF MICHIGAN LIBRARIES

THE PHYSICAL REVIEW

A journal of experimental and theoretical physics established by E. L. Nichols in 1893

Published by the American Institute of Physics for the

American Physical Society

OFFICERS

President

JOHN T. TATE
University of Minnesota
Minneapolis, Minnesota

Vice President

JOHN ZELENY
Yale University
New Haven, Connecticut

Secretary

W. L. SEVERINGHAUS
Columbia University
New York, New York

Treasurer

G. B. PEGRAM
Columbia University
New York, New York

Local Secretary for the Pacific Coast

PAUL KIRKPATRICK
Stanford University
California

Editor

JOHN T. TATE
University of Minnesota
Minneapolis, Minnesota

BOARD OF EDITORS

JOHN T. TATE, *Editor* J. W. BUCHTA, *Assistant Editor*

Associate Editors

K. T. BAINBRIDGE	A. L. HUGHES	W. BLEAKNEY
H. P. ROBERTSON	T. H. JOHNSON	G. BREIT
H. B. WAHLIN	F. A. JENKINS	D. M. DENNISON

Manuscripts for publication should be submitted to John T. Tate, University of Minnesota, Minneapolis, Minnesota.

Proof and all correspondence concerning papers in the process of publication, should be addressed to the Publications Manager, American Institute of Physics, 175 Fifth Avenue, New York, New York.

Subscription Price

United States and Possessions and Canada $15.00
Foreign $16.50

Back Numbers

Complete set: Series 2,[1] Vol. 1, 1913–Vol. 54, 1938—$390.00
Yearly rate: $16.50
Single copies: $1.50 each prior to July, 1929; $.75 each after July, 1929.

Subscriptions and orders for back numbers should be addressed to Prince and Lemon Streets, Lancaster, Pennsylvania, or to the American Institute of Physics, 175 Fifth Avenue, New York, New York.

Advertising is not accepted for the *Physical Review* but attention is called to the *Review of Scientific Instruments* and the *Journal of Applied Physics* companion publications of the Institute, and media through which the field of physics can be reached most effectively. Rates and other information will be furnished on request.

Changes of address in the case of members of the American Physical Society, should be addressed to the Treasurer; in the case of other subscribers, to the Publications Manager.

[1] For Series 1 inquire of Physics Department, Cornell University, Ithaca, N. Y.

The Physical Review is published semi-monthly at Prince and Lemon Streets, Lancaster, Pennsylvania.

Entered at the Post Office at Lancaster, Pennsylvania, as second class matter.

Acceptance for mailing at special rate of postage provided for in section 1103, Act of October 3, 1917, authorized September 6, 1926.

Physics
Physics-LSA
Johnson
Replace.

THE
PHYSICAL REVIEW

A Journal of Experimental and Theoretical Physics Established by E. L. Nichols in 1893

VOL. 56, NO. 12 DECEMBER 15, 1939 SECOND SERIES

Spin-Orbit Coupling in the Alpha-Model of Light Nuclei

D. R. INGLIS
Rowland Physical Laboratory, The Johns Hopkins University, Baltimore, Maryland
(Received September 25, 1939)

If light nuclei are approximated by the alpha-model, with the particles localized in clusters of four (or less), the particle with uncompensated spin is accelerated by the relatively weak attraction of alphas, or by the difference of the attractions of two clusters. Then the Thomas relativistic term is not in general larger than the Larmor magnetic term in the spin-orbit coupling in contrast to the result of the central model, wherein the acceleration may be attributed to unsaturated forces toward one center. The relative magnitudes of these terms are estimated for the alpha-model of Li^7 and C^{13}, two of the few nuclei to which it is here considered that the model might apply. The magnetic moment consistent with the Larmor-Thomas coupling in the alpha-model of B^{11} is found to be considerably larger than the experimental value. The quadrupole moment of the deuteron implies a spin-orbit coupling arising directly from angle-dependent nuclear forces. The appropriate "spin-orbit-spin" angle dependence suggested by the meson theory causes no first-order coupling in the alpha-model of Li^7, however, and a rough estimate of the second-order doublet splitting shows that it may be considerably smaller than that due to the Larmor and Thomas terms.

FOR nuclei which may be approximated by a central-field model, it has been pointed out[1] that the Thomas relativistic term may be expected to be considerably larger than the Larmor magnetic term, and to determine the sign and order of magnitude of the spin-orbit coupling due to spherically symmetric forces between the particles in light nuclei. This may not be said in general for nuclei which may be approximated by the alpha-model, in which the protons and neutrons are treated[2, 3] as being clustered into alphas and possibly an extra particle or a triton or He^3. The difference arises largely from the fact that the Thomas term contains the acceleration of the particle with uncompensated spin toward the center of mass of the system, and in the alpha-model this acceleration is due to inter-alpha-forces which are supposedly considerably weaker than intra-alpha-forces, in keeping with the saturation requirement.

The validity of explaining nuclear doublet splittings by means of the Larmor-Thomas precession depends on whether or not its effect is masked by the effect of the angle-dependent nuclear interaction responsible for the deuteron quadrupole moment. Such an interaction, of "spin-orbit-spin" angle dependence $(\mathbf{s}_1\cdot\mathbf{r})(\mathbf{s}_2\cdot\mathbf{r})$, is suggested by the meson theory, but specification of its radial dependence requires an arbitrary cut-off. The contribution of this interaction to the doublet splitting in the alpha-model, of Li^7, for example, is a second-order effect and is expected to be quite sensitive to details of the model and of the radial dependence,

[1] D. R. Inglis, Phys. Rev. **50**, 783 (1936).
[2] L. R. Hafstad and E. Teller, Phys. Rev. **54**, 681 (1938).
[3] H. Bethe, Phys. Rev. **53**, 842 (1938).

so it does not at present seem wise to try to compute the splitting. Since a very rough estimate below indicates that this contribution and the Larmor-Thomas splitting have about the same order of magnitude, an estimate of the Larmor and Thomas terms remains physically interesting, especially in view of such minor successes as its explanation of the sign of the spin-orbit coupling in the relatively simple nuclei Li^7 and O^{15}.

Among the $(4n-1)$-particle stable nuclei, Li^7 is probably the only promising application of the alpha-model.[4] This is indicated first by the fact that the magnetic moment of Li^7 calculated by the alpha-model[3] disagrees[5] with experiment considerably less severely than that calculated by a perturbation theory starting from the central model;[6] second, by the relatively high ratio of "internal" to "external" binding of the triton in Li^7; and third, by the failure of the alpha-model to furnish a correlation between the electrostatic energies of the various $(4n-1)$-particle nuclei.[7] For the $(4n+1)$-particle nuclei, such as C^{13}, which do not contain an easily distorted triton, the use of the alpha-model seems more plausible.

It is here shown that the magnetic term is at least of the same order of magnitude as the Thomas term in the alpha-model of the ground state of Li^7 and of C^{13}, and in Li^7 probably even larger. Only in the odd-neutron case C^{13} (and Be^7) can a preponderant magnetic term change the sign of the spin-orbit coupling, since the negative gyromagnetic ratio of the neutron here makes the magnetic and Thomas terms have opposite signs. It is further shown that the Larmor-Thomas splitting in B^{11} is too small to lead to agreement of the result of the alpha-model with the observed magnetic moment.

The Larmor-Thomas Precession in Li^7

For the sake of numerical simplicity in the dynamical problem we approximate the alpha-model of Li^7 by two clusters of $3\frac{1}{2}$ particles each, having their center of mass at the geometrical center. Each cluster has a displacement $\mathbf{r}$ and a velocity $\mathbf{v}$, relative to the center of mass, and a mass $(7/2)M$. The magnetic field at the triton due to the motion of the alpha relative to the triton is then

$$\mathbf{H}=(2e/c)(2\mathbf{r})\times(2\mathbf{v})/(2r)^3=(e\mathbf{L}/7Mcr^3),$$

where $\mathbf{L}=7M\mathbf{r}\times\mathbf{v}$ is the orbital angular momentum.

The Larmor energy is

$$E_L=-(ge/2Mc)\mathbf{S}\cdot\mathbf{H},$$

where $\mathbf{S}$ is the spin angular momentum, $(ge/2Mc)\mathbf{S}$ the spin magnetic moment, and g the spin gyromagnetic ratio (5.6 for the proton in Li^7 and about -4 for the neutron in Be^7). $\mathbf{S}\cdot\mathbf{L}$ contributes a factor $3\hbar^2/2$ to the doublet splitting, $\Delta E=E(^2P_{1/2})-E(^2P_{3/2})$, so we have the Larmor splitting of the Li^7 doublet

$$\Delta E_L=3ge^2\hbar^2/(28M^2c^2r^3)$$
$$=(3g/28)(137/1830)^2(e^2/mc^2r)^3mc^2$$
$$=0.003_5(e^2/mc^2r)^3mc^2.$$

The Thomas relativistic term is

$$E_T=\mathbf{S}\cdot\mathbf{a}\times\mathbf{v}/2c^2$$

the mean value of which is due mainly to the radial component of the acceleration $\mathbf{a}$ and the tangential component of the velocity $\mathbf{v}$. We may consider the radial acceleration in two parts. First there is a centripetal acceleration a_e accompanying the exchange of particles between the two clusters, and, second, the familiar centripetal acceleration $a_r=v^2/r$ of a particle at rest in a rotating coordinate system.

In treating the exchange, each particle may be described by a wave function having two

[4] Compare, however, B. O. Grönblom and R. E. Marshak, Phys. Rev. **55**, 229 (1939).
[5] D. R. Inglis, Phys. Rev. **55**, 329 (1939).
[6] D. R. Inglis, Phys. Rev. **53**, 882 (1938).
[7] H. Brown and D. R. Inglis, Phys. Rev. **55**, 1182 (1939). In that paper it appears that the electrostatic energy of a light nucleus is as much as about half as great as the binding energy *between alphas*. This fact furnishes an easy rough indication of the preponderance of the magnetic term in the alpha-model if the spin stays with a triton; it favors the Thomas term by only a factor 2 in a comparison of nuclei with the well-known situation in atoms (wherein the electric field is the accelerating field, and the magnetic term is twice as large as the Thomas term). The magnetic term in nuclei is equally favored by the anomalously large gyromagnetic ratios of the proton and neutron, leaving the magnetic term preponderant as in atoms. Values of nuclear masses newer than used in that paper (compare W. H. Barkas, Phys. Rev. **55**, 691 (1939)) alter the comparison with experiment but do not decrease the discrepancy. The following may be substituted in Table I:

	H^3-He^3	Li^7-Be^7	$B^{11}-C^{11}$	$N^{15}-O^{15}$
α-model	0.86*	2.00	3.14*	4.28
obs.	0.86	1.87	3.14	3.66

extremes, one at each of the clusters.[2] Each of these "molecular orbital" wave functions may be considered in the distant-cluster approximation to be a symmetric or antisymmetric combination of the s functions of the two clusters, as in the perturbation treatment of the H_2^+ ion. If we call the energy difference between the antisymmetric and symmetric states $\hbar\omega$, the "frequency of exchange" between the clusters in the single-particle problem is $\omega/2\pi$. The order of magnitude of the corresponding acceleration we take from simple harmonic motion, $a_e \approx -\omega^2 r$. Using this and $\mathbf{L}=7M\mathbf{r}\times\mathbf{v}$, we have

$$\Delta E_T \approx (3/28M)(\hbar\omega/c)^2.$$

The magnitude of $\hbar\omega$ is given in Fig. 4 of reference 2 as $\hbar\omega = Q \approx mc^2$, but this depends upon the application of the alpha-model to B^{11} and N^{15} where it is probably not valid. A more generous estimate of $\hbar\omega$ may be made as follows: The binding energy of the alphas in Be^8 would be about $5mc^2$ if there were no Coulomb energy,[7] and the binding energy of the triton to the alpha in Li^7 would be about $7mc^2$. Of this, roughly $(3/4)5mc^2 \approx 4mc^2$ might be due to the same sort of interaction as binds Be^8, there being $\frac{3}{4}$ as many intercluster heavy-particle interactions in Li^7, so we might attribute the remaining $3mc^2$ to "exchange"—that is, to the fact that Li^7 has one more particle in the low energy symmetric state than in the antisymmetric state, whilst in Be^8 both states are filled. Using $\hbar\omega = 3mc^2$, we obtain

$$\Delta E_T \approx (m/M)mc^2 \approx 5\times 10^{-4}\ mc^2.$$

The "rotational" centripetal acceleration is

$$\mathbf{a}_r = -(v/r)^2\mathbf{r} = -(L/7Mr^2)^2\mathbf{r}$$

and the consequent doublet splitting is

$$\Delta E_T' \approx (3/4)\hbar^2L^2/(7^3M^3c^2r^4) = (3/2)\hbar^4/(7^3M^3c^2r^4) \approx 3\times 10^{-4}(e^2/mc^2r)^4mc^2.$$

For the value of r suggested below, this is considerably larger than the previous term ΔE_T.

The contribution of the tangential component of $\mathbf{a}$ and the radial component of $\mathbf{v}$ to $|\mathbf{a}\times\mathbf{v}|_{Av}$ is $\langle(\dot{r}/r)(d/dt)r^2\dot{\varphi}\rangle_{Av}$, which does not in general vanish in the alpha-model as it does in the central model. In the case of a simple harmonic motion along the figure axis (if one considers $\dot{\varphi}$ constant and so retains only the Coriolis acceleration), this becomes $\omega^2r^2\dot{\varphi}$, which is just $|a_e r\dot{\varphi}|$. The effect of the Coriolis term is thus just equal to the rather small effect ΔE_T of the radial exchange acceleration, in this approximation. In the alpha-model of more complex nuclei, in which the particle is not so nearly constrained to move on a rotating line, the tangential acceleration would be expected to be even less important than here.

The value of r to be used in the comparison of the various terms should be indicated by the mass difference of Li^7 and Be^7, which is attributed to Coulomb energy according to the usual assumption that the Hamiltonian is otherwise symmetrical between protons and neutrons. The atomic mass difference Be^7-Li^7 is roughly[8] 1.0 Mev $= 2.0mc^2$, and that of He^3-H^3 is about zero. The Coulomb energy difference of Be^7-Li^7 minus that of He^3-H^3 is then about $2mc^2$ and the corresponding radius $r = \frac{1}{2}r_{1a} = \frac{1}{2}\cdot 2e^2/(2mc^2) = \frac{1}{2}e^2/mc^2$. Using this value we obtain $\Delta E_L \approx 7\Delta E_T' \approx 50\Delta E_T$ and a total splitting $\Delta E \approx 0.03mc^2 = 15$ kev. Although these estimates are rough, they indicate that the magnetic term is almost certainly larger than the Thomas term in the alpha-model of Li^7. The same is true of the alpha-model of Be^7, the sign of its Larmor-Thomas coupling being thus altered and its ground state $^2P_{1/2}$.

The fact that the "rotational" centripetal acceleration appears to be greater than the acceleration associated with exchange is an indication of the manner in which the alpha-model should be treated in rotational problems. Since the triton and alpha change places by rotation more frequently than they exchange identity by migration of a particle, it is more consistent to consider a triton and an alpha rotating about a center of gravity somewhat nearer the alpha than it is to picture two clusters of $3\frac{1}{2}$ particles each rotating about the geometrical center. This makes a slight difference[3,9] in the expected magnetic moment of Li^7, favoring the

[8] L. H. Rumbaugh, R. B. Roberts and L. R. Hafstad, Phys. Rev. **54**, 657 (1939), especially p. 680.

[9] R. G. Sachs, Phys. Rev. **55**, 825 (1939). I wish to thank Dr. Sachs for discussion of his results, especially on C^{13}, in connection with the present paper, and for pointing out that his reason for neglecting the Larmor term was a desire to make a formal comparison between the results of the two models, introducing the same assumptions, as nearly as possible, in both.

value 0.405 $\mu_N+\mu_\tau$ of reference 3 over the value 0.433 $\mu_N+\mu_\tau$ of reference 9.

The Larmor-Thomas Precession in C^{13}

C^{13} has an extra neutron which, in the alpha-model, occupies free space on both sides of the plane containing the three alphas. It is attracted by the alphas and may be pictured as being accelerated continually toward the plane in which they lie. In the ground state, the nucleus rotates about an axis in the plane of the alphas with one unit of angular momentum.[2] About this axis the moment of inertia is almost the same as that of the Li^7 nucleus, if the alpha-alpha distance $r_{\alpha\alpha}$ is nearly equal to the triton-alpha distance $r_{t\alpha}$. The angular velocities are therefore about the same. The C^{13} calculation differs from that for Li^7 principally in the fact that the extra particle has a greater centripetal acceleration because it is not bound into a cluster with other particles.

We can get a rough idea of the average distance of the neutron from the plane of the alphas in C^{13} by assuming that it is the same as (or slightly less than) that of the proton in N^{13}, and by using the observed Coulomb energy of the latter, 3.21 mMU$=6mc^2$. This is $6e^2/r_{\tau\alpha}$, where $r_{\tau\alpha}$ is the average proton-alpha distance in N^{13}. We thus have for the average neutron-alpha distance in C^{13}, $r_{\nu\alpha}\approx e^2/mc^2$. Taking $r_{\alpha\alpha}\approx e^2/mc^2$, as suggested by the Li^7-Be^7 Coulomb energy, we have the average position of the neutron on each side of the plane forming a regular tetrahedron with the alphas. The average radial component of the electric field at the neutron is only slightly reduced by the vectorial addition of the fields of the three alphas. This electric field is thus

$$F\approx 6e/r_{\tau\alpha}{}^2\approx 6m^2c^4/e^3$$

or somewhat less. With the magnetic field $\mathbf{H}=\mathbf{v}\times\mathbf{F}/c$ and with $\mathbf{v}\times\mathbf{r}=\mathbf{L}/2M$, the Larmor splitting is roughly

$$\Delta E_L\approx(9/4)g(137/1830)^2mc^2=-0.05mc^2.$$

The binding energy of the last neutron in C^{13} is about $10mc^2$. Although it moves in a non-Coulomb field so that we cannot apply the virial theorem exactly, we may assume as a rough approximation that the average kinetic energy has the same magnitude. Of this, part corresponds to motion in the two dimensions parallel to the plane of the alphas, but probably as much or more corresponds to motion along the z axis. To calculate the partition would require quite detailed treatment of the forces, so we merely assume that about $5mc^2$ corresponds to z motion. Approximating the z motion by a simple harmonic motion of frequency $\omega/2\pi$ and amplitude r, and considering E_T to be mainly due to this motion, we have $\ddot{z}\approx-\omega^2z\approx-4(5mc^2/Mr^2)z$ and, due to the rotation, $v_{\text{tangential}}=(L/2Mr_{\alpha\alpha}{}^2)z$. These lead to a Thomas splitting

$$\Delta E_T\approx(15/4)(137/1830)^2mc^2=0.02mc^2$$

(or somewhat more with the Coriolis term). This is thus weaker than the magnetic effect, but so slightly that it remains for a more accurate estimate to decide definitely whether the spin-orbit coupling arising from the Larmor-Thomas precession is positive or negative in the alpha-model of C^{13}. This rough estimate serves at least to show that the Larmor term may not be merely neglected, and suggests that the coupling is more apt to be negative, in agreement with the central model[10] and with experimental indications.[11]

Larmor-Thomas Coupling in B^{11} and the Consequent Magnetic Moment

A study of Coulomb energies does not exclude the possibility that the alpha-model applies to B^{11}, but makes this seem unlikely by showing that the model does not apply both to B^{11} and to N^{15}. Recent papers[9, 12] suggest that the alpha-model of B^{11}, with the Larmor-Thomas coupling, stands in agreement with the observed magnetic moment, but this is due to apparently excessive caution in avoiding specification of parameters in the model: Even a relatively safe order-of-magnitude estimate of the spin-orbit coupling limits the plausible μ to a narrow range which does not include the experimental value,[12] 2.68 μ_N. The treatment of Li^7 suffices to estimate the coupling due to body rotation and exchange acceleration (corresponding to β of reference 9)

[10] M. E. Rose and H. A. Bethe, Phys. Rev. **51**, 205 (1937).
[11] C. H. Townes, Phys. Rev. **56**, 850 (1939).
[12] S. Millman, P. Kusch and I. I. Rabi, Phys. Rev. **56**, 165 (1939).

as $10^{-2}mc^2$. An upper limit of the coupling due to rotation of the "hole" around the triangle (the parameter α of reference 9) is had by considering the entire axis-projection $\Lambda=\hbar$ of the angular momentum to be due to rotation of one particle about the circumscribed circle. This gives an upper limit because a hole has less mobility (greater effective mass in the theory of metals) than a particle. Taking a radius $3^{-\frac{1}{2}}e^2/mc^2$, one finds the Thomas term $\Delta E_T \approx \frac{1}{4}mc^2$ (or $\alpha \approx mc^2/6$) and the magnetic splitting much smaller. The ground state might differ from $^2P_{3/2}$ by admixture of $^2D_{3/2}$. The rotational kinetic energy difference of the states is $\epsilon \approx 3\hbar^2/2I \approx 7mc^2$, so the admixture of D wave function is of the order of magnitude $\frac{1}{4}mc^2/7mc^2=0.03$. The operator $g_L L_z+g_S S_z$ being diagonal, the magnetic moment μ of the ground state would thus be expected to differ from $\mu(^2P_{3/2})=\mu_\pi+5/11=3.23\mu_N$ by only about one-tenth of one percent, $(0.03)^2$. (Specializing the formulas of reference 9 gives $b_2=3^{\frac{1}{2}}\alpha/16\epsilon$ and $\mu \approx (1-10^{-5})\mu(^2P_{3/2})$. The lower limit $1.5\,\mu_N$ suggested in reference 9 and quoted in reference 12 corresponds to about equal mixture of P and D states, which is quite implausible.)

Angle-Dependent Nuclear Forces in Li^7

The above remarks have been directed toward an investigation of the possibility that nuclear properties may be derived from rather simple spherically symmetric exchange forces between the particles. The quadrupole moment of the deuteron indicates that such forces (if retained at all) must be supplemented by a torque between spin and position vectors, so as to mix virtual states with the low S state of the deuteron. The appropriate angle-dependent interaction, or "spin-orbit-spin coupling," suggested by the meson theory, has the form

$$H'=\{\mathbf{s}_1\cdot\mathbf{s}_2-3(\mathbf{s}_1\cdot\mathbf{u})(\mathbf{s}_2\cdot\mathbf{u})\}f(r),$$

where $\mathbf{u}=\mathbf{r}/r$, and $\mathbf{r}=\mathbf{r}_2-\mathbf{r}_1$, the difference of the position vectors of the particles. Because of the present difficulties in the meson theory,[13] it still seems desirable to investigate the possibility of supplementing the old central exchange forces by a term H' only strong enough to account for the deuteron quadrupole moment. We shall here estimate the magnitude of the spin-orbit coupling thereby introduced in the alpha-model of the relatively simple nucleus Li^7.

Considering H' as a perturbation, the first-order spin-orbit coupling would be due to a difference of the $^2P_{1/2}$ and $^2P_{3/2}$ diagonal elements of H'. According to the sum rule, this may be calculated as the difference between the sum of the diagonal elements for the two states with $(M_L, M_S)=1, -\frac{1}{2}$, or $0, \frac{1}{2}$ and that for the state with $(M_L, M_S)=1, \frac{1}{2}$. (Here M_L and M_S are the usual orbit and spin projection quantum numbers.) The wave function of the ground state in the alpha-model, as in a molecule, is a product of a function of the internal coordinates, with M_S as a subscript, and a function of the orientation of the line between the clusters, with M_L as a subscript. The function of internal coordinates may be written as an antisymmetric sum of products of the form

$$s^{\nu+}s^{\nu-}s^{\pi+}s^{\pi-}a^{\nu+}a^{\nu-}a^{\pi\pm},$$

where s and a are the symmetric and antisymmetric "molecular orbital" wave functions, orthogonal to one another, the superscripts ν and π are the isotopic spin quantum numbers[14] referring to neutron and proton, respectively, and the superscripts $+$ and $-$ refer to single-particle spin projection m_s, or to the spin functions α and β, respectively. For calculating the matrix elements, the essential "spin-orbit-spin" coupling factor of H' may be written

$$\begin{aligned}(\mathbf{s}_1\cdot\mathbf{r})(\mathbf{s}_2\cdot\mathbf{r})=\tfrac{1}{4}[&(s_x+is_y)_1(s_x-is_y)_2\\&+(s_x-is_y)_1(s_x+is_y)_2](x^2+y^2)\\&+s_{z1}s_{z2}z^2+\text{terms which alter } M_S,\end{aligned}$$

and the spin operators may be used in the form

$$(s_x+is_y)\begin{pmatrix}\alpha\\\beta\end{pmatrix}=\begin{pmatrix}0\\\alpha\end{pmatrix},\quad (s_x-is_y)\begin{pmatrix}\alpha\\\beta\end{pmatrix}=\begin{pmatrix}\beta\\0\end{pmatrix},$$
$$s_z\begin{pmatrix}\alpha\\\beta\end{pmatrix}=\begin{pmatrix}\alpha/2\\-\beta/2\end{pmatrix}.$$

The diagonal element of this coupling factor consists of direct terms, between the product written above and itself, and of exchange terms, between the product as written and a similar product with two of its factors interchanged, with

[13] H. A. Bethe, Phys. Rev. **55**, 1261 (1939).

[14] B. Cassen and E. U. Condon, Phys. Rev. **50**, 846 (1936).

a negative sign because of the Pauli antisymmetry. One thus finds six direct terms in $-z^2/4$ from like-particle, unlike-spin pairs (two $s-s$, three $a-s$, and one $a-a$). There are also three terms in $z^2/4$ from like-particle, like-spin, $a-s$ pairs, making the direct terms from $a-s$ pairs vanish. Unlike-particle pairs contribute as many positive as negative terms. (x^2+y^2) is absent from the direct terms because of orthogonality introduced by the accompanying spin operations. Among the exchange terms, we first have three terms $-\frac{1}{4}(x^2+y^2)$ from the like-particle, $s-s$ or $a-a$ pairs (two $s-s$ and one $a-a$). We may combine the terms involving $s-s$ pairs into a space integral of $-\frac{1}{2}(x^2+y^2+z^2)f(r)$, independent of the sign of M_S, $\pm$. Due to its symmetry it is also independent of M_L, and gives no splitting. Similarly for the $a-a$ pairs. Further, we have the exchange terms due to like-particle, $a-s$ pairs which amount to $-\frac{3}{4}(x^2+y^2)$ from the unlike-spin pairs and $-\frac{3}{4}z^2$ from the like-spin pairs, all involved in the same "internal" space integral of an exchange nature, again centrally symmetric, so not contributing to the splitting. Unlike-particle pairs have no exchange terms for an H' independent of isotopic spin. There is thus no first-order doublet splitting in the alpha-model of Li^7.

The second-order splitting arises from admixture of excited P and F states to the two levels of the low ^2P. (Excited S and D states are not admixed because the space factor of H' transforms as the product of two vectors.) The magnitude of the matrix elements responsible for the admixture would depend in great detail upon the form of $f(r)$ and of the alpha-model. We shall therefore make only a very rough order-of-magnitude estimate of the splitting by comparison of this problem with that of the deuteron quadrupole moment.

By numerical integration of an $f(r)$ based on cut-off of the neutral meson theory, Bethe has shown that the 7-percent admixture of D wave function which he obtains in the ground state of the deuteron is quite adequate to explain the quadrupole moment.[13] While dependent on a special form of the interaction, his result indicates roughly the amount of D admixture required by the quadrupole moment with any interaction giving about the same "size of the deuteron," except for the possibility[15] of a considerably larger admixture which requires the small quadrupole moment to be a difference of the effects of the $S-D$ and $D-D$ quadrupole matrix elements. For interactions of which H' is a small perturbation this latter possibility seems to be ruled out by comparison of the stability of the deuteron and alpha-particle,[15] together with new measurements of the range of the proton-neutron interaction.[16] So it seems that the matrix element responsible for the D admixture is about $(S|H'|D)\approx 0.07(E_D-E_S)$ in order of magnitude, and this might be about $1mc^2$. This gives us an idea of the magnitude of the corresponding matrix elements in the alpha-model of Li^7, between the excited $^2,{}^4P$ and ^4F states and the low ^2P states. The "internal" space factors of these excited states have an extra node making them orthogonal to the ground state, so that the matrix elements in question would vanish for very short or very long range of H', and for intermediate range the integrations must contain strong cancellation of positive and negative parts. This leads one to expect the matrix elements to be much smaller than in the deuteron, of the order of magnitude $10^{-1}mc^2$. The energy involved in the excitation is intermediate between that for a triton and that for an alpha, perhaps about $30mc^2$. For the depression of one of the low ^2P levels by one excited F state we may thus estimate $(F|H'|P)^2/(E_F-E_P)\approx 3\times 10^{-3}mc^2$. The excited P states depress both the levels $^2P_{1/2}$ and $^2P_{3/2}$, but the ^4F depresses only the $^2P_{3/2}$, suggesting that this type of doublet splitting would also be apt to make the $I_{Li^7}=\frac{3}{2}$, as observed. Since it depends on the detailed difference of the depressions of the two low ^2P levels due to several excited states, the splitting might be either larger or smaller than the depression ($\approx 3\times 10^{-3}mc^2$) due to one excited state. We may at least make the very rough estimate that the second-order splitting due to H' is of about the same order of magnitude as, and might be considerably smaller than, the Larmor-Thomas splitting ($\approx 3\times 10^{-2}mc^2$) in the alpha-model of Li^7.

[15] D. R. Inglis, Phys. Rev. **55**, 988 (1939).
[16] E. O. Salant, R. B. Roberts and P. Wang, Phys. Rev. **55**, 984 (1939).

The Scattering of Alpha-Particles by Nitrogen

GORDON BRUBAKER*
Sloane Physics Laboratory, Yale University, New Haven, Connecticut
(Received October 13, 1939)

A study has been made of the scattering of alpha-particles by nitrogen into four angular ranges of mean angles 53°, 66°, 88°, and 104°. Anomalies in the scattering are observed for energies as low as 3.5 Mev. Curves showing the ratio of observed to Coulombian scattering as a function of energy show several maxima and minima. The form of the curves varies greatly with the scattering angle.

NEXT to those elements which may be obtained in the form of thin foils, elements which exist in gaseous form are the most convenient for use in investigations of scattering. Nitrogen is such an element, and one of the lightest. Although, presumably, the scattering of alpha-particles by nitrogen nuclei would show marked anomalies, it was not investigated during the early work on alpha-particle scattering since the scintillation screen then used as a detector of the scattered particles would not distinguish sharply between scattered alpha-particles and the protons produced by the transmutation of nitrogen. The development in recent years of electrical detectors which will distinguish between the two kinds of particles has made it possible to study the scattering of alpha-particles by nitrogen nuclei. Such studies have been carried out by Devons,[1] who has investigated the scattering at 90°, and by the author.

In the present work the scattering at four different mean angles has been studied. The apparatus used has been previously described.[2] The detectors used were toroidal proportional counters which detected particles scattered from a small volume on the axis of the toroid. The counters were filled with the gas whose scattering was being studied. Proper adjustment of the voltage applied to the counters and the amplification of the impulses produced by them made it possible to detect alpha-particles but not protons.

The use of two of the toroidal counters made it possible simultaneously to observe particles scattered into two different angular ranges. By changing the positions of the edges defining incident and scattered beams of particles, scattering into two other angular ranges could be studied. The scattering of alpha-particles having energies between 3.5 Mev and 7.0 Mev into four somewhat overlapping angular ranges whose mean angles are 53°, 66°, 88°, and 104° was studied.

Since its original description, the apparatus has been altered to improve its resolving power. The size of the angular ranges has been reduced by use of an alpha-particle source 3 mm instead of 9 mm in diameter, and by slightly reducing the angular width of the beam of scattered particles. These changes have also reduced somewhat the spread in energy of incident particles in the scattering volume. The total spread in scattering angle for the 53°, 66°, 88°, and 104° ranges, respectively, are 35°, 36°, 41°, and 37°. A computation of the number of recorded scattered particles as a function of scattering angle, on the assumption of Coulomb forces, shows that, unless the scattering differs a great deal from Coulomb scattering, very few particles are recorded which have been scattered through the very smallest or very largest angles in each angular range. The effective angles of scattering, may, then, be given as $53°\pm11°$, $66°\pm12°$, $88°\pm14°$, and $104°\pm12°$.

The spread in energy of the incident particles is due to the thickness of the scattering volume and to the straggling of the alpha-particles. The thickness of the scattering volume in each case was about 2 mm air equivalent. For an alpha-particle energy of 5 Mev this amounts to 0.2 Mev spread in energy. At the same energy the straggling in energy of the alpha-particles amounts to about 0.09 Mev. The total spread

* Sterling Fellow.
[1] S. Devons, Proc. Roy. Soc. **A172**, 127 (1939).
[2] Gordon Brubaker, Phys. Rev. **54**, 1011 (1938).

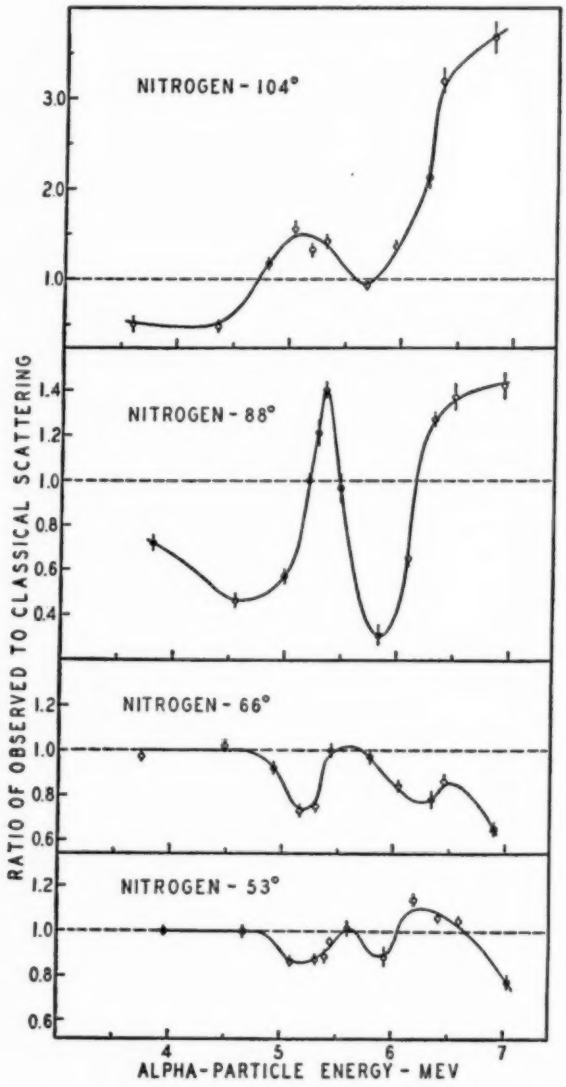

FIG. 1. Experimental results for the scattering of alpha-particles by nitrogen.

in energy of incident particles in the scattering volume was, therefore, about 0.38 Mev.

For calibration of the apparatus, the scattering of alpha-particles by argon was used. The number of particles scattered by argon at energies near 4 Mev (for which the scattering is known to be classical) was determined and, by use of the Rutherford scattering formula, the number which would be scattered by nitrogen on the assumption of Coulomb forces was calculated.

To make sure that no protons were being detected, a foil thick enough to stop the scattered alpha-particles but not the protons was placed between the scattering volume and detectors and alpha-particles of various energies were allowed to pass through the scattering volume. It was found that no protons were counted.

RESULTS

The results which were obtained are shown in the curves of Fig. 1, in which the ratio of observed to Coulomb scattering is plotted against the energy of the incident alpha-particles. From 200 to 1500 particles were counted for each of the experimental points. The curves show that anomalies in the scattering exist for energies as low as 3.5 Mev, as is to be expected since the penetrability of the nuclear potential barrier for this energy is at least 10 percent, and that the course of the anomalies with increasing energy of the particles is very irregular. Particularly noteworthy is the high and narrow peak at 5.3 Mev in the curve for 88° mean scattering angle, the appearance of which strongly suggests that it is due to resonance. The whole curve is similar to that obtained by Devons[1] at 90° mean angle of scattering. The second smaller resonance peak at about 4.6 Mev shown in Devons' curve does not appear here, probably because of lack of experimental points in that region. The difference in height of the higher peak as shown in Devons' curve and in Fig. 1 may be caused by differences in resolving power of the two sets of apparatus.

A somewhat broader peak occurs in the curve for mean scattering angle 104° with its maximum at about 5.0 Mev. It is possible that this is composed of two peaks and that further and more accurate data would separate the two. The subsequent rise in the curve at higher energies is similar to that found in the scattering by oxygen at these same angles,[2] and to those found by Riezler[3] in the scattering at high angles by beryllium, boron, and carbon.

The curves for the scattering into the two lower angular ranges resemble each other, but bear little resemblance to the curves for the two higher angular ranges. The first anomaly evident from the data is a depression of the scattering ratio below unity having its minimum at about 5.2 Mev. Following this there are two maxima in each of the curves. More data are needed to

[3] W. Riezler, Ann. d. Physik **23**, 198 (1935).

determine the exact positions and heights of these maxima. It seems probable that the depression at 5.2 Mev is produced by the same resonance level as is responsible for the high peak in the curve for angle 88°. The difference (0.1 Mev) in the positions of the minimum and the maximum is felt to be real and not the result of experimental error. Such an error could arise only through errors in the measurement of the dimensions of the apparatus. This measurement was carefully repeated and found to be correct.

Discussion

Bethe[4] has given a formula based on the many-body theory of scattering which is valid in the neighborhood of resonance for any spin of scattering nucleus and incident particle but for only zero orbital angular momentum of the particle. For the particular case of nitrogen this formula is

$$\frac{\sigma(\theta)}{\sigma_0}=1+\frac{\rho^2+2\rho\sin\zeta+2\rho x\cos\zeta}{1+x^2},$$

where $\sigma(\theta)/\sigma_0$ is the ratio of actual to Coulomb scattering, $\zeta=\alpha\log\sin^2\theta/2$, $\alpha=e^2zZ/\hbar v$, θ is the angle of scattering in the center of gravity system,

$$\rho=(2/\alpha)(\Gamma^r{}_{Pp}/\Gamma_r)\sin^2\theta/2,\quad x=2(E-E_r)/\Gamma_r,$$

and $\Gamma^r{}_{Pp}/\Gamma_r$ is the ratio of the partial width of the resonance level corresponding to scattering to the total level width.

Consideration of this formula shows that, a given resonance energy having been assumed, the behavior of $\sigma(\theta)/\sigma_0$ as the energy is varied slightly from the resonance value is as follows:

For angles θ greater than a certain high value θ_1, the numerator of the fraction is positive and $\sigma(\theta)/\sigma_0$ decreases as E either increases or decreases: that is, the evidence of resonance is a peak in the curve of $\sigma(\theta)/\sigma_0$ against E.

For another range of angles $\theta_2<\theta<\theta_1$ the numerator is negative and the evidence of resonance is a depression in the curve.

This alteration in the character of the curve continues as the angle is further decreased.

In the curves of Fig. 1 there is apparent evidence of resonance in the high peak of the curve for angle 88°, and further evidence of the same resonance level in the depression at approximately the same energy in the curves for the two lower angles. This change from a peak to a depression agrees qualitatively with the behavior predicted by the theory. Quantitatively, however, the formula cited above predicts only depressions at an assumed resonance energy of 5.3 Mev for all the angles concerned. This indicates that incident particles of zero angular momentum are not involved in the resonance process. This is not in disagreement with the conclusion of Devons that particles of angular momentum two are involved.

The irregularities at the higher energies in the curves for the two lower angular ranges are not well defined by the present data. For this reason and because of the variability in the character of evidence for resonance discussed above, no assignment of the energies of the resonance level or levels presumably responsible for the irregularities has been made.

The author wishes to express his gratitude to Professor A. F. Kovarik and Professor E. Pollard for helpful discussions during the course of this work.

[4] H. A. Bethe, Rev. Mod. Phys. 9, 176 (1937).

On Transition Probabilities in Double Beta-Disintegration

W. H. FURRY
Physics Research Laboratory, Harvard University, Cambridge, Massachusetts

(Received October 16, 1939)

The phenomenon of double β-disintegration is one for which there is a marked difference between the results of Majorana's symmetrical theory of the neutrino and those of the original Dirac-Fermi theory. In the older theory double β-disintegration involves the emission of four particles, two electrons (or positrons) and two antineutrinos (or neutrinos), and the probability of disintegration is extremely small. In the Majorana theory only two particles—the electrons or positrons—have to be emitted, and the transition probability is much larger. Approximate values of this probability are calculated on the Majorana theory for the various Fermi and Konopinski-Uhlenbeck expressions for the interaction energy. The selection rules are derived, and are found in all cases to allow transitions with $\Delta i = \pm 1,0$. The results obtained with the Majorana theory indicate that it is not at all certain that double β-disintegration can never be observed. Indeed, if in this theory the interaction expression were of Konopinski-Uhlenbeck type this process would be quite likely to have a bearing on the abundances of isotopes and on the occurrence of observed long-lived radioactivities. If it is of Fermi type this could be so only if the mass difference were fairly large ($\epsilon \gtrsim 20$, $\Delta M \gtrsim 0.01$ unit).

I. INTRODUCTION

THE probability of double β-disintegration was calculated some years ago by Goeppert-Mayer[1] on the basis of the Fermi theory.[2, 3] The result obtained was extremely small, corresponding to a lifetime of the order of 10^{25} years in the case of two isobars whose masses differ by 0.002 mass unit and whose atomic numbers differ by two units. Thus one can account for the large number of isobaric pairs with $\Delta Z = 2$, as compared to the scarcity of isobars with $\Delta Z = 1$. Although not strictly stable, the heavier isobar of a pair with $\Delta Z = 2$ may be supposed to be metastable, having a lifetime large compared to geologic time.

An inspection of the calculations shows that the results would not be changed by any significant factor by the use of an expression for the interaction energy involving derivatives of the neutrino wave function, as suggested by Konopinski and Uhlenbeck.[4] The same is true as regards the generalizations in structure of this expression,[5] which make it possible to obtain selection rules[6] for ordinary β-decay decidedly different from those originally given by Fermi. The original Fermi picture of the fundamental interaction processes concerned in β-decay has now been generally supplanted by a picture in which mesons play the role of mediaries between the heavy particles and the electrons and neutrinos. In this case also, as is evident from a consideration of the arguments of Yukawa,[7] the results of Goeppert-Mayer will remain unchanged.

The situation is, however, decidedly altered if one admits a change in the theory of the neutrino itself as an elementary particle. Such a change was suggested by Majorana[8] in a paper on the symmetry properties of the Dirac theory. Majorana's suggestions have been more generally developed in the case of the positron theory by Kramers,[9] and for the neutral particle by the writer.[10] Racah[11] has also discussed the application to the neutrino theory of β-decay.

The essential difference between the Majorana theory of the neutrino and the usual form of the Dirac theory is that in the former there are only

[1] M. Goeppert-Mayer, Phys. Rev. **48**, 512 (1935).
[2] E. Fermi, Zeits. f. Physik **88**, 161 (1934).
[3] For a review of the theory and its various modifications and applications up to the beginning of 1936, see pages 186–206 of the article by Bethe and Bacher, Rev. Mod. Phys. **8** (1936).
[4] E. J. Konopinski and G. E. Uhlenbeck, Phys. Rev. **48**, 7 (1935).
[5] Cf. reference 3, pp. 190–192.
[6] G. Gamow and E. Teller, Phys. Rev. **49**, 895 (1936).
[7] H. Yukawa, Proc. Phys.-Math. Soc. Japan, **17**, 55–56 (1935); H. Yukawa, S. Sakata, M. Kobayasa and M. Taketani, Proc. Phys.-Math. Soc. Japan **20**, 731–734 (1938).
[8] E. Majorana, Nuovo Cimento **14**, 171 (1937).
[9] H. A. Kramers, Proc. Amsterdam Akad. **40**, 814 (1937).
[10] W. H. Furry, Phys. Rev. **54**, 56 (1938), referred to as *N*.
[11] G. Racah, Nuovo Cimento **14**, 322 (1937).

two states for a given momentum, corresponding to the two possibilities for the spin; there are no negative energy neutrinos, and no "holes," or antineutrinos. If in applying the usual Dirac-Fermi theory to β-decay one assumes that the emission of a neutrino accompanies that of a positron, then the emission of an electron must be accompanied by the emission of an *antineutrino*, or else the *absorption* of a neutrino. In the Majorana theory the emission of *either* an electron *or* a positron is accompanied by *either* the emission *or* the absorption of a neutrino.

It can be shown that the use of the Majorana form of neutrino theory instead of the usual theory makes no difference in the case of ordinary β-decay.[12] For the double β-disintegration, however, there is a marked qualitative difference between the results of the two theories. In the ordinary form of the theory four particles must be emitted in such a process: two neutrinos (or antineutrinos) must accompany the emission of two positrons (or electrons). In the Majorana theory there can occur not only these four-particle disintegrations, but also disintegrations in which only the two charged particles—electrons or positrons—are emitted, unaccompanied by neutrinos. In these two-particle disintegrations the neutrino plays only a transitory or virtual part, such as is played by electron-positron pairs in certain hypothetical radiative processes.[13] Subject to the usual limitations on the meaning of such language, one can say that a (virtual) neutrino is emitted together with one of the electrons (or positrons), and reabsorbed when the other electron (or positron) is emitted.

In calculating the probability amplitude for such a process, one must integrate over the momentum space of the neutrino. This introduces a quantity which is a sort of "form factor" of the nucleus. In most cases the integral converges, giving a finite "form factor" without any arbitrary "cutting off" procedure; one has to resort to "cutting off" only for certain types of Konopinski-Uhlenbeck expressions for the interaction energy. The results obtained for the disintegration probability are, nevertheless, greater than those for the four-particle process by a factor which ranges from 10^5 to 10^{15} or more, depending on the particular interaction expression used. The fact that the neutrino momentum is not limited by the amount of energy available in the transition also makes the probability less strongly dependent on the energy.

In the following section we carry through the calculation for the simplest case, using the "scalar-type" interaction energy expression[14] and assuming that the nuclear spin does not change and that the transition is of even-even or odd-odd type. In Section III we consider the effects of using various other expressions for the interaction energy, and determine the selection rules governing changes in the nuclear spin i and the even-odd or even-even, odd-odd character of the transitions.

Before we continue beyond the introduction it should be remarked that the Majorana form of the theory is not the only one which permits this new type of disintegration. The same sort of result can be obtained with the more usual theory if one introduces an interaction expression involving a linear combination of the neutrino wave function and its conjugate. Such an introduction has never been suggested, however, in the neutrino-antineutrino type of theory. The Majorana theory is the natural one to use for our purpose, both because, in the elimination of the antineutrino, it provides an independent motive for the use of such expressions, and because it provides, so to speak, a canonical form for them.

II. Scalar-Type Interaction without Derivatives; $\Delta i = 0$, Even-Even, Odd-Odd Transitions

We consider the transition of two neutrons in the nucleus into two protons, with the emission of electrons into states having wave functions ψ_s and ψ_t and energies H_s and H_t. The formula for the probability amplitude must contain two terms, since either electron may be emitted first. These terms are of opposite signs because of the antisymmetry of the electronic wave functions; whether or not they actually cancel strongly depends on the interaction expression used.

[12] Reference 10, pp. 66–67; but see limitation stated in footnote 22 of reference 10.

[13] Cf. for example M. Delbrück, Zeits. f. Physik **84**, 144 (1933); N. Kemmer, Helv. Phys. Acta, **10**, 112 (1937); H. Euler, Ann. d. Physik **26**, 398 (1936).

[14] Cf. Eq. (208a) of reference 3.

The neutrino wave functions are taken to be expanded in terms of plane waves subject to a periodic boundary condition in a box of volume V, as expressed in Eqs. (30) and (31) of N. Only the neutrino amplitudes are regarded as quantized, and all other wave functions are treated as c-numbers.

Apart from a resonance factor, the square of whose absolute value may be set equal to $(2\pi t/\hbar)\delta(E_N+H_e+H_\iota-E_M)$, the probability amplitude is

$$a_{N\leftarrow M}=g^2\sum(\mathbf{k})\sum_L\int\Psi_N^\dagger\{\sum_i\beta_iQ_i^\dagger(\mathbf{r}_i|\mathbf{k})\}\Psi_L d\tau$$
$$\cdot\int\Psi_L'^\dagger\{\sum_j\beta_jQ_j^\dagger(\mathbf{r}_j'|-\mathbf{k})\}\Psi_M'd\tau'$$
$$\cdot\left[\frac{(\psi_\iota^\dagger\beta a(\mathbf{k}))(\psi_e^\dagger\beta a(-\mathbf{k}))}{E_M-E_L-H_e-K_k}\right.$$
$$\left.-\frac{(\psi_e^\dagger\beta a(\mathbf{k}))(\psi_\iota^\dagger\beta a(-\mathbf{k}))}{E_M-E_L-H_\iota-K_k}\right]. \quad (1)$$

Here g is Fermi's constant; K_k is the neutrino energy in the virtual intermediate state; and ψ_M, ψ_N, and ψ_L are the wave functions of the nucleus in the initial, final, and intermediate states. They are functions not only of the space coordinates of all the heavy particles, but also of the four-valued Dirac spin coordinates on which matrices such as β operate, and of a two-valued fifth coordinate for each particle which indicates whether it is a neutron or a proton. The indicated integrations must be understood as including summation over the fourth and fifth coordinates. It is on the fifth coordinates that the Fermi operators $Q_i^\dagger$ act in such a way as to change a neutron into a proton; if the ith particle is already a proton, the operator $Q_i^\dagger$ gives the result zero. The operators $\beta_iQ_i^\dagger$ are symmetrized by summing over all the particles in the nucleus, and the factor $(\mathbf{r}_i|\mathbf{k})$ appears because the neutrino wave function must be given its value at the position of the heavy particle. The electron wave functions ψ_e and ψ_ι are to be evaluated at the "outer edge of the nucleus," as is usual in calculations on β-decay.[1,2]

According to the Majorana theory, the four-component neutrino amplitudes $a(\mathbf{k})$ are given by Eqs. (36), (50), and (53) of N. We have to substitute from these equations into (1), and then put

$$B_iB_j=0, \quad B_i^*B_j=0 \quad (2)$$

and

$$B_i(\mathbf{k})B_j^*(\mathbf{k})=\delta_{ij}, \quad B_i^*B_j^*=0. \quad (3)$$

Eq. (2) corresponds to the initial condition that no neutrinos are present, and (3) indicates our intention to calculate the process in which no neutrinos are emitted and not that in which two neutrinos are emitted. As indicated in N, the calculation can be simplified by using Eq. (51) of N instead of (50), and then discarding all terms in b_3, b_4, b_3^*, and b_4^*. Our conditions (2) and (3) can be satisfied by using instead of Eq. (51) of N just

$$b(\mathbf{k})\rightarrow b(\mathbf{k}) \quad (4)$$

for the left-hand factor and

$$b(\mathbf{k})\rightarrow T^*(\mathbf{k})b^*(-\mathbf{k}) \quad (4')$$

for the right-hand factor. Then, remembering that in the Majorana form of β-decay theory it is consistent to regard the factors $(2)^{-\frac{1}{2}}$ given by Eq. (53) of N as absorbed in the disposable constant g, we obtain

$$(\psi_\iota^\dagger\beta a(\mathbf{k}))(\psi_e^\dagger\beta a(-\mathbf{k}))$$
$$=\sum_{i=1,\,2}(\psi_\iota^\dagger\beta S(\mathbf{k}))_i(\psi_e^\dagger\beta S(-\mathbf{k})T^*(-\mathbf{k}))_i$$
$$=\psi_\iota^\dagger\beta S(\mathbf{k})\cdot\tfrac{1}{2}(1+\rho_3)\cdot T^\dagger(-\mathbf{k})S'(-\mathbf{k})\beta'\psi_e^*. \quad (5)$$

Here ρ_3 is a matrix originally defined by Dirac,[15] and quoted in N, Eq. (39). Then we can use the value of $T(\mathbf{k})$ as given in N, Eq. (43), and obtain

$$(\psi_\iota^\dagger\beta a(\mathbf{k}))(\psi_e^\dagger\beta a(-\mathbf{k}))=\psi_\iota^\dagger\beta S(\mathbf{k})$$
$$\cdot\tfrac{1}{2}(1+\rho_3)S^\dagger(\mathbf{k})A^\dagger\beta'\psi_e^*=\psi_\iota^\dagger M\psi_e^*. \quad (6)$$

It is readily verified that (6) has the same invariance properties as Eq. (56) of N with respect to changes in the form of the matrices α_i, β, and $S(\mathbf{k})$, and that if the neutrino mass is equal to zero M is a symmetrical matrix, independently of such changes. We shall use the representation of α_i, β which was originally given by Dirac, and has usually been employed in explicit calculations; it is quoted in N, Eqs. (59), (62). We can accordingly substitute Eqs.

[15] P. A. M. Dirac, Proc. Roy. Soc. **A117**, 614 (1928).

(60)–(62) of N into (6); we shall, however, replace both ϵ and $\epsilon+1$ by k, which corresponds to setting the neutrino mass equal to zero. The result is

$$M=-\tfrac{1}{2}k^{-1}\{k+(\boldsymbol{\alpha}\cdot\mathbf{k})\}\cdot i\alpha_y\beta=M'. \tag{7}$$

It is certainly correct to set the neutrino mass equal to zero, since important contributions to the result will come only from large values of the neutrino momentum. This step leads to a formal difficulty, however, because in N the vector $\mathbf{k}$ represents the propagation vector in units $mc/\hbar$, where m is the neutrino mass. We must, accordingly, change the units of k; this makes no difficulty, because (7) is homogeneous of degree zero in k. We shall from now on take k to be expressed in c.g.s. units, and replace Eq. (31) of N by

$$(\mathbf{r}|\mathbf{k})=V^{-\frac{1}{2}}\exp(i\mathbf{k}\cdot\mathbf{r}). \tag{8}$$

When (7) is substituted into (1), we see that on account of the symmetry of the matrix M the two numerators are equal. The minus sign due to the antisymmetry of the electronic wave function thus causes a strong cancellation, and we get

$$a_{N\leftarrow M}=g^2V^{-1}\sum(\mathbf{k})\sum_L\int\Psi_N^\dagger\{\sum_i\beta_iQ_i^\dagger\exp(i\mathbf{k}\cdot\mathbf{r}_i)\}\Psi_L d\tau\cdot\int\Psi_L'^\dagger\{\sum_j\beta_jQ_j^\dagger\exp(-i\mathbf{k}\cdot\mathbf{r}_j')\}\Psi_N' d\tau$$
$$\cdot(H_s-H_t)(E_M-E_L-H_s-K_k)^{-1}(E_M-E_L-H_t-K_k)^{-1}\psi_t^\dagger M\psi_s^*. \tag{9}$$

The main difficulty in the calculation occurs in the evaluation of the factor

$$\Gamma=g^2\sum_L\int\Psi_M^\dagger\{\sum_i\beta_iQ_i^\dagger\exp(i\mathbf{k}\cdot\mathbf{r}_i)\}\Psi_L d\tau\cdot\int\Psi_L'^\dagger\{\sum_j\beta_jQ_j^\dagger\exp(-i\mathbf{k}\cdot\mathbf{r}_j')\}\Psi_M' d\tau'\cdot f(E_L) \tag{10}$$

where $$f(E_L)=(E_M-E_L-H_s-K_k)^{-1}(E_M-E_L-H_t-K_k)^{-1}.$$

For values of the neutrino energy small enough to allow us to put $\exp(i\mathbf{k}\cdot\mathbf{r}_i)=1$, the first factor of the summand is

$$\int\Psi_M^\dagger\{\sum_i\beta_iQ_i\}\Psi_L d\tau. \tag{11}$$

This is just the sort of factor which occurs in calculations on single β-disintegration. It is usually assumed to have the value 1 if the angular momentum selection rule is obeyed, and, of course, the value 0 otherwise. Actually this is a decidedly crude assumption, as has been pointed out by Nordheim and Yost;[16] for moderately heavy nuclei it seems likely that the expression (11) cannot have a value larger than perhaps 0.1. Since, however, the value of g given by Fermi was assigned to agree with experiment on the basis of setting an expression such as (11) equal to 1, we shall not make any very large net error if we use this value of g and assume that there is at least one value of L for which both of the first two factors of the summand in (10) can be set equal to 1. There still remains, however, the question as to how many terms in the summation will yield similarly appreciable contributions to the value of Γ.

At first one might suppose that there would be a great many such values of L, because of the large number of energy levels possesed by any moderately heavy nucleus and because $\mathbf{k}$ is not restricted to small values, so that limitations on the angular momentum of the state L do not appear in the usual way. Such a conclusion, however, would in all probability be erroneous. The nature of nuclear states is such that any appreciable excitation energy is practically certain to be distributed effectively among a considerable number of particles, so that a factor $\exp(i\mathbf{k}\cdot\mathbf{r}_i)$, which involves the coordinates of one particle only, is unlikely to be very effective in removing the orthogonality of two wave functions. The assumption that there is only one intermediate state L which makes an important contribution to the sum is accordingly not an unreasonable one; we shall proceed in this way, with the reservation that our result is perhaps best regarded as a lower limit, from which the correct result should not differ by any very large factor.

[16] L. W. Nordheim and F. L. Yost, Phys. Rev. **51**, 942 (1937). Very recently (Phys. Rev. **56**, 519 (1939)) the matrix elements for a number of light radioactive elements have been calculated explicitly by Wigner.

In accordance with the above considerations, we shall use in our further calculations the simple formula

$$\Gamma = g^2 f(E_L)(4\pi\rho^3/3)^{-2} \int\int\int_{r<\rho} \exp(i\mathbf{k}\cdot\mathbf{r}) d\tau \cdot \int\int\int_{r'<\rho} \exp(-i\mathbf{k}\cdot\mathbf{r}') d\tau'. \quad (12)$$

Here the integral is over the interior of a three-dimensional sphere of radius ρ, the nuclear radius. The factor $(4\pi\rho^3/3)^{-2}$ comes from normalization. The formula has been written on the assumption that the angular momentum of the state L is the same as that of M and N, but this assumption has actually rather little to do with our final result. If, for example, $i_L - i_M = i_L - i_N = \pm 1$, we should have to use some such expression as

$$\Gamma' = g^2 f(E_L)(4\pi\rho^3/3)^{-2} \cdot 3 \cdot \int\int\int_{r<\rho} \cos\theta \cdot \exp(i\mathbf{k}\cdot\mathbf{r}) d\tau \cdot \int\int\int_{r'<\rho} \cos\theta' \exp(-i\mathbf{k}\cdot\mathbf{r}') d\tau', \quad (12')$$

and we shall verify later that this makes no decided difference.

Further simplification in Eq. (9) can easily be made. Since k is in c.g.s. units, the energy of the neutrino is $K_k = \hbar c k$. The main contributions to (9) come from values of k so large that the other energies can be neglected compared to K_k; the occurrence of a vanishing denominator is of course ruled out by the postulated impossibility of single β-disintegration for the nucleus in question. Accordingly we set

$$f(E_L) = K_k^{-2} = (\hbar c)^{-2} k^{-2}. \quad (13)$$

The sum over the allowed values of $\mathbf{k}$ in the box of volume V can be replaced by an integral in the usual way:

$$\sum(\mathbf{k}) \cdots = (2\pi)^{-3} V \int_0^\infty k^2 dk \int\int d\Omega \cdots. \quad (14)$$

Substituting (12), (13) and (14) in (9), we obtain

$$a_{N\leftarrow M} = -(2\pi)^{-3}(g/\hbar c)^2 C^{0,0} \cdot (H_s - H_t)\psi_t^\dagger \cdot \tfrac{1}{2} i\alpha_y \beta \psi_s^*, \quad (15)$$

where

$$C^{0,0} = \int_0^\infty dk \int\int d\Omega \left| (3/4\pi\rho^3) \int\int\int_{r<\rho} \exp(i\mathbf{k}\cdot\mathbf{r}) d\tau \right|^2 = (9/4\pi\rho^6) \int_0^\infty dk \left| \int\int\int_{r<\rho} e^{ikz} d\tau \right|^2; \quad (16)$$

the superscripts 0,0 refer to the values of $i_L - i_M$ and $i_L - i_N$. The second term in (7) is omitted from (15), since it makes no contribution for even-even or odd-odd transitions.

Following Goeppert-Mayer, we express the energies of the electrons and the total available energy in terms of dimensionless quantities: $H_s = h_s mc^2$, $H_t = h_t mc^2$, $E_M - E_N = \epsilon mc^2$, where m is the mass of an electron. Let us also put $p_s = (h_s^2 - 1)^{\frac{1}{2}}$, $p_t = (h_t^2 - 1)^{\frac{1}{2}}$, and make the abbreviation

$$R_s = (16\pi/|\Gamma(3+2S)|^2)(mc/h)^3(2mc\rho p_s/\hbar)^{2S} \cdot \exp(\pi\gamma h_s/p_s)|\Gamma(1+S+i\gamma h_s/p_s)|^2, \quad (17)$$

where $\gamma = Z/137$, $S = (1-\gamma^2)^{\frac{1}{2}} - 1$. We follow Goeppert-Mayer in replacing R_s by the following approximation, valid because $|S| \ll 1$:

$$R_s \cong (16\pi/|\Gamma(3+2S)|^2)(mc/h)^3(2mc\rho/\hbar)^{2S} \cdot 2\pi\gamma h_s/p_s. \quad (17')$$

A similar definition and approximation hold for R_t.

When the resonance factor is included, the squared amplitude for the transition to two particular states s and t is $(2\pi t/\hbar)|a_{N\leftarrow M}|^2 \delta(\epsilon mc^2 - h_s mc^2 - h_t mc^2)$. The total probability per unit time for transitions in which one electron gets an energy between $h_s mc^2$ and $(h_s + dh_s)mc^2$ and the other receives the rest of the energy ϵmc^2 is then

$$P(h_s)dh_s = (2\pi/\hbar mc^2)(dh_t)^{-1} \sum_{dh_t} \sum_{dh_s} |a_{N\leftarrow M}|^2. \quad (18)$$

Here the symbol $\sum_{dh_t}$ means the sum over all states having energy between $h_t mc^2$ and $(h_t+dh_t)mc^2$; the result is of course proportional to dh_t. Using the Dirac wave functions for an electron in the Coulomb field, evaluated at $r=\rho$, we obtain, to the lowest order in γ^2:

$$\sum_{dh_s}\sum_{dh_t}|\psi_t^\dagger\cdot\tfrac{1}{2}i\alpha_y\beta\psi_s^*|^2 = \tfrac{1}{4}R_sR_tp_sp_t(h_sh_t-1)dh_sdh_t. \quad (19)$$

Then

$$P(h_s)dh_s=2^{-7}\pi^{-5}g^4\hbar^{-5}mc^{-2}|C^{0,0}|^2 \times R_sR_tp_sp_t(h_sh_t-1)(h_s-h_t)^2dh_s. \quad (20)$$

The energy spectrum of the electrons is, of course, symmetrical around the value $\frac{1}{2}\epsilon mc^2$. The factor $(h_s-h_t)^2$ in (20), which makes the intensity vanish for the energy $\frac{1}{2}\epsilon mc^2$, comes directly from the cancellation due to the antisymmetry of the electronic wave function.

To get the total probability of disintegration per unit time, we must integrate (20) from $h_s=1$ to $h_s=\epsilon-1$. According to the approximation (17′) the quantity R_sp_s/h_s is essentially independent of h_s. This enables us to write for the total probability of disintegration per unit time:

$$P_1=\int_1^{\epsilon-1}P(h_s)dh_s=2^{-7}\pi^{-5}g^4\hbar^{-5}mc^{-2}|C^{0,0}|^2(R_sp_s/h_s)^2\cdot\int_1^{\epsilon-1}h_s(\epsilon-h_s) \times\{h_s(\epsilon-h_s)-1\}(\epsilon-2h_s)^2dh_s. \quad (21)$$

Then

$$P_1=2^{-7}\pi^{-5}g^4\hbar^{-5}mc^{-2}|C^{0,0}|^2(R_sp_s/h_s)^2\cdot\varphi(\epsilon-2), \quad (22)$$

where

$$\varphi(x)=(x^4/3)\{1+(11x/10)+(x^2/5)+(x^3/70)\}. \quad (23)$$

We shall now evaluate P_1 numerically for $Z=31$, the value used as an example by Goeppert-Mayer. Taking $\rho=8\times10^{-13}$ cm, we get from (17′) the value $R_sp_s/h_s=1.52\times10^{30}$ cm^{-3}. The integral (16) can be evaluated by a rather tedious elementary calculation, or more elegantly by means of Fourier's integral theorem:

$$\int_0^\infty dk\left|\iiint_{r<\rho}e^{ikz}d\tau\right|^2=\tfrac{1}{2}\int_{-\infty}^{\infty}dk\cdot\iiint_{r<\rho}e^{ikz}dzdxdy\cdot\iiint_{r'<\rho}e^{-ikz'}dz'dx'dy'=\pi\int\int\int\int\int dxdydx'dy'dz,$$

where in the last expression the limits for x' and y' depend on the value of z in the same way as those for x and y. Then

$$\int_0^\infty dk\left|\iiint_{r<\rho}e^{ikz}d\tau\right|^2=\pi\int_{-\rho}^{\rho}\pi^2(\rho^2-z^2)^2dz=16\pi^3\rho^5/15.$$

Thus

$$C^{0,0}=12\pi^2/5\rho. \quad (24)$$

A similar calculation shows that if (12′) were used instead of (12) we should have simply to replace $C^{0,0}$ by a quantity $C^{1,1}=9\pi^2/5\rho=(3/4)C^{0,0}$. Using $g=4\times10^{-50}$ erg cm^3, we obtain finally

$$P_1=1.07\times10^{-28}\varphi(\epsilon-2)\ \text{sec}^{-1}. =3.4\times10^{-21}\varphi(\epsilon-2)\ \text{year}^{-1}. \quad (25)$$

Some values of φ are as follows:

$\epsilon=$	3	4	6	8	10	12	20
$\varphi(\epsilon-2)=$	0.77	22	8.1×10^3	7.7×10^4	4.1×10^5	1.54×10^6	5.9×10^6

(26)

For small values of ϵ the P found here is about 10^6 times that given by Goeppert-Mayer. For larger values of ϵ the ratio is not so large. This is natural, since for large ϵ there is plenty of energy available for the emission of neutrinos along with the electrons.

III. Other Interaction Expressions

In the preceding section we calculated the value of P by using the scalar-type expression for the interaction energy. We now want to consider what would be the effect of using any

of the various other energy expressions which have been proposed.

Since we are interested only in the order of magnitude of P, we shall neglect the effect of using a different matrix instead of $\frac{1}{2}i\alpha_\nu\beta$ in calculating the expression corresponding to (19). This would at most replace the factor $(h_s h_t - 1)$ by some factor such as $h_s h_t$ or $(h_s h_t + 1)$, and for $\epsilon - 2 \gtrsim 1$ such a change amounts to only a factor of perhaps two in the answer. Hence we shall simply keep the factor $(h_s h_t - 1)$ throughout.

To begin with we shall consider the two main differences in the size of P which can arise from changes in the interaction energy expression. We shall then list the various expressions and indicate the main types of terms which they give in the integrand of the equation corresponding to Eq. (1) in the general case. This classification makes it possible to state the selection rules for the different types of interaction expression.

Differences in order of magnitude of P

The first important difference which may come from the use of a different interaction expression is the absence of the strong cancellation due to the antisymmetry of the electronic wave function which occurred in Section II. If the matrix[17] M is not purely symmetric, the main contribution to $a_{N\leftarrow M}$ will come from the antisymmetric part of M, $M_A = \frac{1}{2}(M - M')$. Eq. (15) is then replaced by

$$a_{N\leftarrow M} = (2\pi)^{-3}(g^2/\hbar c) D^{0,0} \psi_t^\dagger M_A \psi_s^* \qquad (27)$$

and Eq. (20) by

$$P(h_s)dh_s = 2^{-7}\pi^{-5} g^4 \hbar^{-3} m^{-1} c^{-4} |D^{0,0}|^2 \times R_s R_t p_s p_t (h_s h_t - 1) dh_s, \qquad (28)$$

where

$$D^{0,0} = \int_0^\infty 2k dk \int\int d\Omega \times \left| (3/4\pi\rho^3) \int\int\int_{r<\rho} \exp(i\mathbf{k}\cdot\mathbf{r}) d\tau \right|^2. \qquad (29)$$

The spectrum now has a maximum at $h_s = \frac{1}{2}\epsilon$, instead of vanishing there.

The total probability of disintegration per unit time is now

$$P_2 = 2^{-7}\pi^{-5} g^4 \hbar^{-3} m^{-1} c^{-4} |D^{0,0}|^2 \times (R_s p_s / h_s)^2 \cdot \chi(\epsilon - 2), \qquad (30)$$

where

$$\chi(\epsilon - 2) = \int_1^{\epsilon - 1} h_s(\epsilon - h_s)\{h_s(\epsilon - h_s) - 1\} dh_s$$

or

$$\chi(x) = x^2\{1 + (7x/6) + (x^2/3) + (x^3/30)\}. \qquad (31)$$

Integration of (29) by elementary methods gives

$$D^{0,0} = 18\pi/\rho^2. \qquad (32)$$

Then

$$P_2 = 1.43\times 10^{-24}\chi(\epsilon - 2) \text{ sec.}^{-1} = 4.6\times 10^{-17}\chi(\epsilon - 2) \text{ year}^{-1}. \qquad (33)$$

$\epsilon =$	3	4	6	8	10	12	20
$\chi(\epsilon-2) =$	2.5	19.7	2.1×10^2	9.8×10^2	3.1×10^3	7.9×10^3	1.05×10^5

(34)

Another important effect on the disintegration probability is obtained if we use a Konopinski-Uhlenbeck form of interaction expression. The use of such an expression is subject to certain theoretical difficulties,[18] and it has been suggested[19] that the experimental results can perhaps be fully explained without using an interaction expression involving derivatives; nevertheless it is not without interest to see what such expressions give for the double β-disintegration.

The use of a Konopinski-Uhlenbeck expression means essentially the insertion of a factor k^2 into the integrand in (16) or (29), and the replacement of the constant g by a constant which differs from it by the dimensions of a length. The length by which g is multiplied to give the new constant should be $(2\pi)^{-1}$ times a typical de Broglie wave-length of the neutrino in an ordinary β-disintegration, in order that the probabilities for single β-disintegration may be kept the same. Hence we shall replace g by $(\hbar/2mc)g$. The total disintegration probability per unit time is then

$$P_3 = 2^{-11}\pi^{-5} g^4 \hbar^{-1} m^{-3} c^{-6} |F^{0,0}|^2 \times (R_s p_s / h_s)^2 \cdot \varphi(\epsilon - 2), \qquad (35)$$

[17] In general it is actually a matrix *function* which has to be used, as is indicated below in Eq. (45). In the case treated in Section II this function could conveniently be split into factors, only one of which is a matrix (Cf. Eq. (46)). In any case it is only the symmetry or antisymmetry under the interchange of two four-valued indices which comes into question in determining the presence or absence of the cancellation.

[18] Cf. M. Fierz, Helv. Phys. Acta **10**, 123, 284 (1937).

[19] H. A. Bethe, F. Hoyle and R. Peierls, Nature **143**, 200 (1939).

where

$$F^{0,0}=\int_0^\infty k^2dk\int\int d\Omega \times\left|(3/4\pi\rho^3)\int\int\int_{r<\rho}\exp(i\mathbf{k}\cdot\mathbf{r})d\tau\right|^2 \quad (36)$$

if M is a pure symmetric matrix. If M is asymmetric we get

$$P_4=2^{-11}\pi^{-5}g^4\hbar m^{-5}c^{-8}|G^{0,0}|^2\times(R_sp_s/h_s)^2\chi(\epsilon-2), \quad (37)$$

where

$$G^{0,0}=\int_0^\infty 2k^3dk\int\int d\Omega \times\left|(3/4\pi\rho^3)\int\int\int_{r<\rho}\exp(i\mathbf{k}\cdot\mathbf{r})d\tau\right|^2. \quad (38)$$

The integral (36) can be evaluated elegantly by using Fourier's integral theorem:

$$\begin{aligned}F^{0,0}&=(3/4\pi\rho^3)^2\int_{-\infty}^{\infty}dk_x\int_{-\infty}^{\infty}dk_y\int_{-\infty}^{\infty}dk_z\\&\cdot\int\int\int_{r<\rho}\exp(i\mathbf{k}\cdot\mathbf{r})dxdydz\\&\cdot\int\int\int_{r'<\rho}\exp(-i\mathbf{k}\cdot\mathbf{r}')dx'dy'dz'\\&=(3/4\pi\rho^3)^2\cdot(2\pi)^3\cdot\int\int\int_{r<\rho}dxdydz=6\pi^2/\rho^3.\end{aligned} \quad (39)$$

Numerical computation then gives:

$$\begin{aligned}P_3&=2.28\times10^{-22}\varphi(\epsilon-2)\text{ sec.}^{-1}\\&=7.17\times10^{-15}\varphi(\epsilon-2)\text{ year}^{-1}.\end{aligned} \quad (40)$$

The integral (38) diverges logarithmically, so that in order to obtain a finite value it is necessary to "cut off" at some value of k. It is generally assumed that the value at which the theory becomes unreliable and the cutting off should be done is about mc^2/e^2. In evaluating $G^{0,0}$ it is particularly convenient to cut off at a value which makes $k\rho=\pi$. One then readily finds by elementary methods that

$$G^{0,0}=(72\pi/\rho^4)\left\{\int_0^\pi\sin^2 y\cdot dy/y-\tfrac{1}{2}\right\}\leqq162/\rho^4. \quad (41)$$

The cut-off occurs rather beyond the first maximum of the integrand. The range $0<k<\pi/\rho$ includes the essential contributions to the integrals $C^{0,0}$, $D^{0,0}$, and $F^{0,0}$, so that their values are genuinely independent of whether one cuts off or not.

Using the value (41), one obtains

$$\begin{aligned}P_4&=3.99\times10^{-18}\chi(\epsilon-2)\text{ sec.}^{-1}\\&=1.26\times10^{-10}\chi(\epsilon-2)\text{ year}^{-1}.\end{aligned} \quad (42)$$

We have now listed four typical formulas for the disintegration constant P. Next we must classify the various possible expressions for the interaction energy in such a way as to show what value of P each would give.

Classification of interaction energy expressions

By methods analogous to those used in deriving Eq. (7) one can readily calculate the value of $a_{N\leftarrow M}$ corresponding to any particular expression for the interaction energy. The formulas obtained are, however, for the most part very long and cumbersome. Accordingly we shall indicate only the typical characteristics of the dominant terms, which suffice to determine the order of magnitude of the disintegration constant and to determine the selection rules.

Usually in calculations using the neutrino theory of β-decay one neglects terms involving the small components of the wave functions of the heavy particles compared to those which involve only the large components. This is done because the small components are of order $\bar{v}/c$ compared to the large, $\bar{v}$ being a typical velocity of a heavy particle, and $\bar{v}/c$ is only about 0.2. For our present purposes we can neglect such terms usually, but not always; if the terms involving only the large components give purely symmetric matrices M and other terms give asymmetric matrices, then the latter will be more important because of the absence of any strong cancellation. This situation arises with Fermi's original "vector-type" interaction expression.

Usually only the product of the time components is used in calculations, because the product of the space components brings in small components of the heavy particle wave functions. In our present case, however, such a procedure gives a symmetric matrix M, and the space components appear in the actual dominant terms.

To avoid useless multiplication of the number of types listed, we shall write the typical expressions in terms of just the matrices 1 and $\boldsymbol{\sigma}$ for the heavy particles, whose wave functions may then be thought of as two-component Pauli wave functions Any occurrence of the small components in the dominant terms will then be indicated by a suitable power of $(\bar{v}/c)$. Explicitly, so far as the heavy particles are concerned we set

$$\begin{aligned}&\beta\rightarrow 1, \quad \gamma_5=\rho_1\rightarrow(\bar{v}/c)\\ &\beta\boldsymbol{\sigma}\rightarrow\boldsymbol{\sigma}, \quad \boldsymbol{\alpha}\rightarrow(\bar{v}/c)\boldsymbol{\sigma}, \quad \beta\boldsymbol{\alpha}\rightarrow(v/c)\boldsymbol{\sigma}.\end{aligned} \tag{43}$$

We use the abbreviations:

$$\begin{aligned}\Psi_L^\dagger\{\textstyle\sum_i Q_i^\dagger(\mathbf{r}_i|-\mathbf{k})\}\Psi_M&=a_1,\\ \Psi_L^\dagger\{\textstyle\sum_i \boldsymbol{\sigma}_i Q_i^\dagger(\mathbf{r}_i|-\mathbf{k})\}\Psi_M&=\mathbf{b}_1,\\ \Psi_N^\dagger\{\textstyle\sum_i Q_i^\dagger(\mathbf{r}_i|\mathbf{k})\}\Psi_L&=a_2,\\ \Psi_N\{\textstyle\sum_i \boldsymbol{\sigma}_i Q_i^\dagger(\mathbf{r}_i|\mathbf{k})\Psi_L&=\mathbf{b}_2.\end{aligned} \tag{44}$$

The quantity $a_{N\leftarrow M}$ can always be expressed in the form

$$\begin{aligned}a_{N\leftarrow M}=g^2\textstyle\sum(\mathbf{k})\int d\tau\int d\tau'\sum_L\sum_{lm}\psi_{ll}^*\\ \times\left\{\frac{\Lambda_{lm}{}^L(\mathbf{r},\mathbf{r}';\mathbf{k})}{E_M-E_L-H_s-K_k}\right.\\ \left.-\frac{\Lambda_{ml}{}^L(\mathbf{r},\mathbf{r}';\mathbf{k})}{E_M-E_L-H_l-K_k}\right\}\psi_{sm}^*.\end{aligned} \tag{45}$$

In the case treated in Section II the matrix function Λ was simply

$$\Lambda(\mathbf{r},\mathbf{r}';\mathbf{k})=a_2(\mathbf{r};\mathbf{k})M(\mathbf{k})a_1(\mathbf{r}';\mathbf{k}), \tag{46}$$

with M given by Eq. (7). Eq. (9) gives the result of substituting (46) and (44) in (45), provided (43) is taken into account.

We now list the types of expression which can appear as the dominant terms of the matrix function Λ:

Symmetric Terms:

$$S_1=a_2\cdot i\alpha_y\beta a_1, \tag{47a}$$

$$S_2=a_2(\boldsymbol{\alpha}\cdot\mathbf{n})i\alpha_y\beta a_1 \quad (\mathbf{n}=\mathbf{k}/k). \tag{47b}$$

Many other types of symmetric term occur, but only in combination with antisymmetric terms which give the dominant contributions to the result.

Antisymmetric Terms:

$$A_1=i([\mathbf{b}_1\times\mathbf{b}_2]\cdot\boldsymbol{\sigma})i\alpha_y\beta, \tag{48a}$$

$$A_2=i([\mathbf{b}_1\times\mathbf{b}_2]\cdot\mathbf{n})\rho_1 i\alpha_y\beta, \tag{48b}$$

$$A_3=i([\mathbf{b}_1\times\mathbf{b}_2]\cdot\mathbf{n})(\mathbf{n}\cdot\boldsymbol{\sigma})i\alpha_y\beta, \tag{48c}$$

$$A_4=\beta([\mathbf{b}_1\times\mathbf{n}]\cdot[\mathbf{b}_2\times\mathbf{n}])i\alpha_y\beta, \tag{48d}$$

$$A_5=i([(a_1\mathbf{b}_2-a_2\mathbf{b}_1)\times\mathbf{n}]\cdot\boldsymbol{\sigma})i\alpha_y\beta. \tag{48e}$$

We give the different expressions for the interaction energy the same designations as used by Bethe and Bacher.[3] The types of the dominant terms in Λ and the order of magnitude of the disintegration constant P are given in the following list:

Fermi Expressions:

Scalar: $\Lambda\sim S_1, S_2$; $P\approx P_1$, (49a)

Vector: $\Lambda\sim(\bar{v}/c)A_5$; $P\approx(\bar{v}/c)^2P_2$, (49b)

Tensor: $\Lambda\sim A_1, A_2$; $P\approx P_2$, (49c)

Pseudovector: $\Lambda\sim A_1, A_2$; $P\approx P_2$, (49d)

Pseudoscalar:

$$\Lambda\sim(\bar{v}/c)^2S_1, (\bar{v}/c)^2S_2; \quad P\approx(\bar{v}/c)^4P_1. \tag{49e}$$

Konopinski-Uhlenbeck Expressions:

Vector: $\Lambda\sim qS_1, qS_2$; $P\approx P_3$, (50a)

Tensor: $\Lambda\sim qA_2, qA_3$; $P\approx P_4$, (50b)

Pseudovector:

$$\Lambda\sim qA_1, qA_2, qA_3, qA_4; \quad P\approx P_4. \tag{50c}$$

Here

$$q=k^2(\hbar/2mc)^2 \tag{51}$$

is the essential factor which distinguishes the Konopinski-Uhlenbeck from the Fermi formulas,

and which was taken into account in calculating P_3 and P_4.

Selection rules

The expressions

$$\sum_L \psi_i^\dagger S_j \psi_s^* \quad \text{and} \quad \sum_L \psi_i^\dagger A_j \psi_s^*$$

are all scalars with respect to the three-dimensional rotation-reflection group: so far as transformation properties are concerned we can think of $i\alpha_y\beta\psi_s^*$ as replaced by a function ψ_σ.[20] To find the selection rules corresponding to the expressions (47) and (48) we may inspect the transformation properties of either the factors involving a_n, $\mathbf{b}_n$, and $\mathbf{n}$ or the matrix factors, apart from the factors $i\alpha_y\beta$. We obtain:

S_1 and A_4: Scalars: $\Delta i=0$; odd-odd and even-even transitions.

A_2: Scalar, but with reflection character -1: $\Delta i=0$; odd-even and even-odd transitions.

S_2: Polar vector: $\Delta i=0$ or ± 1, but not $0\rightarrow 0$; odd-even and even-odd transitions.

A_1, A_3, and A_5: Axial vectors: $\Delta i=0$ or ± 1, but not $0\rightarrow 0$; odd-odd and even-even transitions.

The selection rules for each interaction expression can then be read off from (49) or (50). The selection rules in general bear more resemblance to those of Gamow and Teller than to those of Fermi, since some $\Delta i=\pm 1$ transitions are always allowed. Transitions forbidden by these rules can occur only if at least one electron is emitted in a state with $j\neq\frac{1}{2}$, and their probabilities will be decidedly smaller than those given by (49) and (50). For $\epsilon-2\gtrsim 2$ the probabilities will be decreased by a factor of roughly $\{(\epsilon-2)\rho mc/2\hbar\}^2$ for a change in parity type of the transition or for each extra unit of Δi. For smaller values of $\epsilon-2$ the decrease will be more drastic.

[20] Cf. discussion in *N*, p. 66; also W. H. Furry, Phys. Rev. **51**, 125 (1937), Eq. (8) with $A=i\alpha_y\beta$. The free electron functions form a complete set.

Dependence of transition probability on atomic number

The numerical results which we have given were all computed for $Z=31$, $\rho=8\times 10^{-13}$ cm. The quantity $(R_s p_s/h_s)$ is roughly proportional to Z, and ρ may be taken to be proportional to $Z^{\frac{1}{3}}$. Approximate relations for changing the results to different values of Z or a different estimate of the nuclear radius are, accordingly:

$$P_1\propto Z^2\rho^{-2}\propto Z^{4/3}, \quad P_2\propto Z^2\rho^{-4}\propto Z^{\frac{1}{3}},$$
$$P_3\propto Z^2\rho^{-6}\propto \text{cons.}, \quad P_4\propto Z^2\rho^{-8}\propto Z^{-\frac{1}{3}}. \quad (52)$$

The results as calculated are for emission of two negative electrons. In the case of positron emission the probabilities will be smaller, because R_s contains an additional factor $\exp(-2\pi\gamma h_s/p_s)$, and R_t a similar factor. These factors decidedly complicate the evaluation of the integrals from which the functions φ and χ have to be determined. It is evident, however, that for $\epsilon-2\gtrsim 2$ the decrease will be by a factor not much smaller than $e^{-4\pi\gamma}=e^{-0.092Z}$. As is the case for the forbidden transitions, the decrease is more decided for smaller values of $\epsilon-2$.

IV. Conclusion

We have seen that the phenomenon of double beta-disintegration is one for which there is a decided difference between the results of the Majorana theory and those of the older theory of the neutrino. According to the older theory it seemed certain that double beta-disintegration could never be capable of observation because of its extremely minute probability, but the Majorana theory indicates that this is by no means necessarily the case. Indeed, if the interaction expression were of Konopinski-Uhlenbeck type this process would be quite likely to have a bearing on the abundances of isotopes and on the occurrence of observed long-lived radioactivities. If it is of Fermi type this could be so only if the mass difference were fairly large ($\epsilon\gtrsim 20$, $\Delta M\gtrsim 0.01$ unit).

Phase Shift Calculations for Proton-Proton Scattering at High Energies

H. M. THAXTON* AND L. E. HOISINGTON
University of Wisconsin, Madison, Wisconsin

(Received October 17, 1939)

The theoretical s wave shift for the square well and the Gauss error well which is fitted to experiment from 0.7 to 2.6 Mev is calculated up to energies of 10 Mev. Coulomb functions needed for this purpose are tabulated and the phase shift, as well as the ratio of theoretical scattering to that expected according to Mott's formula, is represented graphically as a function of the energy. The Gauss error well and the square well are found to give very similar extrapolations of the experimental phase shifts to high energies.

ANALYSIS[1,2] of the experimental data[3] on proton-proton scattering has shown that the p state scattering is small in the energy interval 0.9 to 2.4 Mev. The analysis also shows that on the assumption of pure s state scattering in this energy region the experimental data are closely fitted by the scattering expected from a square potential well of depth 10.50 Mev and range e^2/mc^2 without Coulomb potential inside, or from a Gauss error potential well $Ae^{-\alpha r^2}$ where $A=51.44\ mc^2$ and $\alpha=21.59\ Mmc^2/\hbar^2$, cut off at $r=3e^2/mc^2$ and with Coulomb potential inside. Comparisons with experimental data were also made[2] with the use of square wells of depth 6.3452 Mev and range $1.25\ e^2/mc^2$, and of depth 19.690 Mev and range $0.75\ e^2/mc^2$.

The probability that proton-proton scattering experiments will soon be done at energies from 3 to 10 Mev has made it desirable to have the phase shifts and the expected scattering for the above wells calculated for these higher energies. Graphs up to 9 Mev have already been published[2] for the square wells of depth 10.50 Mev and radius e^2/mc^2, and of depth 46.78 Mev and radius $0.5\ e^2/mc^2$. In this paper the high energy calculations for the others of the above potential wells are reported.

The notation and the values of the physical constants are the same as those used in BTE. The quantities Φ_0^*/Φ_0, $\Phi_0\Theta$ and $C_0^2\rho\Phi_0^2$ used in the calculation of the phase shift K_0 (BCP Eq. (7.8)) are given in Table I. In the other tables are listed the values of the quantities necessary to find the ratio $\mathfrak{R}$ of the expected scattering to Mott scattering (BTE Eqs. (2.1) and (2.2), and see BCP Eqs. (6) to (6.7)). Tables II, IV and VI give the values of the coefficient of $-\sin K_L \cos K_L$ in the formula for $\mathfrak{R}$ for $L=0$, 1, 2. Tables III, V and VII give the values of the coefficient of $\sin^2 K_L$ for $L=0$, 1, 2. Tables II to VII are extensions of the BCP tables of the same numbers, and Tables II and III are extensions of BTE Tables I and II.

The calculations with the Gauss error potential were made at energy intervals of 1 Mev. The joining to the Coulomb functions was made at $r=3e^2/mc^2$. Interpolations were necessary to obtain the value of $x\mathfrak{F}'/\mathfrak{F}$ at the value of x (here $x=\alpha^{\frac{1}{2}}r$) corresponding to $r=3e^2/mc^2$; these interpolations were made parabolically. At energies of 6 and 7 Mev the value of $x\mathfrak{F}'/\mathfrak{F}$ changes so rapidly with x that interpolations of $\mathfrak{F}$ and $\mathfrak{F}'$ separately were necessary.

Figures 1 to 4 show the phase shifts K_0 for the different potential wells as a function of the energy E of the incident protons. Figs. 1, 2 and 3 illustrate the effects of varying the depths of the square wells of radius 0.75, 1.00 and 1.25 e^2/mc^2 without Coulomb potential inside. Increasing the depth of the well mainly raises the K_0, E curve as a whole, and does not change its shape or slope much. Fig. 4 shows how the shape of the K_0, E curve for the square well without Coulomb potential inside is affected by changing the radius of the well. Decreasing the radius increases the slope and slightly reduces the curva-

* Now at the Agricultural and Technical College of North Carolina.

[1] G. Breit, E. U. Condon and R. D. Present, Phys. Rev. **50**, 825 (1936). This paper will be referred to as BCP.

[2] G. Breit, H. M. Thaxton and L. Eisenbud, Phys. Rev. **55**, 1018 (1939). This paper will be referred to as BTE.

[3] R. G. Herb, D. W. Kerst, D. B. Parkinson and G. J. Plain, Phys. Rev. **55**, 603(A) and 998 (1939); N. P. Heydenberg, L. R. Hafstad and M. A. Tuve, Phys. Rev. **55**, 603(A) (1939). For analysis of the data, see BTE pp. 1035–6.

TABLE I. *Coulomb functions. This table is probably accurate to ±0.02 percent. It is an extension of the table in the appendix of BTE and gives the quantities needed for Eq. (7.8) of BCP.*

E (Mev)	η	$r=0.5\ e^2/mc^2$ Φ_0^*/Φ_0	$\Phi_0\Theta_0$	$C_0^2\rho\Phi_0^2$	$r=0.75\ e^2/mc^2$ Φ_0^*/Φ_0	$\Phi_0\Theta_0$	$C_0^2\rho\Phi_0^2$	$r=e^2/mc^2$ Φ_0^*/Φ_0	$\Phi_0\Theta_0$	$C_0^2\rho\Phi_0^2$
3.0	0.091279	1.0005	0.9228	0.2034	0.9829	0.8789	0.3029	0.9530	0.8215	0.3972
3.5	.084508	.9965	.9189	.2239	.9739	.8678	.3319	.9367	.8003	.4324
4.0	.079050	.9925	.9146	.2429	.9649	.8561	.3583	.9204	.7784	.4635
4.5	.074529	.9886	.9098	.2606	.9559	.8439	.3824	.9040	.7562	.4912
5.0	.070704	.9845	.9048	.2772	.9470	.8314	.4047	.8875	.7338	.5161
5.5	.067414	.9806	.8996	.2929	.9377	.8186	.4254	.8708	.7114	.5385
6.0	.064544	.9765	.8942	.3075	.9285	.8057	.4446	.8540	.6890	.5587
6.5	.062012	.9725	.8886	.3215	.9193	.7927	.4625	.8372	.6667	.5770
7.0	.059756	.9685	.8829	.3348	.9101	.7795	.4792	.8202	.6446	.5935
7.5	.057730	.9645	.8771	.3476	.9009	.7663	.4949	.8031	.6225	.6084
8.0	.055897	.9604	.8712	.3597	.8916	.7531	.5096	.7858	.6009	.6219
8.5	.054228	.9564	.8653	.3713	.8823	.7400	.5234	.7685	.5793	.6340
9.0	.052700	.9524	.8593	.3825	.8729	.7268	.5364	.7510	.5583	.6449
9.5	.051294	.9483	.8532	.3932	.8635	.7136	.5486	.7334	.5372	.6547
10.0	.049996				.8541	.7006	.5602			
E (Mev)	η	$r=1.25\ e^2/mc^2$ Φ_0^*/Φ_0	$\Phi_0\Theta_0$	$C_0^2\rho\Phi_0^2$	$r=2\ e^2/mc^2$ Φ_0^*/Φ_0	$\Phi_0\Theta_0$	$C_0^2\rho\Phi_0^2$	$r=3\ e^2/mc^2$ Φ_0^*/Φ_0	$\Phi_0\Theta_0$	$C_0^2\rho\Phi_0^2$
3.0		0.9108	0.7516	0.4818	0.7004	0.4781	0.6544	0.1728	0.08249	0.6451
3.5		.8851	.7183	.5194	.6282	.4063	.6764	−.03225		.6027
4.0		.8591	.6847	.5515	.5538	.3387	.6880	−.2555	−.07356	.5510
4.5		.8329	.6512	.5791	.4771	.2755	.6914	−.5005		.4942
5.0		.8063	.6179	.6028	.3980	.2169	.6883	−.7715	−.16425	.4359
5.5		.7795	.5851	.6231	.3163	.1623	.6796	−1.0742		.3780
6.0		.7524	.5529	.6404	.2318	.1133	.6666	−1.416	−.2045	.3243
6.5		.7250	.5213	.6550	.1444	.06805	.6500	−1.806		.2700
7.0		.6972	.4904	.6672	.05367	.02701	.6306	−2.259	−.2080	.2219
7.5		.6692	.4601	.6773	−.04038	−.01005	.6089	−2.795		.1784
8.0		.6409	.4306	.6855	−.1382	−.04325	.5854	−3.440	−.1867	.1399
8.5		.6122	.4020	.6919	−.2398	−.07283	.5606	−4.239		.1064
9.0		.5831	.3740	.6967	−.3460	−.09894	.5349	−5.262	−.1498	.07794
9.5		.5537	.3467	.7001	−.4568	−.12187	.5086	−6.627		.05437
10.0		.5241	.3205	.7022				−8.479	−.10579	.03601

ture. Fig. 4 also shows the close agreement of the K_0's as calculated for the square well of radius e^2/mc^2 and depth 10.5 Mev and for the Gauss error well $Ae^{-\alpha r^2}$ with $A=51.44\ mc^2$ and $\alpha=21.59\ Mmc^2/\hbar^2$, the latter potential well being supposed to be superposed on the Coulomb potential. A slight change in the depth and radius of the square well should bring the two curves almost into coincidence. This indicates

TABLE II. *Values of the coefficient (i.e., $2\mathbf{X}/\eta\mathfrak{M}$) of $-\sin K_0 \cos K_0$ for $\mathbf{P}/\mathbf{P}_M$. This table is an extension of Table I of BTE. For expansions of $\mathbf{X}$ and $\mathfrak{M}$ in terms of E see BTE Tables III and V.*

E (Mev)	η	$\Theta=15°$	20°	25°	30°	35°	40°	45°
6.0	0.064544	2.348	4.592	8.069	13.23	20.20	27.51	30.96
7.0	0.059756	2.541	4.967	8.722	14.30	21.83	29.72	33.44
8.5	0.054228	2.806	5.482	9.621	15.77	24.06	32.76	36.85
10.0	0.049996	3.050	5.952	10.44	17.10	26.11	35.54	39.98

TABLE III. *Values of the coefficient (i.e. $4/\eta^2\mathfrak{M}+2\mathbf{Y}/\eta\mathfrak{M}$ of $\sin^2 K_0$ for $\mathbf{P}/\mathbf{P}_M$. This table is an extension of Table II of BTE. For expansions of $2\mathbf{Y}/\eta$ and $\mathfrak{M}$ in terms of E see BTE Tables IV and V.*

E (Mev)	η	$\Theta=15°$	20°	25°	30°	35°	40°	45°
6.0	0.064544	4.225	14.26	36.11	76.17	137.3	205.7	238.7
7.0	0.059756	4.994	16.73	42.26	89.02	160.4	240.2	278.7
8.5	0.054228	6.146	20.44	51.51	108.3	195.1	291.9	338.7
10.0	0.049996	7.303	24.15	60.72	127.6	229.7	343.6	398.7

TABLE IV. *Values of the coefficient of $-\sin K_1 \cos K_1$ for $\mathbf{P}/\mathbf{P}_M$. Interpolations linear in E may be correct only to about ±0.1 percent.*

E (Mev)	η	$\Theta=15°$	20°	25°	30°	35°	40°	45°
3.0	0.091279	11.34	17.31	21.37	21.16	15.13	5.329	0.000
4.0	0.079050	13.10	19.99	24.67	24.43	17.46	6.122	0.000
5.0	0.070704	14.66	22.36	27.58	27.30	19.51	6.841	0.000
7.0	0.059756	17.35	26.45	32.67	32.30	23.07	8.090	0.000
10.0	0.049996	20.75	31.62	38.99	38.59	27.56	9.664	0.000

TABLE V. *Values of the coefficient of $\sin^2 K_1$ for $\mathbf{P}/\mathbf{P}_M$. Interpolations linear in E are very good.*

E (Mev)	η	$\Theta=15°$	20°	25°	30°	35°	40°	45°
3.0	0.091279	45.69	116.4	205.3	260.0	218.6	84.38	0.000
4.0	0.079050	61.27	155.8	273.7	346.8	291.5	112.5	0.000
5.0	0.070704	76.85	195.0	342.3	433.6	360.1	140.6	0.000
7.0	0.059756	108.0	273.4	479.6	607.1	510.3	196.8	0.000
10.0	0.049996	154.8	390.8	685.8	867.5	729.1	281.1	0.000

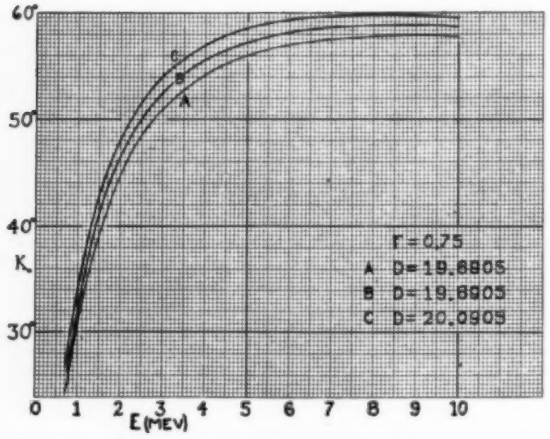

FIG. 1. The phase shift K_0 as a function of the energy E of the incident protons for square potential wells of radius 0.75 e^2/mc^2 and depths 19.690, 19.890 and 20.090 Mev without interior Coulomb potential.

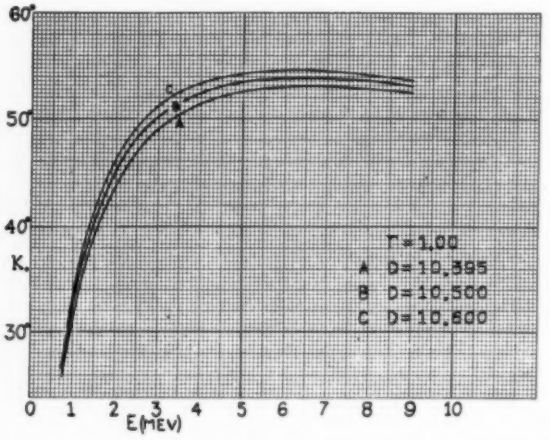

FIG. 2. The phase shift K_0 as a function of the energy E for square wells of radius e^2/mc^2 and depths 10.305, 10.50 and 10.60 Mev without interior Coulomb potential.

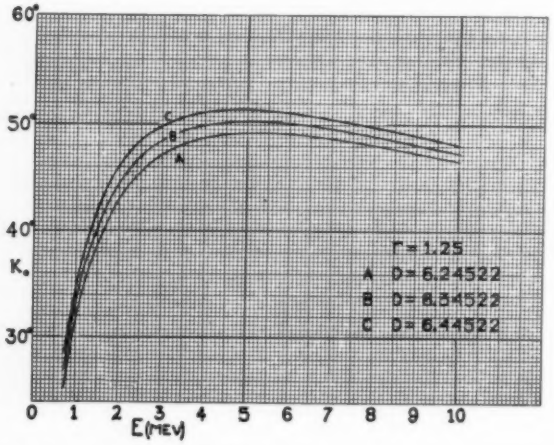

FIG. 3. The phase shift K_0 as a function of the energy E for square wells of radius 1.25 e^2/mc^2 and depths 6.2452, 6.3452 and 6.4452 Mev without interior Coulomb potential.

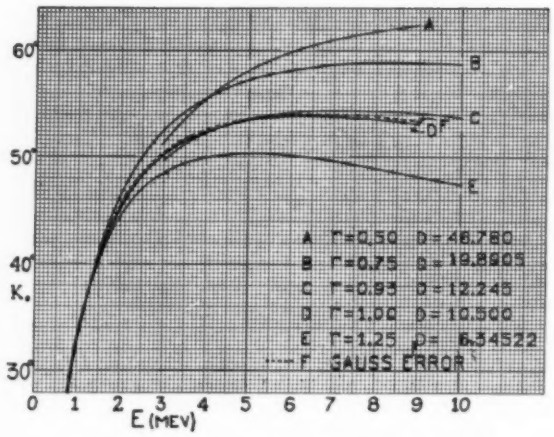

FIG. 4. The phase shift K_0 as a function of the energy E for square wells of differing radii (r is in e^2/mc^2). The depth (in Mev) is adjusted for each radius so as to give coincidence with the experimental K_0 at approximately 1.4 Mev. There is no interior Coulomb potential. The broken line F is for the Gauss error potential well $Ae^{-\alpha r^2}$, where $A=51.44$ mc^2 and $\alpha=21.59$ $Mmc^2/\hbar^2$, cut off at $r=3e^2/mc^2$ and with interior Coulomb potential.

that the high energy region will not be more useful than the low energy region in distinguishing between the two types of potential wells by means of the s wave phase shift.

Figure 5 shows how the ratio $\mathfrak{R}$ of theoretical scattering to Mott scattering varies with the energy and the scattering angle. The curves for the square well of depth 10.5 Mev and radius e^2/mc^2 lie very close to those for the Gauss error well.

The curves in Figs. 6 and 7 show the theoretical number of proton counts as a function

TABLE VI. *Values of the coefficient of* $-\sin K_2 \cos K_2$ *for* $\mathbf{P}/\mathbf{P}_M$. *Interpolations linear in E may be correct only to about* ± 0.1 *percent.*

E (Mev)	η	$\Theta=15°$	20°	25°	30°	35°	40°	45°
3.0	0.091279	5.241	6.177	3.390	− 5.764	−22.78	−43.35	−53.57
4.0	0.079050	6.060	7.150	3.929	− 6.686	−26.44	−50.33	−62.21
5.0	0.070704	6.780	8.005	4.402	− 7.495	−29.65	−56.46	−69.78
7.0	0.059756	8.029	9.486	5.221	− 8.896	−35.20	−67.05	−82.88
10.0	0.049996	9.602	11.35	6.251	−10.66	−42.17	−80.37	−99.34

TABLE VII. *Values of the coefficient of* $\sin^2 K_2$ *for* $\mathbf{P}/\mathbf{P}_M$. *Interpolations linear in E are very good. (For the calculation of d scattering there is a third term, which is* $+(40/\eta^2)\sin K_0 \sin K_2 \cos[K_2-K_0+2\sigma_2-2\sigma_0]$. *See BCP Eq. (6.7).)*

E (Mev)	η	$\Theta=15°$	20°	25°	30°	35°	40°	45°
3.0	0.091279	22.72	27.37	7.085	14.03	177.8	525.9	738.7
4.0	0.079050	30.23	36.31	9.290	19.06	238.6	704.4	988.7
5.0	0.070704	37.74	45.26	11.498	24.08	299.4	882.8	1238.7
7.0	0.059756	52.77	63.14	15.91	34.12	421.0	1239.6	1739
10.0	0.049996	75.31	89.97	22.53	49.19	603.4	1775	2489

of the energy of the incident protons. The number given is the number expected from the scattering chamber used by Herb, Kerst, Parkinson and Plain[3] per microcoulomb of incident proton current per mm of oil hydrogen pressure in the chamber. Fig. 6 is for the square well of depth 19.690 Mev and radius 0.75 e^2/mc^2 without interior Coulomb potential; added as broken lines are the curves for the Gauss error potential well $Ae^{-\alpha r^2}$, where $A=51.44\ mc^2$ and $\alpha=21.59\ Mmc^2/\hbar^2$, with interior Coulomb potential. Fig. 7 is for the square well of depth 6.3452 Mev and radius 1.25 e^2/mc^2 without interior Coulomb potential; the dotted lines are the same Gauss error curves as in Fig. 6. For a similar graph for square wells of radius 0.5 and 1.0 e^2/mc^2 see BTE Fig. 14. In each case pure s state scattering is assumed.

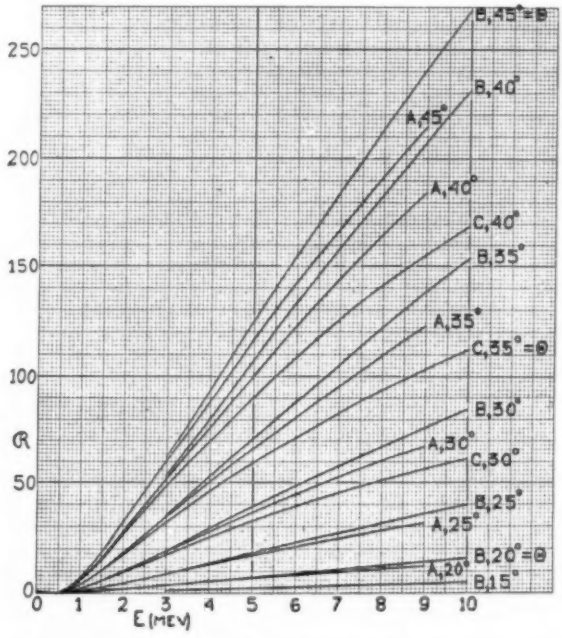

FIG. 5. The ratio ℜ to Mott scattering, as a function of the energy E and the scattering angle Θ, of the scattering calculated for: A, Gauss error well $Ae^{-\alpha r^2}$, where $A=51.44\ mc^2$, and $\alpha=21.59\ Mmc^2/\hbar^2$; B, square well of radius 0.75 e^2/mc^2 and depth 19.690 Mev, and C, square well of radius 1.25 e^2/mc^2 and depth 6.3452 Mev. The curves for a square well of depth 10.50 Mev and radius e^2/mc^2 would lie very close to A.

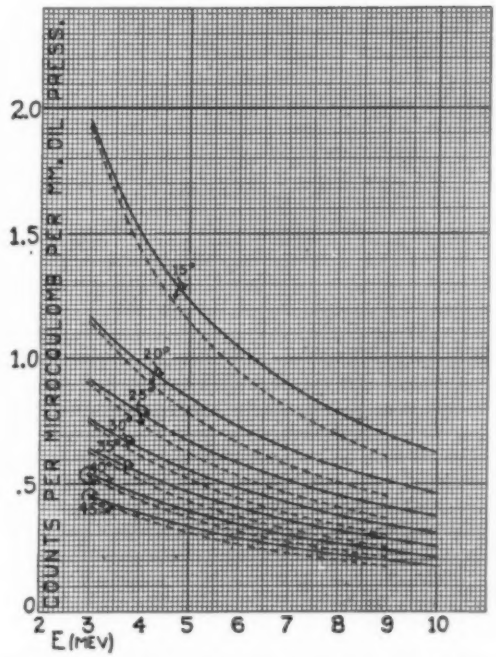

FIG. 6. The number of proton counts expected plotted as a function of the energy E of the incident protons and as a function of the scattering angle Θ. The unbroken curves are for the square well of radius 0.75 e^2/mc^2 and depth 19.690 Mev without interior Coulomb potential. The broken-line curves are for the Gauss error well $Ae^{-\alpha r^2}$, where $A=51.44\ mc^2$, and $\alpha=21.59\ Mmc^2/\hbar^2$ with interior Coulomb potential. For curves for the square well of radius e^2/mc^2 and depth 10.50 Mev, see BTE Fig. 14. The number plotted is the number of counts expected from the scattering chamber of HKPP[3] per microcoulomb of incident proton current per mm of oil hydrogen pressure in the scattering chamber (see BTE). Pure s state scattering is assumed.

Figures 6 and 7 show that the sensitivity of the number of counts to a change in the range of nuclear force is no greater at higher energies than at energies below 3 Mev. (It must be remembered that the energy of the point of intersection of two phase shift curves for different ranges of force is determined by the depth of the wells.) For the larger values of the scattering angle Θ experiments at energies from 1 to 3 Mev may be best for determining the range of the well. (See BTE Fig. 14 and discussion on p. 1059 regarding small angle scattering.) Thus it appears that as far as the s state scattering is concerned

TABLE VIII. *Values of K_1 for the constant potential ±10.5 Mev of radius e^2/mc^2.*

ENERGY OF INCIDENT PROTONS (MEV)	3	4	5	6	7	8	9	10
K_1 (attractive potential)	0.40°	0.63°	0.90°	1.1(9)°	1.5(4)°	1.8(7)°	2.2(3)°	2.6(1)°
K_1 (repulsive potential)	−0.23°	−0.36°	−0.51°	−0.67°	−0.85°	−1.0(4)°	−1.2(3)°	−1.4(2)°

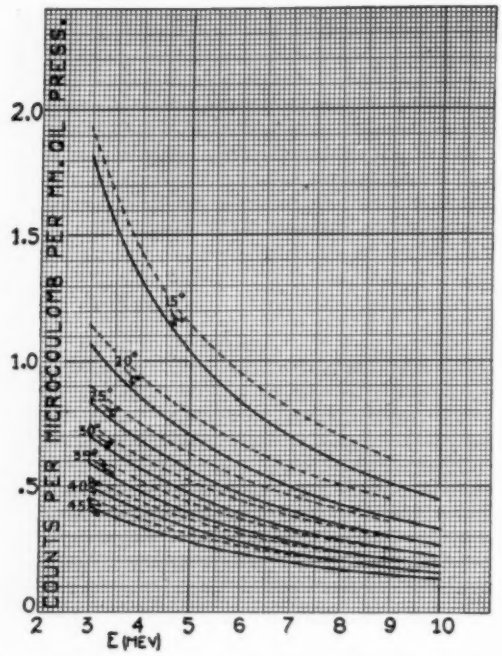

FIG. 7. The same type of curve as Fig. 6. The unbroken curves are for a square well of radius 1.25 e^2/mc^2 and depth 6.3452 Mev. The broken-line curves are the same as in Fig. 6.

the chief value of high energy experiments will be to corroborate the results of the low energy experiments and to make possible better determinations of the range and depth of the potential well by increasing the length of the K_0, E curve to be fitted by theory. The determination of K_0 may be more complicated because of the presence of phase shifts K_1 and K_2.

The experiments at energies above 3 Mev are, however, expected to be very valuable in determining the p state interaction (see BTE pp. 1059–61). In Table VIII are given values of the phase shift K_1 calculated for a constant potential of ± 10.5 Mev with a range of e^2/mc^2 and without interior Coulomb potential. The second and third rows of the table correspond, respectively, to attractive and repulsive p interactions. In both cases it is seen that the absolute values of K_1 increase with energy as would be expected. For the Gauss error potential $\pm Ae^{-\alpha r^2}$ with $A=51.44\ mc^2$ and $\alpha=21.59\ Mmc^2/\hbar^2$ superposed on the Coulomb potential, one finds, by integrating the wave equation numerically and joining to the Coulomb function at $r=3\ e^2/mc^2$, that for a repulsive p state interaction $K_1=-0.74°$ at 5 Mev, while for an attractive interaction $K_1=+1.23°$ at the same energy. These values are larger than the corresponding values for the constant potential because the Gauss error potential extends to larger values of r. Beyond showing that the values of K_1 are probably large enough to appear in high energy scattering experiments, these values of K_1 have little direct significance, since it is improbable that the singlet s state and triplet p state interactions are the same.

If the Coulomb potential is considered to be effective inside a square potential well, the depth of the well must be increased in compensation if one wishes to obtain the same phase shift K_0 as was obtained without the interior Coulomb potential. The necessary increase in depth of the square well of depth 10.5 Mev and radius e^2/mc^2 was found to be 0.849 Mev at the energy 7 Mev, and 0.860 Mev at the energy 10 Mev. The calculations were made by the use of BTE Eq. (11.2) and checked by BTE Eq. (11.5). It may be noted that, as a very rough empirical rule, $\delta D=0.826+0.00333\ (E-0.2)$, for this well, where δD and E are in Mev.

The authors are glad to express their thanks to Professor G. Breit for very helpful discussion and advice.

The Townsend Ionization Coefficients for Ni and Al Cathodes in an Atmosphere of Hydrogen

DONALD H. HALE
Department of Physics, University of California, Berkeley, California
(Received September 5, 1939)

Measurements of the first and second Townsend coefficients for ionization by collision have been carried out for surfaces of Ni and Al in an atmosphere of hydrogen. The Al surface was evaporated in an atmosphere of argon and is estimated to be a few hundred molecular layers thick. The values found for the α- and γ-coefficients are compared with the results previously reported for a Pt surface in hydrogen. The values of α/p, in pure hydrogen, plotted as a function of X/p show a decreasing characteristic between values of X/p from 900 to 1400. The curves of values of γ plotted as a function of X/p show a characteristic photoemission peak at an X/p of 131, and a gradual rise at the higher values of X/p. Sparking potential curves are calculated from the γ-values and are compared with the experimentally determined curves.

INTRODUCTION

MEASUREMENTS of the Townsend ionization coefficients for Pt and NaH surfaces in an atmosphere of hydrogen have been previously reported.[1] These measurements have been extended to surfaces of Ni and Al. An improved ionization chamber has been constructed with which it was possible to extend the measurements of α/p to an X/p of 1700 volts/cm per mm Hg.

A diagram of the ionization chamber is shown in Fig. 1. The chamber is of glass 18 cm in diameter and 45 cm in length. Fitted inside the glass wall of the chamber is a grounded wire gauze which is not shown in the diagram. The electrodes are of Ni. The rod supporting the upper electrode is threaded and this electrode can thus be raised or lowered by turning the armature with an exterior electromagnet. The electrodes are 6 cm in diameter and the distance between them may be varied from zero to 6 cm. A quartz window is attached to a side arm by a graded seal. Light from a quartz mercury lamp passed through a quartz lens and the window and then fell upon a spot near the center of the cathode. This radiation gave the photoelectric current i_0 at the surface of the cathode. From 2 to 10 cm^2 of the cathode surface was illuminated, the larger area being used in the case of the Ni cathode. The data taken with the larger area of illumination showed some irregularities when the plate separation was greater than 2 cm. This was taken to indicate that in these cases there was some field distortion at the greater values of the plate separation.

The Al surface was evaporated directly upon the Ni surface of the cathode. This evaporation was carried out in an atmosphere of argon at a pressure of 0.8 mm of mercury. The side arm, shown sealed off in Fig. 1, was extended to 32 cm in length and carried a support for a filament and a soft iron armature. By means of an external

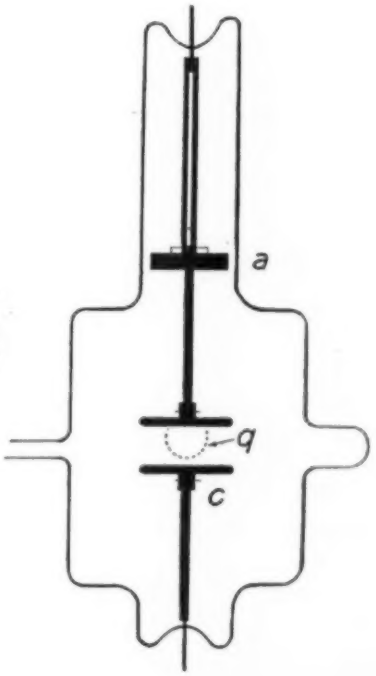

FIG. 1. The ionization chamber. *a* is a soft iron armature, *c* the cathode and *q* a quartz window.

[1] Donald H. Hale, Phys. Rev. **55**, 815 (1939).

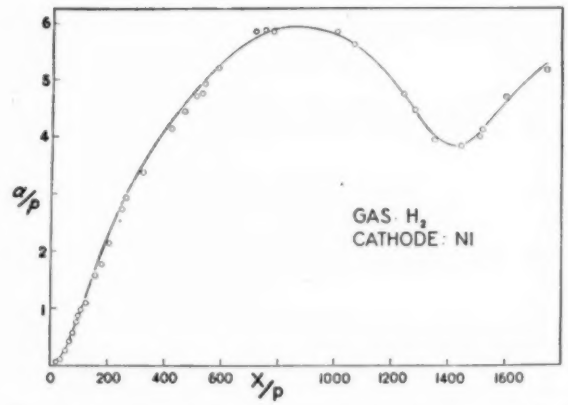

FIG. 2. The values of α/p plotted as a function of X/p.

electromagnet the filament could be moved to a position about 1.5 cm above the cathode and after the evaporation was complete the filament and its supports retracted into the side arm. The filament consisted of three 20-mil tungsten wires loosely twisted together. To this filament were fastened several small pieces of aluminum plate 0.4 mm thick and about 0.25 cm² in area. The metal was analytical grade and contained 0.32 percent of iron and 0.45 percent of SiO_2 as impurities. The filament was first heated while retracted into the side arm until the sheets melted. This treatment removed the surface contamination which was deposited on the walls of the side arm.

Tank hydrogen was used. The gas was purified by passing it through a purifying train in the conventional manner and then through two liquid-air traps and a fine leak before it entered the chamber. The photoelectric current was kept at a minimum at all times in order that the measurements might not be falsified by space charge effects.

The ionization chamber was built into an oven and was baked out at a temperature of 425°C for 16 hours each time air was admitted. A discharge in hydrogen was run for one hour after each baking and before any data were taken. The reason for this treatment of the cathodes was that in the presence of hydrogen neither the clean Ni surface nor the freshly evaporated Al surface was stable photoelectrically but the photoemission changed continually with time and in these measurements it was essential to have a stabilized surface. Thus these surfaces were carefully formed probably as hydrogen coated surfaces of some stability. In each case this treatment increased the photoelectric sensitivity of the surface. In the case of Al the treatment also apparently shifted the photoelectric threshold towards the long wave-length side of the spectrum as it was found that this surface was sensitive to visible light after the discharge had been run. It was therefore necessary in all measurements on the Al surface to have the ionization chamber covered by a light-tight box. The Al surface was not baked after it was deposited upon the surface of the Ni cathode.

In this type of measurement it is necessary that a fairly steady source of ultraviolet radiation be used as a source of the photoelectric current i_0. It was found that a lamp designed by Mr. E. H. Guyon of this laboratory was quite satisfactory when used with a stabilizer of the iron wire-hydrogen type.[2]

All data given in this paper are reduced to a temperature of 22°C.

EXPERIMENTAL RESULTS

The Al and Ni surfaces gave the characteristic curves, as shown by Bowls,[3] when $(1/p)\ln(i/i_0)$ was plotted as a function of the plate separation x. The exact amount of Al evaporated in forming the Al cathode could not be determined but it was estimated that the surface was a few hundred molecular layers thick. The values of α/p plotted as a function of X/p are shown in Fig. 2. Here α is the first Townsend ionization

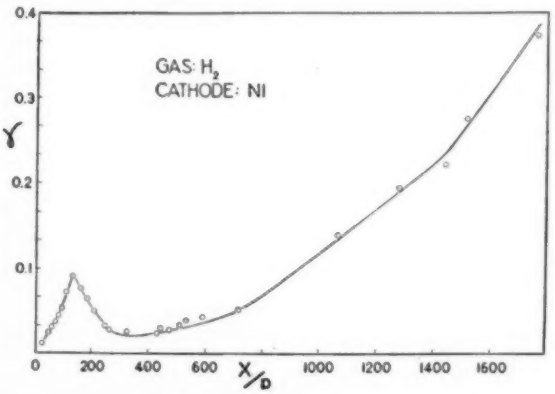

FIG. 3. The values of γ plotted as a function of X/p for the Ni cathode.

[2] Francis A. Jenkins and Harvey E. White, *Fundamentals of Physical Optics* (McGraw-Hill Book Company, 1937), p. 248.

[3] W. E. Bowls, Phys. Rev. **53**, 293 (1938).

coefficient and represents the number of electrons produced by each electron in 1 cm of path in the direction of the electric field. X is the field strength in volts/cm and p is the pressure in mm Hg. The Al cathode gave values of α/p which lay along this curve within experimental error. The values of α/p found for the Pt surface[1] also agree with those shown in Fig. 2. In the case of the Pt surface the measurements were reliable only to an X/p of about 900. With the new ionization chamber reliable measurements of α/p could be extended to an X/p of 1700. This curve shows a falling characteristic between values of X/p of 900 to 1400. Above an X/p of 1400 the curve starts a second sharp rise.

The values of the second coefficient γ were computed from the equation of Townsend[4] which was also derived by Thomson,[5]

$$i=i_0\frac{e^{\alpha x}}{1-\gamma(e^{\alpha x}-1)}. \qquad (1)$$

This equation assumes a secondary emission process at the cathode. Loeb[6] has shown that under the conditions obtaining in the ionization chamber in this work it is likely that Eq. (1) properly describes the mechanism. This may be either a secondary emission of electrons at the cathode due to positive ion bombardment or a photoelectric mechanism. The values of the second coefficient plotted as a function of X/p are shown in Figs. 3 and 4. These curves show

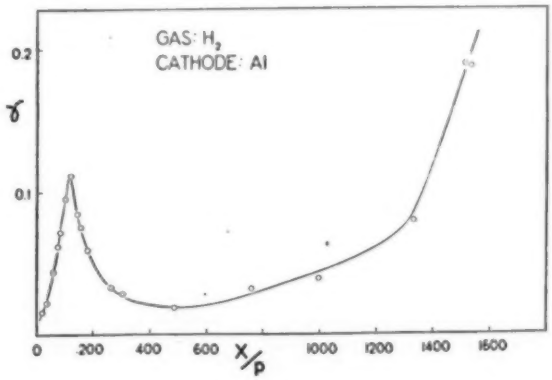

FIG. 4. The values of γ plotted as a function of X/p for the Al cathode.

[4] J. S. Townsend, *Electricity in Gases* (Oxford University Press, 1914), p. 314.
[5] J. J. Thomson and G. P. Thomson, *Conduction of Electricity through Gases* (Cambridge University Press, third edition, 1933), Vol. II, p. 518.
[6] L. B. Loeb, Rev. Mod. Phys. **8**, 267 (1936).

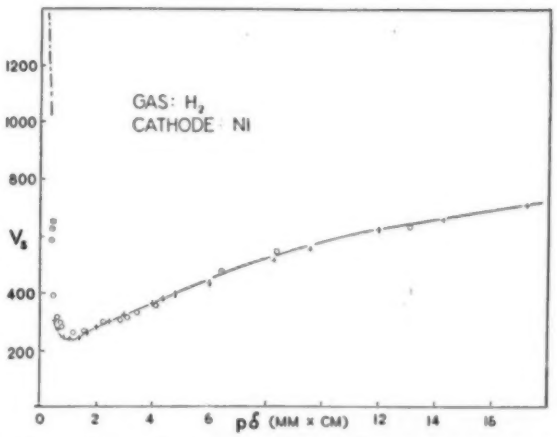

FIG. 5. The sparking potential curve for the Ni cathode. The crosses are experimentally determined points. The circles are values of the sparking potential calculated from the γ values determined in this work.

the same general characteristics. It is quite probable that the values of γ for the Ni surface are somewhat less accurate than those for Al. In the case of Ni the larger area of the cathode was illuminated and there were indications that at plate separations above 2 cm there was a small field distortion. Such a distortion would tend to lower the measured values of γ but these values are of the right order of magnitude. This error would not alter the form of the curve. There is a pronounced peak at the lower values of X/p and at the higher values of X/p both curves show a general rise. The maxima, at the lower values of X/p, occur, within experimental error, at an X/p of 131. The maximum in the similar peak as shown by the Pt surface in hydrogen was at an X/p of 120 which is nearly the same. The maximum value of γ, at an X/p of 131, for the Al surface is greater than for the Ni surface. However, this may be due to the field distortion which is suspected in the case of the Ni surface. The ratio of the value of γ for Al to that for Ni, at an X/p of 131, is 1.25.

In the range of values of X/p from 300 to 1400 the value of γ for the Al surface is smaller and the rise with increasing values of X/p is more gradual than is the case for the Ni cathode. However, above an X/p of 1400 the Al surface gives γ values which increase more rapidly than is the case for the Ni cathode. This again may be due to field distortion as such distortion in falsifying α would have more effect on the value of γ at the lower values of X/p.

The sparking potentials for both surfaces in hydrogen were experimentally determined. These data are shown in Fig. 5 for the Ni cathode. The crosses are the experimentally determined sparking potentials. The dotted line at the lower values of $p\delta$ is taken from data published by Quinn.[7] The circles in this figure are calculated break down potentials which are found by use of the values of γ shown in Fig. 4. The agreement is good except at the minimum values of the sparking potential. The data for the Al surface gave about the same sort of agreement.

Discussion

The α/p curve shows the same values for the Pt, Ni and Al cathodes as it should since this coefficient is a function of the gas between the electrodes. Above an X/p of 900 the values of α/p show a decline and then rise again starting at an X/p of 1400. The decline is analogous to the results of Huxford[8] for argon-filled tubes. This behavior may logically be ascribed to a decrease in the cross section for ionization by electron impact at the higher energies as shown by the Compton-van Voorhis curves. The effect observed at the higher values of X/p is not, in any case, to be confused with the decline observed in hydrogen contaminated with a volatile sodium compound[1] which is caused by a secondary ionization of the volatile compound by hydrogen photons. The subsequent rise, as shown by the curve of Fig. 2, above an X/p of 1400 is unexplained. If as conjectured the decline is a reflection of the decline of probability of ionization with increasing electron energies, one must assume that the subsequent rise in α/p is caused by the failure of the electrons to gain their terminal energy in the gap at the pressures used and thus the increase in α/p is due to the fact that below the maximum terminal energy their chance to ionize is greater. The pressures of 0.1 mm used in determining the values of α/p in the range of values of X/p from 900 to 1400 make this explanation plausible. However, at the rise in the curve the pressures were reduced by less than 10 percent below those near the minimum. Hence it is possible that the entire decline may be caused by failure of the electrons to achieve their terminal energy and that the hump corresponding to the Compton-van Voorhis curve may occur at much higher values of X/p.

It is seen that, except for minor differences due in part to experimental errors, the values of γ for the Ni and Al surfaces are nearly the same. There is for all three surfaces a definite photoelectric peak. These peaks occur at the same value of X/p for the Ni and Al surfaces and at nearly this value of X/p for Pt. However, it is to be remembered that a discharge was run in hydrogen, in the case of the Ni and Al surfaces before any data were taken. It must also be remembered that Pt is notoriously sensitive to absorption of hydrogen as shown by Langmuir in 1918.[9] The values found for γ for Pt surfaces in nitrogen[3] and for NaH surfaces in hydrogen[1] are not alike nor do they resemble the values found for the Pt, Ni and Al surfaces in hydrogen. This indicates the probability that for secondary emission by positive hydrogen ion bombardment surfaces of Pt, Ni and Al in hydrogen are essentially the same.

In a measure the similarity of these curves for Pt, Ni and Al cathodes in hydrogen for γ as a function of X/p is disappointing as it was hoped to find that different surfaces had markedly different properties. Since, however, Ni and Pt are noted catalysts for hydrogenation reactions, this result might have been expected. The behavior of Al is interesting in that it indicates its affinity for hydrogen. Further less reactive metals should be deposited by the Beeck[10] process and the γ values determined for such cathodes. It is unfortunate that hydrogen, one of the few gases free from metastables, should be so chemically active with metals. This fact must lead one to seek another nonreactive vehicular gas free from metastables in which to test the intrinsic properties of surfaces for secondary electron libration in the Townsend gap.

The calculated values of spark breakdown at low values of $p\delta$ agree satisfactorily with the experimentally determined values.

It is a pleasure to acknowledge that Professor L. B. Loeb has contributed much to this paper by many helpful discussions of the interpretation of the experimental results.

[7] Robert B. Quinn, Phys. Rev. **55**, 482 (1939).
[8] W. S. Huxford, Phys. Rev. **55**, 754 (1939).
[9] I. Langmuir, J. Am. Chem. Soc. **40**, 1361 (1918).
[10] Otto Beeck, A. Wheeler and A. E. Smith, Phys. Rev. **55**, 601(A) (1939).

The Absorption of High Energy Electrons. IV

M. M. SLAWSKY AND H. R. CRANE
University of Michigan, Ann Arbor, Michigan

(Received October 18, 1939)

The scattering of electrons in lead and in aluminum has been studied, mainly under the conditions used previously for the study of energy loss. The primary object of the investigation was to determine the extent to which the existing energy loss data (up to 13.5 Mev) are affected by multiple scattering. The conclusion reached is that the measurements so far made in lead with electrons below 9 Mev are so much affected by multiple scattering within the absorbing material that they are of very little use as a direct check on the theory for energy loss. In the measurements from 9 to 13.5 Mev the scattering is found to be small enough so that a comparison of the energy losses with the theoretical values is possible. The observed losses are roughly 40 percent in excess of the theoretical. Some measurements on the multiple scattering of 0.9-Mev electrons in thin sheets of aluminum were made, and it was found that the most probable angle of scattering and the average angle of scattering were in good agreement with theoretical predictions.

INTRODUCTION

A CONSIDERABLE amount of data is now available on the loss of energy suffered by electrons passing through solid materials such as lead, carbon and aluminum. During the past two years the work carried on in this laboratory has covered the energy range from 0.5 Mev to 17 Mev.[1–4] Results from the University of California[5] and the California Institute of Technology[6] are in essential agreement with those obtained here. It may be said with some certainty that, for the experimental method used at present, the results on energy loss are well established. The main uncertainties lie in the interpretation of the results, and one difficulty which overshadows all others is the estimation of the actual distance traveled by an electron inside the absorber.

On the assumption that the measured thickness of a given absorber corresponds to the actual path traversed by an electron, the experimental results have consistently shown losses greater than those predicted by theory. The discrepancy is not the same over the whole range but varies from a factor of more than two at the low energies to about one and a half at the high end of the range. The question is: How much of this discrepancy is due to the fact that the path taken by an electron does not correspond to the actual thickness of the absorber? The number we wish to find is called the path length-thickness ratio, or the ratio of the actual path length to the thickness of the absorber. This ratio is greater than unity for all absorbers, because the electron suffers an extremely large number of deflections, taking a zigzag path. In cases where there is much scattering the direction of emergence of a particular electron from the material tells little or nothing about its path length, since its final direction is a result of very many deflections in random directions. It therefore seems to be of no advantage to restrict the data to those electrons which emerge in a direction normal to the surface, or to try to make individual allowance for the effective thickness traversed by each electron, depending upon its angle of emergence. The best procedure seems to be to include all tracks in the data and to try to make a correction which applies to the average path length.

The complexity of the theoretical treatment of the path length-thickness ratio may be indicated by listing some of the important facts to be taken into account.

(1) The probability of a deflection varies with the size of the deflection.

(2) The probability of a deflection of a given

[1] J. J. Turin and H. R. Crane, Phys. Rev. **52**, 63 (1937).
[2] J. J. Turin and H. R. Crane, Phys. Rev. **52**, 610 (1937).
[3] A. J. Ruhlig and H. R. Crane, Phys. Rev. **53**, 618 (1938).
[4] B. R. Curtis, Phys. Rev. **53**, 986 (1938).
[5] L. J. Laslett and D. G. Hurst, Phys. Rev. **52**, 1035 (1937).
[6] W. A. Fowler and J. Oppenheimer, Phys. Rev. **54**, 320 (1938).

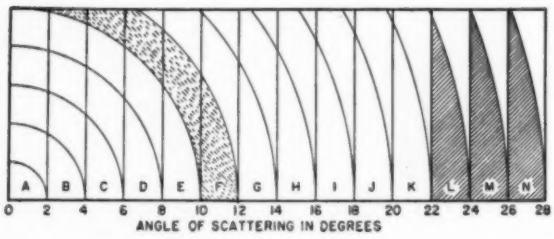

FIG. 1. Graphical device which is used in obtaining the true (three-dimensional) angular distribution of scattered electrons, from the cloud-chamber data.

size is a function of the energy of the electron, while the energy of the electron changes at an appreciable rate along its path due to two processes: ionization and radiation.

(3) The electrons finally must be separated into two classes: those which lose their entire energy in the absorber, and those which succeed in passing through the absorber. It is the average path length for the latter group alone that must be found, if the result is to be compared with the experimental data that are available.

(4) The situation has been made even more difficult to handle because the validity of the single scattering formulae has been placed in some doubt recently,[7–10] both in regard to large angles of scattering and in regard to the small angles which are important in multiple scattering. This is of direct concern because the theoretical estimates of path length are derived necessarily from the laws of single scattering.

The calculations can be simplified if the scattering is so small that at all times the deviation from the initial direction is not great ($\sin\theta \leqq \theta$). The treatment simplifies also if the scattering is so great that the mathematics of diffusion become applicable. It is desired, in the measurement of energy loss, to approach as nearly as possible the condition in which the scattering is small. Unfortunately the choice of an absorber which is thin enough to insure the electron path is nearly straight, and yet thick enough to cause a loss of energy large enough to be accurately measurable seems to be difficult in the range of energy with which we have been concerned, at least when a material of high atomic number is used. However, with the aid of the experimental results which we shall present, we have been able to arrive at some general statements which simplify the problem somewhat, at least in regard to the interpretation of the energy loss measurements already existing.

[7] A. Barber and F. C. Champion, Proc. Roy. Soc. **A168**, 159 (1938).
[8] E. J. Williams, Proc. Roy. Soc. **A169**, 531 (1939).
[9] N. L. Oleson, K. T. Chao, J. Halpern and H. R. Crane, Phys. Rev. **56**, 482 (1939); Phys. Rev. **56**, 1171 (1939).
[10] W. A. Fowler, Phys. Rev. **54**, 773 (1938).

PROCEDURE

Electrons were allowed to enter the cloud chamber through a thin window in the side wall and to fall normally upon a piece of absorbing material placed across the center of the chamber, as described in previous papers.[1–4]. The energy and the angle of deflection in the horizontal projection were measured for each track passing through the absorber. Although stereoscopic pairs of photographs were taken in all cases, it was found more satisfactory to measure only the component of deflection in the horizontal plane and to convert the distribution thus obtained into a three-dimensional one by a graphical method. This conversion can be made uniquely, because of the cylindrical symmetry about the initial direction of motion of the electrons. The reason for adopting this procedure rather than the direct three-dimensional measurement from the stereoscopic pictures is the following: Because of the limited depth of the chamber many tracks deflected through large angles away from the plane of the chamber are invisible or at least unmeasurable. Therefore an important correction would have to be made in this case, and the amount of the correction would be difficult to determine. By restricting the data to those tracks which lie within definite, small angular limits in the vertical direction (the plane of the chamber is horizontal), the correction to be applied becomes more definite and calculable. The data pertaining to the geometry are as follows.

TABLE I. *Area ratios for angles larger than those given in Fig. 1.*

ANGLE	PERCENT	ANGLE	PERCENT	ANGLE	PERCENT
26–28	42	36–38	28	46–48	22
28–30	37	38–40	26	48–50	21
30–32	35	40–42	24	50–52	21
32–34	32	42–44	23	52–54	20
34–36	30	44–46	23	54–56	20

(1) The depth of the visible region of the chamber is well defined by the light beam and is taken to be 3 cm.

(2) The incident electrons are passed through a slit system outside the chamber, so that their paths lie within 5 degrees of the horizontal plane and so that they strike the center of the absorber.

(3) The scattering is cylindrically symmetric about the direction of the incident electron.

(4) Only those tracks were included in the data which, after passing through the absorber, did not pass out of the light beam. This means that only those tracks were included whose vertical component of scattering was smaller than 10 degrees. All angles in the horizontal plane (up to 90 degrees) were included.

For the actual operation of making the conversion to the three-dimensional case the diagram in Fig. 1 is used. This shows the fraction of each scattering cone which falls within the horizontal and vertical angles defined above, and together with the supplementary data in Table I gives the numerical values necessary for conversion of the data to the three-dimensional case. The actual measurements yield the number of tracks in a particular vertical strip. This number then has to be distributed among those parts of the circular zones which lie within the vertical strip. It is necessary to start with the largest angle and work toward the center. An example of the procedure is as follows: Suppose we measure the number of tracks which fall in the rectangular column between 26 and 28 degrees. Since the angle is large, we can assume that the density of population in this rectangle is uniform, and therefore we can determine the number of tracks to assign to the shaded area N. Let us call this number N. The density of population in the *unshaded* part of the 24–26-degree rectangle is the same as that of the area N, because of the cylindrical symmetry about the origin. The number of tracks in the unshaded part of the 24–26-degree rectangle is therefore $0.47N$, because this is the ratio of the areas. The number of tracks which belong to the shaded area M is now determined by counting the number in the 24–26-degree rectangle and subtracting $0.47N$.

TABLE II. *Ratio of the complete ring about the origin to that of the curved figure.*

ANGLE	FACTOR	ANGLE	FACTOR	ANGLE	FACTOR
10–12	5.2	30–32	18.5	50–52	28.0
12–14	7.2	32–34	19.6	52–54	28.7
14–16	9.3	34–36	20.6	54–56	29.4
16–18	10.5	36–38	21.6	58–60	30.8
18–20	11.7	38–40	22.5	62–64	32.1
20–22	12.9	40–42	23.5	66–68	33.5
22–24	14.1	42–44	24.5	70–72	34.4
24–26	15.2	44–46	25.4	74–76	35.1
26–28	16.3	46–48	26.3	78–80	35.6
28–30	17.4	48–50	27.2	82–84	35.8
				86–88	36.0

TABLE III. *Energy distribution of electrons striking aluminum.*

THICKNESS OF ALUMINUM	NUMBER	ENERGY MEV
0.0025 cm	31	0.6 to 0.8
	87	0.8 to 1.0
	32	1.0 to 1.2
0.01 cm	45	0.6 to 0.8
	78	0.8 to 1.0
	35	1.0 to 1.2
0.025 cm	43	0.6 to 0.8
	99	0.8 to 1.0
	53	1.0 to 1.2

The number in the shaded area L is equal to the number in the 22–24-degree rectangle, minus $0.52M$. By continuing this process to zero degrees, the density of population in all parts of the diagram is found. A continuation of these area-ratios for larger angles than those which appear on the diagram is given in Table I.

To get the data finally in terms of the number of tracks in a given interval of solid angle or interval of angle, we make use of Table II. This table gives the ratio of the complete ring around the origin to that of the curved figure (for example the shaded one whose base lies between 10 and 12 degrees in the diagram).

EXPERIMENTAL RESULTS

The experimental results are represented by the curves in Figs. 2 and 3. In these figures the points represent number of tracks scattered into an angular interval between ϕ and $\phi+\Delta\phi$, in the plane of the chamber. In each case two curves are given. The full line curve is drawn smoothly through the experimental points, the dashed curve is the angular distribution which includes the entire cone of scattering, obtained by the

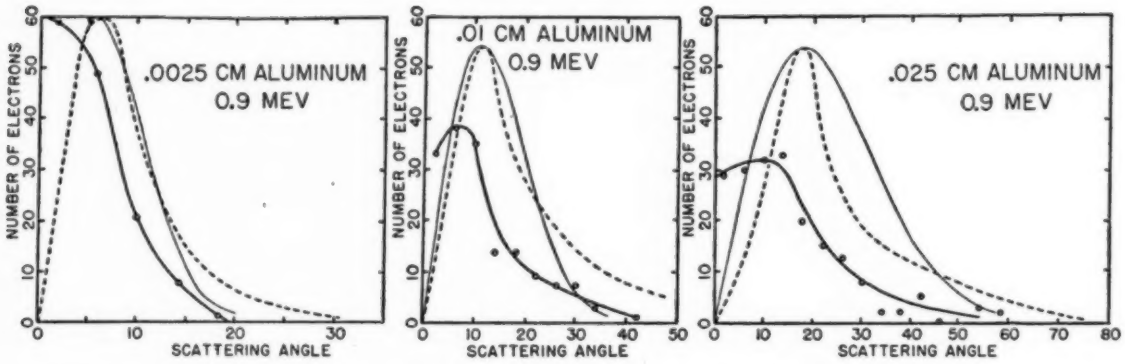

FIG. 2. Angular distribution of electrons scattered by aluminum.

use of Fig. 1. In Fig. 2 an additional curve is given to represent a theoretical distribution of the form: $y=Axe^{-Bx^2}$ with the parameters chosen arbitrarily. The reason for including the latter curve will be indicated in the discussion which follows later in the paper. The electrons which were incident upon the aluminum scatterers had an average energy of 0.9 Mev, and the actual distribution in energy is given in Table III. The electrons incident upon the 0.0038-cm and 0.0066-cm lead scatterers had an average energy of 0.9 Mev and a distribution as given in Table IV.

THEORETICAL CONSIDERATIONS

There can be little doubt that in the experimental data we have presented, we are dealing mainly with the effects of multiple scattering, even for the fastest electrons and the thinnest absorbers. In such cases, where a large number of deflections occurs inside the absorber, the distribution in direction of the emergent electrons must be found by compounding statistically effects of the large number of deflections. The result can be represented approximately by the simple error curve of the form

$$N(\theta)d\theta=A\theta e^{-B\theta^2}d\theta.$$

However, there is always a small number of large deflections due to single encounters, whose effect is to distort the distribution from the form mentioned above, especially at large angles. One must expect a noticeable deviation from the error curve at angles which are several times the most probable angle; this is the region of the so-called plural scattering. At extreme angles the distribution is expected to correspond closely to that predicted by the formula for single scattering. The angle beyond which the single scattering formula applies can be estimated by the use of Wentzel's criterion.[11] The 4ω used by Wentzel is approximately equal to the most probable angle, and it is customary to use 3 or 4 times this as the limiting angle. Referring to our curves, we may say that the scattering is essentially single at angles equal to about 4 times the angle at which the peak occurs in the dashed curve. The experimental distributions will be expected to conform to an error curve in the region of the maximum, and to have a plural or single scattering "tail" at the large angles, which will lie above the tail of the error curve.

It is essential at this point to tell what happens as the most probable angle approaches 25 or 30 degrees. In cases of thick absorbers, where the scattering is very great, the electrons will lose completely their original directions of motion, and take up random directions inside the absorber. Thus the case will resemble diffusion. Obviously any further increase in the thickness of the absorber will not alter the distribution in direction of the emerging electrons, but will only

TABLE IV. *Energy distribution of electrons striking lead.*

THICKNESS OF LEAD	NUMBER	ENERGY MEV
0.0038	81	0.6 to 0.8
	75	0.8 to 1.0
	56	1.0 to 1.2
0.0066	63	0.6 to 0.8
	65	0.8 to 1.0
	38	1.0 to 1.2

[11] G. Wentzel, Ann. d. Physik **69**, 335 (1922).

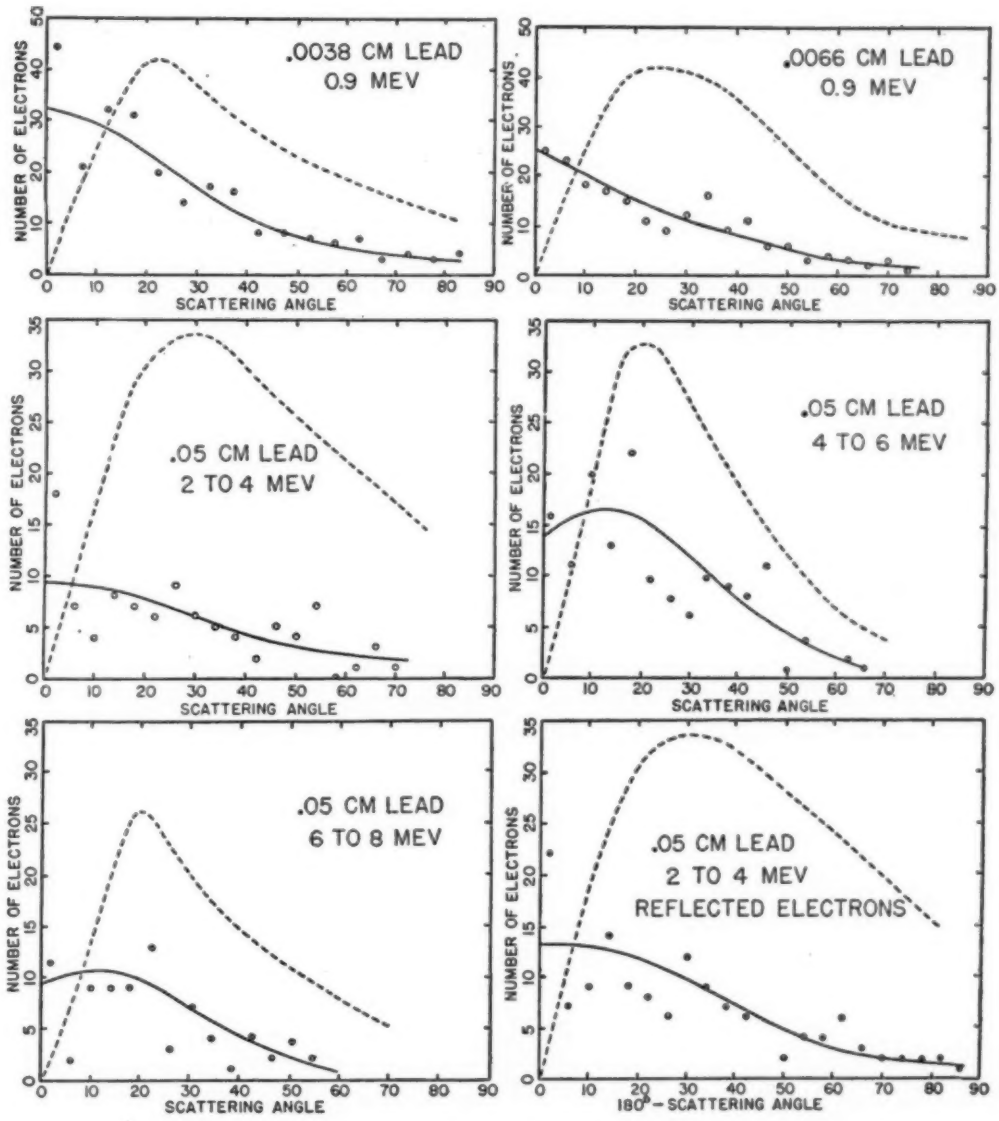

FIG. 3. Angular distribution of electrons scattered by lead.

change the number emerging. We have found experimentally that in those cases in which diffusion seems to exist, the most probable angle of emergence of the electrons is 25 to 30 degrees (measured from the normal to the surface). This means that if we start with a very thin absorber and gradually increase its thickness, we will at first get an error curve for the distribution, whose peak will move toward the right with increasing thickness. As the peak approaches 25–30 degrees the form of the distribution will change over into one which is characteristic of diffusion. No matter how much more we increase the thickness after this point has been reached, the curve will not change in any way except in total intensity. The arguments of the preceding paragraphs, which are based upon the error curve, will therefore apply only if the most probable angle is considerably less than 25 degrees.

Bethe, Rose and Smith[12] have treated the problem of multiple scattering and have given a theoretical expression for the "transport mean free path":

$$\frac{1}{\lambda}=\frac{2\pi NZ^2e^4W^2}{(W^2-m^2c^4)^2}\log\frac{2ap}{\hbar Z^{\frac{1}{3}}},$$

[12] H. A. Bethe, M. E. Rose and L. P. Smith, Am. Phil. Soc. Proc. **78**, 573 (1938).

TABLE V. *Comparison of our observed values of θ_{max} with those calculated by Bethe, Rose and Smith.*

MATERIAL	THICKNESS, CM	AVERAGE ENERGY, MEV	θ_{MAX} CALC.	θ_{MAX} OBS.	PATH LENGTH THICKNESS RATIO, CALC.	ENERGY LOSS, EXP./THEOR.
Al	0.0025	0.9	8	6	1.01	—
Al	0.01	0.9	16	11	1.04	—
Al	0.025	0.9	25	19	1.10	1.25
Pb	0.0038	0.9		22		3.
Pb	0.0066	0.9		25		2.7
Pb	0.05	3.0		29	Diffusion	1.8
Pb	0.05	5.0		21		1.8
Pb	0.05	7.0		21		1.8

where W is the energy of the electron including the rest mass, a is the Bohr radius and p is the momentum of the electron. The quantity λ is immediately connected with the most probable angle of scattering:

$$\theta_{max}=(2t/\lambda)^{\frac{1}{2}}.$$

The above formula can be applied to our data only when the most probable angle is considerably less than 25 degrees. Under this condition Bethe, Rose and Smith give as the mean path length for the electron in the absorber,

$$t=t_0(1+\tfrac{1}{2}\theta^2_{max}),$$

where t is the actual path length taken by the electron, t_0 is the measured thickness of the absorber and θ_{max} is the most probable angle of scattering.

Williams[13] has recently treated both single and multiple scattering in detail, and has developed formulae for the angular distribution and also for the average angle of scattering. He has compared our results for the average angle of scattering in 0.0025 cm aluminum at 0.9 Mev with that calculated by means of his formula and finds fairly good agreement. Our experimental value for the average angle in the plane projection is 5.5 degrees and his calculated value, after applying the appropriate correction for our geometrical conditions, is 5.9 degrees. This indicates that theory cannot be seriously wrong for the scattering in aluminum at this energy.

DISCUSSION OF RESULTS

Scattering

A comparison between our results and the values of θ_{max} calculated by the formulae of Bethe, Rose and Smith is shown in Table V. With the help of this the following can be said:

(1) The angular distributions of the electrons are those which would be expected to result mainly from multiple scattering. The positions of the maxima and the shapes of the curves are in fair agreement with the predictions of the multiple scattering formulae, in those cases in which the theory is applicable, namely $\theta_{max}\ll 25°$.

(2) The experiments on 0.0025 cm and 0.01 cm aluminum lie within the region of applicability of the Bethe, Rose and Smith formula, and we see that here the experimental and calculated values of θ_{max} are in fair agreement. The energy loss was too small to be measured in these two absorbers.

(3) The energy loss discrepancy in the 0.025 cm aluminum is somewhat larger than is accounted for by the increase in path length which is calculated, but this probably indicates that at this value of θ_{max} (19 degrees) we are already outside the region in which the formula gives the correct path length.

(4) For all the lead absorbers listed in Table V the scattering is so great that it approaches the case of diffusion. It is important to keep in mind the fact that as the amount of scattering increases θ_{max} approaches the stationary value of about 25 degrees, while the path length-thickness ratio continues to rise. Therefore in all cases in which θ_{max} is near 25 degrees, the formula gives only a lower limit to the path length. The value 25 degrees for the limit which the angle approaches was obtained by referring to the *experimental* data, and may therefore be to some extent characteristic of the particular set-up used for these measurements.

[13] E. J. Williams, Proc. Roy. Soc. **A169**, 531 (1939).

(5) Table VI gives a resumé of results from other papers. Some similar data exist for positrons,[3, 4, 6] but these have not been included in the table. In two of the measurements on lead (0.015 cm, 9 and 13.5 Mev) the results are reasonably free from the effects of diffusion so that the formula for the path length correction may be used. Although this statement is based upon the calculated values of θ_{max} this seems safe, since the experimental values have been lower than the calculated, in cases in which both are available.

(6) The fact that the observed values of θ_{max} are smaller than the theoretical is worth noting, in view of the fact that others[14–17] have recently reported a deficiency in scattering, both single and multiple. It is true that in the case of 0.0025 cm Al the average angle was found to be in accord with Williams' formula. This, however, is only a single case, and there is the possibility that it is in error.

(7) Single scattering could not be checked against theory for any of the cases because the thickness of the foils and the energy of the electrons were such that only those electrons scattered at very large angles would satisfy the requirements. In the case of the thinnest absorber (0.0025 cm Al, 0.9 Mev) Wentzel's criterion requires that only those electrons scattered through ~ 20 degrees or more be considered. Actually no electrons at all were found beyond this angle, for the 0.0025 cm Al.

Energy loss

In the light of the foregoing data, we may now make some statements about the interpretation of the measurements on energy loss.

(1) When we use an absorber of high atomic number which is thick enough to cause an easily measurable loss of energy, the effect of multiple scattering is usually very large. It appears in Tables V and VI that the only values for energy loss in lead which can be accepted (on the basis of scattering) are those for 0.015 cm thickness and 9 and 13.5 Mev. These are measurements by Fowler and Oppenheimer. The value for 0.038 cm thickness and 12.7 Mev, by Ruhlig and Crane is on the borderline (calculated $\theta_{max} = 18$ degrees). In all the other measurements in lead the path in the absorber is so crooked that its average length cannot be estimated with reasonable accuracy. If we are willing to assume that positrons behave exactly as electrons, both in energy loss and in scattering, we may find some acceptable measurements on positrons in the papers already mentioned.[3, 6] These values do not change our conclusions, but only support what has been said in regard to electrons.

(2) The number of electrons which strike the lead absorber and do not emerge at all is found to be large in all those cases in which θ_{max} is large. This is understandable if we believe that in these cases the electrons penetrate the absorber by a process very much like diffusion. Those which fail to emerge are simply those which have traveled a distance equal to several times the thickness of the absorber and have thus "died" inside the material. The fraction of the electrons which fails to emerge from absorbers of various kinds has been measured and reported.[18]

(3) The fact that in some cases in which the scattering would be expected to be extremely great (for example 0.35 to 0.65 Mev in 0.0066 cm lead)[3] the specific energy loss becomes almost as low as the theoretical value, is understandable. The thickness of the absorber is not much less

TABLE VI. *Summary of results from other papers on energy loss of high speed electrons.*

Material	Thickness, cm	Average energy Mev	θ_{max} calc.	Path length thickness ratio, calc.	Energy loss exp./thor.	Reference
Pb	0.038	9.5	22	—	1.2	3
Pb	0.038	12.7	18	1.05	1.3	3
Pb	0.014	2.5	>25	—	2.7	5
Pb	0.015	9.0	15	1.04	1.7	6
Pb	0.015	13.5	11	1.03	1.5	6
Pb	0.05	10.0	24	—	1.5	2
C	0.5	3.0	>25	—	~1	1
C	0.5	5.0	20	1.07	~1	1
C	0.058	2.5	11	1.03	0.5	5

[14] A. Barber and F. C. Champion, Proc. Roy. Soc. **A168**, 159 (1938).
[15] F. C. Champion and A. Barber, Phys. Rev. **55**, 111 (1939).
[16] W. A. Fowler, Phys. Rev. **54**, 773 (1938).
[17] N. L. Oleson, K. T. Chao, J. Halpern and H. R. Crane, Phys. Rev. **56**, 482 (1939); Phys. Rev. **56**, 1171 (1939).
[18] H. R. Crane and J. Halpern, Phys. Rev. **55**, 838 (1939).

than the maximum range of the electrons in the material. Consequently only those which happen to have a fairly straight path will emerge and will be counted. Those whose paths are more crooked will not emerge at all and will not enter into the average. Thus there is a selection in favor of the electrons which are least scattered. This probably accounts for the fact that the energy loss for carbon, 0.5 cm, 3 Mev (see Table VI) is about equal to the theoretical, in spite of the fact that diffusion clearly exists. In this case 65 percent of the electrons failed to emerge from the absorber.

After rejecting such a large part of the existing work on energy loss, it seems as though there remains little upon which to base an opinion as to whether or not theory is in accord with experiment. If, in the three most acceptable measurements on lead, we apply the indicated path length corrections we find that, as an average, the experimental values are at least 1.4 times the theoretical. Aside from the question of whether or not one is inclined to place any faith even in this result, we believe that we have been able to expose some of the pitfalls in energy loss measurement, so that future experiments can be made upon a somewhat firmer basis.

The authors are grateful for the financial support of this work which was made available from the Horace H. Rackham Fund.

DECEMBER 15, 1939 PHYSICAL REVIEW VOLUME 56

The Spin of Carbon Thirteen

C. H. TOWNES AND W. R. SMYTHE
California Institute of Technology, Pasadena, California

(Received October 16, 1939)

Carbon thirteen was concentrated in a Hertz diffusion system to an abundance of 50 percent and enough 35 percent heavy carbon was obtained for a measurement of the nuclear spin of C^{13}. The spin was determined from the relative intensities of the Λ-type doublets of two lines of the O−O Swan band of $C^{13}-C^{13}$. These doublets are so close that a Lummer-Gehrke plate crossed with a 21-ft. grating was needed to obtain sufficient resolving power. An intensity analysis of the combined interference patterns of the two doublets proves that the C^{13} nucleus obeys the Fermi-Dirac statistics and strongly indicates a spin of $\frac{1}{2}$. This is in disagreement with a spin of $\frac{1}{2}$ predicted for this nucleus from the Hartree nuclear model but is the value predicted by the alpha-particle model.

THE determination of the nuclear spin of the ground state of C^{13} has become of considerable interest lately because it is one of the few magnitudes concerning which the predictions from the alpha-particle nuclear model and from the Hartree model are in complete disagreement.[1] The former predicts a spin of $\frac{3}{2}$ and the latter a spin of $\frac{1}{2}$. The most straightforward method of determining the spin is by measuring the relative intensities of alternate lines in the $C^{13}C^{13}$ molecular spectrum. In ordinary carbon, the $C^{13}C^{13}$ bands are only one ten-thousandth as intense as the $C^{12}C^{12}$ bands; so that for a measurement of the C^{13} spin, it is necessary to concentrate the C^{13} isotope considerably.

[1] R. G. Sachs, Phys. Rev. **55**, 825 (1939).

CONCENTRATION OF CARBON THIRTEEN

The enrichment of C^{13} was carried out in a 34-member Hertz diffusion apparatus described by Wooldridge and Smythe.[2] To obtain high concentration the diffusion was in two stages. For the first diffusion, pure methane was pumped slowly and continuously through the light end at 1.4 cm pressure to maintain the normal concentration of C^{13} at this end. Six liters of methane at 8 mm pressure and about 7 percent C^{13} could be collected at the heavy end after a five-day run. Due to the large quantity of gas passed through the light end, considerable amounts of heavy impurities also collected in

[2] D E Wooldridge and W R Smythe, Phys Rev **50**, 233 (1936).

the heavy end. The CO and CO_2 were removed continuously by hot I_2O_5 and a liquid-air trap. Nitrogen was removed from the heavy methane by a simple fractionation. Four five-day runs were made to collect enough methane enriched in C^{13} to refill the diffusion system for a final enrichment. The second diffusion yielded a small quantity of methane containing 50 percent C^{13} and about one liter of methane at 1 cm pressure of 35–40 percent C^{13}.

Spectroscopic Procedure

The nuclear spin and statistics may be determined from the band spectrum of a homonuclear molecule by measuring the ratio of intensities of alternate lines, the statistics determining which lines are stronger, and the relative intensities being given by $s/(s+1)$, where s is the spin. Thus for $s=0$, as in C^{12}, alternate lines are entirely missing, while for spins of $\frac{1}{2}$, 1, and $\frac{3}{2}$ the intensity ratios are $\frac{1}{3}$, $\frac{1}{2}$, and $\frac{3}{5}$, respectively. Unfortunately, the only bands available in the case of carbon are $^1\Pi-{}^1\Pi$ and $^3\Pi-{}^3\Pi$, so that the lines whose relative intensities must be measured are very close Λ-type doublets. The Deslandres-d'Azambuja ($^1\Pi-{}^1\Pi$) bands are usually excited by the continuous breakdown of hydrocarbon gases at fairly high pressures in an electrical discharge, and since no method of exciting them which used a reasonably small quantity of carbon could be found, the Swan bands ($^3\Pi-{}^3\Pi$) were used. Each member of a single branch in a single band of this system consists of six lines. Near the head there are three well separated lines, each of which is a narrow doublet, the relative intensity of the two doublet components being the desired datum. Far from the head the triplet structure has drawn together into a single line and the doublet structure has spread out so that the lines appear double. In the intermediate region a combination situation holds. The only place where the doublet structure is large enough to resolve and where the desired lines are not interfered with by some overlapping band of $C^{13}C^{13}$, $C^{12}C^{13}$ or $C^{12}C^{12}$ seemed to be in the $(0-0)$ band (λ5165) just before it reaches the $(1-1)$ head. Here the triplets of the R branches of $C^{13}C^{13}$, $C^{12}C^{13}$, and $C^{12}C^{12}$ lie side by side with little overlapping

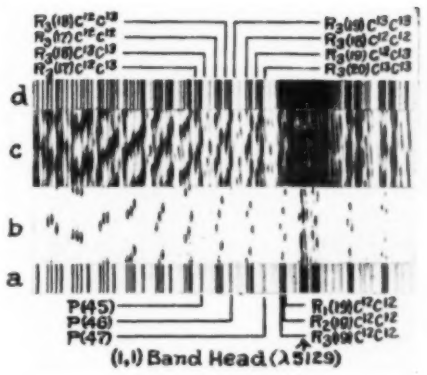

Fig. 1. Spectrogram of carbon bands.

except that one member, R_1, of each molecule is interfered with by the P branch of the next lighter molecule (see Fig. 1, *a* and *d*). Because the carbon molecule approximates Hund's case "a" coupling for low rotational quantum numbers, the triplet members $^3\Pi_0-{}^3\Pi_0(R_3)$ show considerably wider separation of the Λ-type doublets than do the $^3\Pi_1-{}^3\Pi_1(R_2)$ and $^3\Pi_2-{}^3\Pi_2(R_1)$ the separation of the $^3\Pi_0-{}^3\Pi_0$ lines in question being about 0.14 cm. The resolving power required to resolve these doublets, assuming they are very sharp and have equal intensities is about 140,000. Actually the temperature broadening and inequality of intensity of the two components demanded much higher resolving power.

As no grating of sufficient resolving power was available, a 21-ft. grating was crossed with a Lummer-Gehrke plate having a theoretical resolving power of 300,000. Through the kindness of Dr. Badger of the Chemistry Department an Eagle-mounted concave grating very fast in the second order of the green was used. The somewhat complicated optical system required by the Lummer plate and for correcting the astigmatism of the grating was accomplished by suitable lenses supplied by Dr. Bowen.

Such an optical system requires a powerful light source. A discharge tube with a water-cooled quartz capillary 1 mm in diameter and one cm long was constructed. The heavy methane at about 3 mm pressure was admitted to the tube and a discharge run until most of the carbon was deposited in the tube, principally on the electrodes and in the capillary. The tube was then evacuated and 2 cm of pure argon admitted. When a discharge was run through this tube

from a 20,000-volt, 3-kw, transformer with bad voltage regulation, the Swan bands appeared brilliant for hours. To secure this long life from the small quantities of carbon used, it seemed necessary to exclude mercury vapor and to have the aluminum electrodes polished and with rounded edges.

Several plates of varying exposures were taken with ordinary carbon and with 35 percent C^{13}, and step weakener photographs developed with each plate to make possible accurate intensity measurements. In Fig. 1 *b* and *c* were taken on Eastman I-J plates from ordinary carbon and 35 percent C^{13} with exposures 7 min.–60 min., respectively. The $^3\Pi_0-{}^3\Pi_0$ doublets of $C^{12}-C^{13}$, which have equal intensity, are not quite resolved by the Lummer plate, and the corresponding interference fringes of $C^{13}C^{13}$ may be seen to be somewhat asymmetrical, indicating components of unequal intensity.

Analysis of Spectra

There are three lines of measurable doubling, $R_3(17)$, $R_3(18)$ and $R_3(19)$ which, for all the molecules, fall clear of other lines. From the wave-lengths of the C^{12}_2 lines given by Shea,[3] the staggering of alternate lines and hence the doublet separation, can be computed roughly. This calculation indicates about 30 percent greater doublet separation for $R_3(17)$ and for $R_3(19)$ than for $R_3(18)$. This was confirmed qualitatively by a visual examination of the fringes and so only the first two were analyzed.

A simple method of determining the statistics obeyed by the C^{13} nucleus is to compare the position of the center of gravity of an R_3 line relative to the corresponding R_3 line in the C^{12}_2, $C^{12}C^{13}$ and C^{13}_2 bands. Visual measurements of the intensity maxima on a comparator showed at once that the strong component in the C^{13}_2 line was the one which is missing in the C^{12}_2 line, proving that the C^{13} nucleus obeys the Fermi-Dirac statistics. The position of this maximum was visually estimated to be very close to the position of a single component which indicated a very weak second component and a probable spin of $\frac{1}{2}$. Subsequent microphotometer measurements, however, make this conclusion very doubtful and indicate that it may have been an optical illusion caused by the tendency of the eye to judge density by contrast and thus set the cross hair too near the steep edge of the fringe.

If we are given accurate intensity curves on the same horizontal scale of the $R_3(17)$ or $R_3(19)$ lines of C^{12}_2, $C^{12}C^{13}$ and C^{13}_2 the most precise analytical procedure is as follows. Two equal C^{12}_2 profiles are drawn with various separations and summed. By adjusting the vertical scales of the resultant curves only one can be made to coincide with the $C^{12}C^{13}$ profile which gives, quite accurately, the doublet separation. With this separation we now draw two C^{12}_2 curves whose intensities are in the ratio $\frac{1}{3}$, $\frac{1}{2}$, $\frac{3}{5}$, etc., and add them. The vertical scale of the resultant curves are adjusted to fit as closely as possible the C^{13}_2 profile. Only one can be made to fit and this gives the ratio of intensities and hence the spin.

To obtain these intensity curves two plates were available, one being about three times as heavily exposed as the other. On both plates there was a uniform change in intensity across the plate, the intensity ratio of the outside orders being about 2 to 1. On the lighter plate eight or nine orders of each line of C^{12}_2 and $C^{12}C^{13}$ were of suitable density for microphotometering. On the heavier plate eight orders each of the C^{13}_2 lines were suitable but only from 3 to 6 each of the C^{12}_2 and $C^{12}C^{13}$ lines, the others being too dense. Microphotometer curves were run on all orders of the lines involved on both plates, the vertical height averaging about 2.5 cm and the width from 2.5 to 5 cm. From the appropriate step weakener picture appearing on each plate the line profile was converted, point by point, into an intensity profile. The resultant curves present a sawtooth appearance due to the grain of the plate, the average grain size being about 1/15 the width of the line. To determine how completely this grain would average out a microphotometer curve on the same scale was run along one step of the step weakener picture and several such traces were superimposed at random and averaged point by point. The average of eight such curves deviated from a straight line by a maximum of 1 mm in a 3-cm length and crossed a ruled line 20 times in this distance, indicating that the average of eight orders

[3] J. D. Shea, Phys. Rev. **30**, 825 (1927).

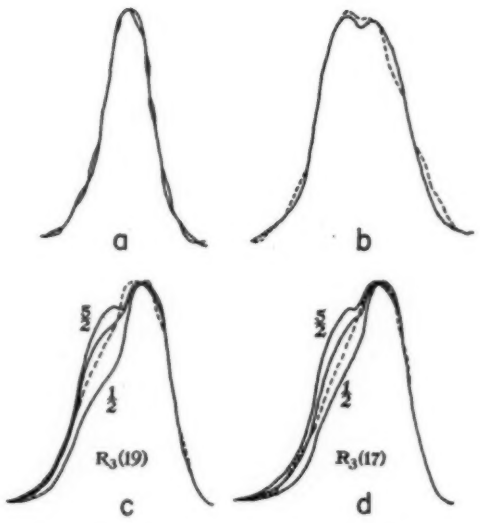

FIG. 2. Microphotometer curves of carbon lines.

should eliminate the grain structure almost completely. This was borne out by the fact that all average curves appeared smooth without artificial smoothing except such as inadvertently occurred by being unable to follow microscopic irregularities through the tracing paper.

The unsmoothed means of 7 orders of $R_3(18)$ $C^{12}{}_2$ and 8 orders of $R_3(17)$ $C^{12}{}_2$ from the light plate are shown superimposed in Fig. 2*a*. It is evident that these two lines have the same shape and we will therefore be justified in using the mean of the same lines on the heavy plate to find the shape of the line to be used in analyzing the $C^{13}{}_2$ lines on that plate. From two curves of this shape with a separation of 1.30 cm we obtain the solid curve, which is shown in Fig. 2*b*, superimposed on the observed dotted curve which is the mean of six orders of $R_3(19)$ $C^{12}C^{13}$ from the light plate. A 1.25-cm separation fits $R_3(17)$ $C^{12}C^{13}$ better on the sides but not as well on the top.

The same shape for a single line cannot be assumed for the heavily exposed plate since changes of temperature of the Lummer plate might have produced a shift in position during exposure. A mean of 3 orders of $R_3(17)$ and four orders of $R_3(18)$ was therefore used for the standard profile on this plate. This turned out to coincide exactly with that of the light plate. The doublet separation was checked on the 3 orders of $R_3(17)$ $C^{12}C^{13}$ and 4 orders of $R_3(19)$ $C^{12}C^{13}$ available on this plate and gave 1.20 and 1.25, respectively, the irregularities being noticeably greater near the tops of the curves as might be expected from the smaller number averaged. The shapes of the peaks to be expected on this plate for $R(19)$ $C^{13}{}_2$ with spins of $\frac{1}{2}$, $\frac{3}{2}$ and 5/2 were then constructed by adding peaks of the standard line shape spaced 1.30 cm apart with intensity ratios 1 to 3, 3 to 5 and 5 to 7, respectively. The resultant curves with the vertical scale suitably adjusted are shown superimposed on the observed dotted mean of 8 orders of $R_3(19)$ $C^{13}{}_2$ in Fig. 2*c*. Corresponding curves for $R_3(17)$, using a 1.25-cm spacing, are shown in Fig. 2*d*. All curves fit almost exactly for two-thirds of the distance up the steep side. On the side of the weak component the $\frac{3}{2}$ curve fits well on the average but the bump which should be present is absent. No known smoothing process, such as the finite microphotometer slit width, could eliminate this bump completely. Accidental deviations of this order have been observed as shown in Fig. 2*b*, but would be unlikely to occur in both lines. On the other hand, the observed curve is much too wide to agree with the calculated $\frac{1}{2}$ curve. No accidental width deviations of this size have been observed even between single unaveraged curves. The standard shape used for the single line was well determined so the use of a wider standard cannot be justified. Use of a wider separation improves the $\frac{1}{2}$ fit at the base but makes it worse in the middle. The spin of 1 is excluded by the statistics.

Wave Reflections from Diffuse Boundaries

C. D. THOMAS AND R. C. COLWELL
West Virginia University, Morgantown, West Virginia
(Received September 18, 1939)

The intensity of the waves reflected from various types of diffuse boundaries in which the dielectric constant changes only slightly is considered. The constant inside the reflection layer is assumed to vary as some power of the distance. It is further assumed that above and below this transition layer the media are uniform. The calculations show that the rate of decrease of intensity of the reflected wave with increasing layer thickness is more rapid for large values of μ the index of refraction, than for values close to unity. Fresnel's equations are therefore applicable to layers of considerable thickness if μ is very close to unity.

IT is customary to consider reflections from a boundary to be of considerable magnitude only if the boundary is very sharp compared to the wave-length of the incident wave. This is the case of importance in optics where the reflected light is usually near the order of magnitude of the incident ray. In the reflection of radio waves, however, the sensitivity of the receiver permits the detection of comparatively feeble waves, and it has been shown that detectable reflections may be produced by non-ionic layers if the boundaries are considered sharp.[1] It does not seem probable, on the other hand, that the layers could have extremely sharp boundaries, relative even to radio wave-lengths. It is therefore desirable to consider whether or not one is justified in using Fresnel's reflection laws here, as has sometimes been done. The important difference between these radio reflections and those of light is that the radio reflections are from regions where the relative refractive index is very close to unity so that the coefficient must be very small even though the boundary is truly sharp.

For the purpose of testing whether or not Fresnel's laws are a good approximation for thicker transition layers as the index approaches unity, a one-dimensional problem will be considered, i.e., plane waves progressing in the direction of variation of the dielectric constant. The region near the origin will be taken as uniform up to some point x_1, above this the dielectric constant will be assumed to vary as some monotonic function of x up to x_2, above this it is to be again uniform.

The wave equation, after removing the time dependent part, becomes

$$d^2X/dx^2 = -\nu^2\epsilon X/c^2, \tag{1}$$

where X is the space dependent part of the electric vector, c is the velocity of light, and ϵ is the dielectric constant which is itself a function of x. The general solution of this equation is

$$X = Af(x) + Bg(x). \tag{2}$$

The boundary conditions which must be satisfied by the solution are that x and its first derivative for the lower region must equal those of the transition layer at its lower boundary, and a similar set relating the upper region to the upper boundary of the layer. Thus there are four conditions for the six constants A, B (A_0, B_0 in the lower space; A_1, B_1 in the layer; A_2, B_2 in the upper space). However, it is only the ratio A_0/B_0 that is required if $f(x)$ and $g(x)$ are made the reflected and incident waves, respectively. Moreover, in the upper space one may assume that the backward component of the wave is zero ($A_2=0$). Hence, there are left only four constants (A_0/B_0, A_1, B_1, B_2), and there are four boundary conditions for determining these. The solutions of (1) in the three regions are now:

$$\begin{aligned} X_0 &= A_0' \exp(ik\epsilon_1^{\frac{1}{2}}x) + B_0' \exp(-ik\epsilon_1^{\frac{1}{2}}x), \\ X_1 &= A_1 f(x) + B_1 g(x), \\ X_2 &= B_2' \exp(-ik\epsilon_2^{\frac{1}{2}}x), \end{aligned} \tag{3}$$

where $k = \nu/c = 2\pi$ frequency$/c$. For convenience,

[1] C. R. Englund, A. B. Crawford and W. W. Mumford, Bell Sys. Tech. J. **14**, 369–387 (1935).

let

$$A_0' \exp(ik\epsilon_1^{\frac{1}{2}}x)+B_0' \exp(-ik\epsilon_1^{\frac{1}{2}}x) = A_0 \exp[ik\epsilon_1^{\frac{1}{2}}(x-x_1)] + B \exp[-ik\epsilon_1^{\frac{1}{2}}(x-x)]. \quad (4)$$

The boundary conditions then become

$$A_0+B_0=A_1f(x_1)+B_1g(x_1), \qquad ik\epsilon_1^{\frac{1}{2}}(A_0-B_0)=A_1f'(x_1)+B_1g'(x_1). \quad (5)$$

And similarly

$$B_2=A_1f(x_2)+B_1g(x_2), \qquad -ik\epsilon_2^{\frac{1}{2}}B_2=A_1f'(x_2)+B_1g'(x_2). \quad (6)$$

The primes on f and g of (5) and (6) indicate differentiation with respect to x before evaluation at x_1 and x_2.

Upon solving Eqs. (5) and (6) for the reflection coefficient when the thickness is t

$$R_t=\frac{A_0}{B_0}=\frac{[f'(x_1)+ik\epsilon_1^{\frac{1}{2}}f(x_1)][g'(x_2)+ik\epsilon_2^{\frac{1}{2}}g(x_2)]-[f'(x_2)+ik\epsilon_2^{\frac{1}{2}}f(x_2)][g'(x_1)+ik\epsilon_1^{\frac{1}{2}}g(x_1)]}{-[f'(x_1)-ik\epsilon_1^{\frac{1}{2}}f(x_1)][g'(x_2)+ik\epsilon_2^{\frac{1}{2}}g(x_2)]+[f'(x_2)+ik\epsilon_2^{\frac{1}{2}}f(x_2)][g'(x_1)-ik\epsilon_1^{\frac{1}{2}}g(x_1)]}. \quad (7)$$

This is applicable to any sort of transition layer of any thickness and for any value of the relative index $\mu=(\epsilon_2/\epsilon_1)^{\frac{1}{2}}$.

More specifically suppose that Eq. (1) inside the layer is

$$\frac{d^2X}{dx^2}+F(x)X=0, \quad (8)$$

where

$$[F(x)]^{\frac{1}{2}}=\frac{\nu}{c}\epsilon_1^{\frac{1}{2}}\frac{x^n}{x_1^n}=\frac{\nu}{c}\epsilon_2^{\frac{1}{2}}\frac{x^n}{x_2^n}. \quad (9)$$

This is not a very serious restriction on $F(x)$ when it is recalled that the layer is not very thick and that n may have any value whatsoever either positive or negative. Since x lies between x_1 and x_2, it is evident that if $(\epsilon_2/\epsilon_1)^{\frac{1}{2}}$ is greater than unity, n must be positive, while if $(\epsilon_2/\epsilon_1)^{\frac{1}{2}}$ is less than unity, n must be negative. In general from Eq. (9)

$$\mu=(\epsilon_2/\epsilon_1)^{\frac{1}{2}}=(x_2/x_1)^n \quad (10)$$

or using

$$x_2-x_1=t, \quad x_1=t/(\mu^{1/n}-1), \quad (11)$$

where t is the thickness of the transition layer.

In the cases under consideration μ is greater than one by a very small amount so that in Eq. (11), x_1 and x_2 are large except for layers which are extremely thin. Under these circumstances, it is allowable to put

$$f=e^{i\Delta+\delta}, \quad g=e^{-i\Delta+\delta}, \quad (12)$$

where

$$\Delta=\frac{k\epsilon_1^{\frac{1}{2}}}{n+1}\frac{x^{n+1}}{(x_1)^n}, \quad \delta=-\frac{n}{2}\log x_1, \quad (13)$$

as may be verified by substitution into Eq. (8) with the aid of (9).

If these values of f and g are put into Eq. (7), the coefficient R_t takes the form

$$R_t=\frac{-in\left\{\exp\left[\frac{ik}{n+1}(\epsilon_2^{\frac{1}{2}}x_2-\epsilon_1^{\frac{1}{2}}x_1)\right]-\frac{1}{\mu}\frac{x_1}{x_2}\exp\left[\frac{-ik}{n+1}(\epsilon_2^{\frac{1}{2}}x_2-\epsilon_1^{\frac{1}{2}}x_1)\right]\right\}}{4k\epsilon_1^{\frac{1}{2}}x_1\exp\left[\frac{ik}{n+1}(\epsilon_2^{\frac{1}{2}}x_2-\epsilon_1^{\frac{1}{2}}x_1)\right]}. \quad (14)$$

If use is now made of the value of x_1 and x_2 from Eq. (11) along with the restriction that μ is always near unity,

$$R_t^2=\frac{n^2(\mu^{1/n}-1)^2\sin^2\left[k\epsilon_1^{\frac{1}{2}}t\left(\frac{\mu+n}{n+1}\right)\right]}{4k^2\epsilon_1 t^2}. \quad (15)$$

The value of R_t^2 reaches zero at approximately

$$kt=\frac{\pi}{\epsilon_1^{\frac{1}{2}}}\frac{n+1}{\mu+n}. \quad (16)$$

It may easily be verified from this that the value of the thickness t for the first zero is greater for a value of μ nearer unity, since the factor

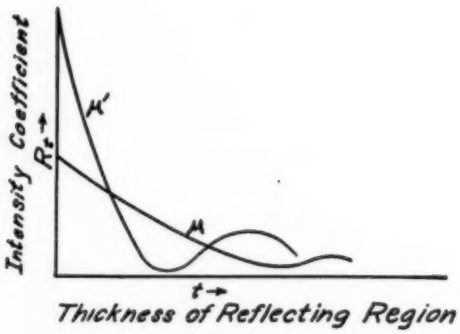

FIG. 1. The variation of the intensity coefficient with layer thickness for two sets of values of ϵ_1 and ϵ_2. The index of refraction $\mu=(\epsilon_2/\epsilon_1)^{\frac{1}{2}}$ is nearer unity than μ'.

$(n+1)/(\mu+n)$ in Eq. (16) increases for smaller values of μ. Also from the value of dR_t^2/dt it may be seen that R_t^2 decreases less rapidly for values of μ nearer unity.

The result on an exaggerated scale is illustrated in Fig. 1. Thus, although the reflection is much greater for truly sharp boundaries if μ differs considerably from one, the rate of decrease is also much greater. Hence, the Fresnel coefficient ($t=0$) becomes a better approximation for a given thickness if the value of μ is closer to one. In order to obtain information as to the exact way in which R_t decreases with t, it is necessary to make some assumptions as to the value of ϵ in the lower and upper regions and regarding the manner in which it changes in the transition layer (i.e., the nature of $F(x)$ of Eq. (8). These calculations will be published later.

The formulas developed here are applicable to the reflection of radio waves from different air masses in the troposphere. It is known from experiment that such reflections take place.[2]

[2] R. C. Colwell and A. W. Friend, Nature **137**, 782 (1936).

DECEMBER 15, 1939 PHYSICAL REVIEW VOLUME 56

On the Interpretation of Atomic Distribution Curves for Liquids

C. A. COULSON, *University College, Dundee, Scotland*

AND

G. S. RUSHBROOKE, *H. H. Wills Physical Laboratory, Bristol, England*

(Received July 24, 1939)

It is shown that if we approximate to a liquid by an Einstein model, in which each atom has a restricted region of motion, wherein it moves independently of its neighbors, and is surrounded by coordination shells of other atoms; and if we denote the density distribution of the atoms by $\rho(r)$, where r is the radial distance from any given atom; then the contribution to $\rho(r)$ made by any coordination shell, e.g., the ith is a function $\rho_i(r)$ for which $r\rho_i(r)$ is symmetrical about its corresponding maximum value. The complete distribution curve, $r\rho(r)$ against r, is the sum of peaks of equal width and similar shape. A semi-empirical application of this theory to liquid sodium (a reapplication of C. N. Wall's theory) gives a latent heat of melting in fair agreement with experiment. The model suggests a change of structure on melting, since agreement with the experimental distribution curve is impossible if the number of atoms in the first coordination shell is that of solid sodium. It is also shown that if the parameters in a partition function developed in this way are chosen to give agreement with any one physical property, then it is incorrect to add to the partition function terms representing "communal entropy."

§1. INTRODUCTION

SEVERAL experimental papers have appeared recently publishing atomic distribution curves for liquids.[1] These curves, found from Fourier analyses of the intensity distributions in x-ray scattering photographs, show $\rho(r)$, or $4\pi r^2\rho(r)$, as a function of r. $4\pi r^2\rho(r)dr$ is proportional to the probability that two unspecified atoms of the liquid are distant r to $r+dr$ apart.

[1] (a) F. H. Trimble and N. S. Gingrich, Phys. Rev. **53**, 278 (1938); (b) C. D. Thomas and N. S. Gingrich, J. Chem. Phys. **6**, 411 (1938); (c) C. D. Thomas and N. S. Gingrich, J. Chem. Phys. **6**, 659 (1938); (d) J. Morgan and B. E. Warren, J. Chem. Phys. **6**, 666 (1938).

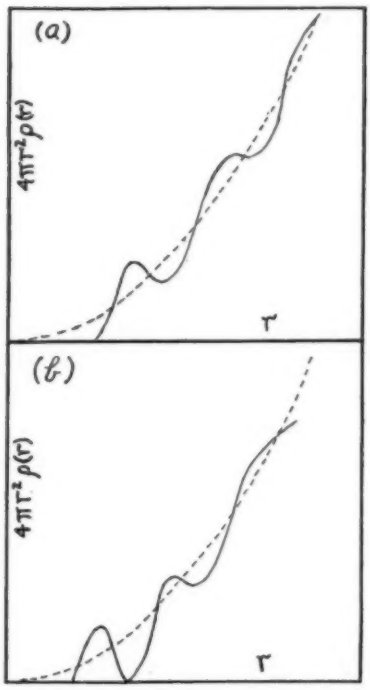

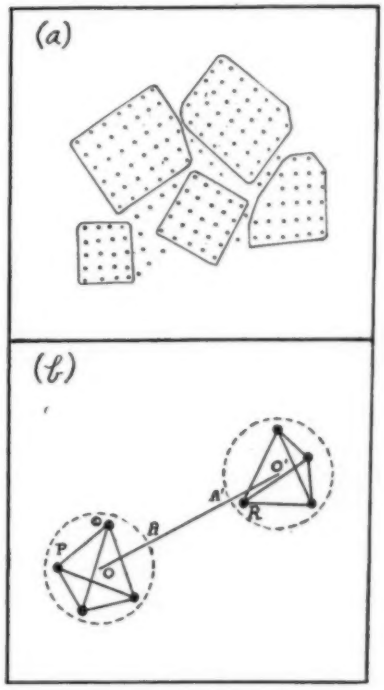

FIG. 1. (Left) Typical distribution curves for a liquid. (a) No structural units present. (b) With structural units.

FIG. 2. (Right) (a) Cybotactic groups in a liquid. (b) Structural units in liquid yellow phosphorus. From the experimental value of the density (found from the parabolas in Figs. 4 and 5 of Thomas and Gingrich's paper), i.e., $\rho_0^{-1}=29.1\ A^3$ at 48°C, and $=31.4\ A^3$ at 226°C, we can calculate an average distance apart for the centroids of two neighboring P_4 units. Since the data of Thomas and Gingrich suggest that each unit has a coordination of about 10, we have taken the mean of the results, which differ by only about 2 percent, found on the assumptions of body-centered and face-centered cubic packing. Thus the length OO′ is found to be 5.42A at 48°C, and 5.55A at 226°C. It is then clear that the first, second and third peaks in the figures of Thomas and Gingrich refer to the mean values of PQ, QR and PR. On account of valence saturation the atoms Q and R try to get as far apart as possible; this is why the distances AA', which are the shortest possible geometrically, do not occur in appreciable numbers.

In each case curves appropriate to various temperatures are given.

It is important to consider with what other experimentally determinable properties of the liquid we can correlate these curves; we may use either the shape of a single curve, the effect of a change of temperature on the curve, or relations between distribution curves for a family of substances such as the alkali metals. And the properties we deal with may be physical ones, e.g., density, viscosity, electrical resistance; or thermodynamic ones, e.g., entropy, vapor pressure, specific heat.

In this note we shall discuss the bearing of atomic distribution curves on the geometry of the atomic structure of a liquid, particularly in the neighborhood of the melting point, and the relation of this structure to the latent heat of melting ($L=T\Delta S$) which occurs at the phase change; incidentally this entails enquiry into the circumstances in which it is *relevant* to introduce the phrase "communal entropy." We shall be concerned mainly with the case of liquid sodium, for which C. N. Wall[2] has already given a theoretical discussion; indeed one object of this note is to reconsider Wall's application of his theory, for it seems to us that this can be done in a more satisfactory way.

§2. The Meaning of Peaks in a Distribution Curve

A typical distribution curve for a liquid, $4\pi r^2\rho(r)$ plotted against r, has peaks as shown in

[2] C. N. Wall, Phys. Rev. **54**, 1062 (1938).

Fig. 1(a). The question arises whether these peaks have any meaning as far as the geometry of the structure of the liquid is concerned.

At temperatures just above the melting point the peaks are sufficiently sharp and characteristically shaped for it to be generally agreed that liquids have some sort of semi-crystalline structure.[3] In particular two types of atomic arrangement have been proposed; one being characterized by molecular homogeneity, i.e., all atoms are thought to be equivalent in the structure of the liquid,[4] and the other by the presence of cybotactic groups,[3] i.e., it is supposed that there are groups of atoms, probably of varying sizes and shapes, which have a more definite crystalline structure within them than the liquid has as a whole.

It is not, however, possible to decide, either from a single distribution curve, or from several curves for different temperatures, whether a liquid is molecularly homogeneous or consists mainly of small cybotactic groups, each containing less than, say, 2000 atoms: Fig. 2(a). For in the latter case the x-ray diffraction lines will be very much blurred by edge effects at the boundaries of the groups, irregularly spaced atoms between the groups and the unequalness of the spacings within the groups, due to their small linear dimensions. This blurring will make the distribution curve indistinguishable from that to be expected with a molecularly homogeneous liquid.

On the other hand, we could see from a distribution curve whether there were only large cybotactic structures, each containing more than about 2000 atoms;[5] for then the peaks would be quite sharp and separate from each other, approaching the lines we should get if we analyzed the intensity distribution in a powder photograph. We can also tell whether the atoms of the liquid form smaller groups, which we may call structural units, as, for example, with liquid yellow phosphorus in which the atoms are grouped, both in the liquid and in the vapor, as P_4 molecules. In this case the fact that the first peak is detached, $\rho(r)$ vanishing, or sensibly vanishing, between the first and second peaks, shows that there are structural units comparatively far apart from each other; Figs. 1(b) and 2(b). We shall indeed have valence saturation in each structural unit and therefore repulsion of any atom not in the same unit; see note under Fig. 2(b). The breadth of the first peak will be due to fluctuations in the atomic distances within the P_4 groups, as a result of vibrations, rotations and occasional collisions. If only a small fraction of the atoms are grouped in structural units, then the detached peak due to them will be masked and not separate from the rest of the atomic distribution curve.

On the assumption of molecular homogeneity the function $4\pi r^2\rho(r)$, which gives the distribution of interatomic distances in the liquid, will give the distribution of the distances of the atoms from any one particular atom. If, for clarity, we suppose that there are no small structural units, then according to Bernal[4] we can define round any atom first, second . . . coordination shells as in a crystalline solid except that now the atoms in these are distributed, somewhat randomly, about mean distances from the central atom. For the shells to be properly defined a suitable probability function for the distribution of the radial distances about the mean radii of the coordination shells ought to be prescribed. Bernal, following earlier work of Prins,[6] assumes a Gaussian distribution, so that in a shell of mean radius R_i, $\rho_i(r)\alpha \times\exp[-\lambda(r-R_i)^2]$. On the other hand, Wall finds that, to his approximation,[2] $r\rho_i(r)$ and not $\rho_i(r)$ or even $r^2\rho_i(r)$ is, for each shell, symmetrical about the mean radius. There seems to us to be insufficient experimental data for deciding between these three possibilities; we shall, however, show theoretically in the following paragraph that for any Einstein model of a liquid, $r\rho_i(r)$ for a single shell, is symmetrical about the mean radius of that shell. Wall's theory, which we are going to reapply to liquid sodium, is based on a particularly simple Einstein model.

An Einstein model is characterized by the assumption that each of the atoms of a substance

[3] (a) P. Debye and H. Menke, Ergebnisse d. Tech. Röntgenkunde II, 1 (1931); (b) N. F. Mott and R. W. Gurney, *Reports on Progress in Physics* (Physical Society of London) **5**, 46 (1938).

[4] J. D. Bernal, Trans. Faraday Soc. **33**, 27 (1937).

[5] It is interesting in this connection that Riley, Chemistry and Industry **58**, 391 (1939) has been able to determine by use of x-rays the mean size of small graphite crystallites, which have about this limiting size.

[6] J. A. Prins, Physica **3**, 147 (1936).

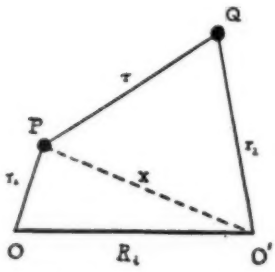

FIG. 3. Mean positions O and O' of the atoms P and Q.

moves independently of its neighbors, vibrating to and fro about a fixed center in some kind of average field which is determined by the rest of the substance. (See papers by Lennard-Jones and Devonshire.[7]) Thus, in Fig. 3, O and O' are the mean positions of two atoms P and Q. R_i, i.e., the length OO', is then the mean radius of the shell in which Q is found relative to P. We denote the average potential field in which each atom is assumed to move independently of its neighbors, by $\phi(s)$, and suppose that it is spherically symmetrical. Then the probability that P lies in a small volume element dV_1, distant $s=r_1$ from O, is proportional to $\exp[-\phi(r_1)/kT]dV_1$; similarly the probability that Q lies in dV_2, distant $s=r_2$ from O', is proportional to $\exp[-\phi(r_2)/kT]dV_2$. And in fact, the joint probability that P lies in dV_1 and Q in dV_2 is

$$\frac{1}{v^2}e^{-[\phi(r_1)+\phi(r_2)]/kT}dV_1dV_2, \qquad (1)$$

where

$$v=\int e^{-\phi(r_1)/kT}dV_1=\int e^{-\phi(r_2)/kT}dV_2.$$

The probability that the length PQ lies between r and $r+dr$ is the integral of (1) taken over all those coordinates of P and Q for which $r\leqslant|PQ|\leqslant r+dr$: thus, if $\rho_i'(r)$ denotes the density contribution per atom in the ith coordination shell, it follows that

$$4\pi r^2\rho_i'(r)dr=\frac{1}{v^2}\int e^{-[\phi(r_1)+\phi(r_2)]/kT}dV_1dV_2,$$

subject to

$$r\leqslant|PQ|\leqslant r+dr.$$

Now if there are N_i atoms in the ith shell, $\rho_i(r)=N_i\rho_i'(r)$: further, if we denote the length $O'P$ by x, and angles about the lines R_i and x by χ_1 and χ_2, then we may write

$$dV_1=xr_1dxdr_1d\chi_1/R_i, \quad dV_2=rr_2drdr_2d\chi_2/x.$$

Introducing these results into (1), and taking the integration over dV_2 to precede that over dV_1, we find that

$$r\rho_i(r)=\frac{\pi N_i}{R_iv^2}\int_{r_1=0}^{\infty}\int_{x=|R_i-r_1|}^{R_i+r_1}\int_{r_2=|r-x|}^{r+x}r_1e^{-\phi(r_1)/kT}\cdot r_2e^{-\phi(r_2)/kT}\cdot dr_2dxdr_1.$$

Now owing to the shape of $\phi(s)$—see Fig. 1 of Lennard-Jones and Devonshire[7]—we can assume that there is a length σ such that $\phi(s)$ is effectively infinite for $s\geqslant\sigma$. The integration over r_2 gives a factor

$$\psi(r+x)-\psi(|r-x|),$$

where $\psi(t)=\int_0^t s\exp[-\phi(s)/kT]ds$. Now $r+x$ is necessarily greater than σ, and clearly $\psi(t)=\psi(\sigma)$ if $t\geqslant\sigma$, so this factor is equal to

$$\psi(\sigma)-\psi(|r-x|).$$

For the integration over r_1 also, only the range from $r_1=0$ to $r_1=\sigma$ is significant, and so we find

$$r\rho_i(r)=\frac{\pi N_i}{R_iv^2}\int_0^{\sigma}r_1e^{-\phi(r_1)/kT}\times\left[2r_1\psi(\sigma)-\int_{R_i-r_1}^{R_i+r_1}\psi(|r-x|)dx\right]dr_1. \qquad (2)$$

This is a function of $|r-R_i|$ and vanishes if $|r-R_i|\geqslant2\sigma$. It therefore represents a contribution to the total function $r\rho(r)$, in the form of a symmetrical peak with a spread at the base given by 4σ, i.e., independent of R_i, and therefore the same for each coordination shell. Wall's Eq. (10) is a particular example of our equation for the case in which $\phi(s)$ is constant for $s\leqslant\sigma$.

According then to Wall's theory, or to any theory based on an Einstein model for a liquid, $4\pi r\rho(r)$ is resoluble into peaks of equal width (4σ) and similar shape. We give below, Fig. 4(a), the result of an empirical attempt which we have made to separate into symmetrical peaks the curve for $4\pi r\rho(r)$ which pertains to the experimental data of Trimble and Gingrich[1a] for liquid

[7] J. E. Lennard-Jones and A. F. Devonshire, Proc. Roy. Soc. **A163**, 53 (1937); **A165**, 1 (1938).

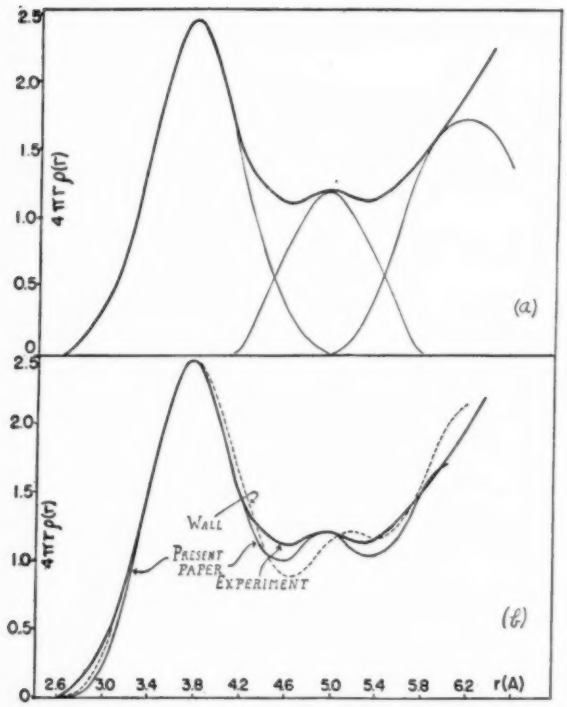

FIG. 4. Distribution curves for liquid sodium at 100°C. (a) Empirical separation into symmetrical peaks. (b) Comparison of predicted distribution curves with the experimental curve.

sodium at 100°C, and we see that the peaks are approximately of equal width and similar in shape. This is as satisfactory as we can reasonably expect, bearing in mind that the peaks are successively more sensitive to the precise shape of the first peak, i.e., to the position of its maximum and its form for small values of r, for which we cannot be certain of the experimental values.

The first two or three peaks do not overlap much and therefore may be supposed to correspond to coordination shells which have some physical meaning. But subsequently there is very considerable overlapping, and so there is little geometrical basis for assigning atoms, at these greater distances from the central atom, to definite coordination shells about that atom. This is even more the case at higher temperatures, and eventually the peaks can have little significance as far as the geometrical structure of the liquid is concerned; for whether this is interpreted in terms of coordination shells or small cybotactic groups, which will subdivide as the temperature is raised, it loses its significance as the structure of the liquid approaches that of a very imperfect gas.

In liquid sodium there will be no structural units other than atoms (or ions) and possibly a small percentage of diatomic molecules if the temperature is great enough. At 100°C, i.e., 2.4° above the melting point, we can ignore the possibility of the latter. We shall make the assumption, which in this case seems to us most reasonable, of molecular homogeneity, and interpret the peaks in the $4\pi r\rho(r)$ curve as corresponding to coordination shells. Unfortunately the small, 2.5 percent, volume change of sodium on melting does not rule out the possibility of cybotactic groups in the way that the comparatively large changes of -9 percent and 11 percent for water and argon, respectively, seem to do in those cases: for large volume changes must imply a radical change of structure, but small volume changes leave the question open.

§3. Reapplication of Wall's Theory to Liquid Sodium at 100°C

Wall's theory is based on the assumption that for each atom (or ion) of the liquid there is a sharply defined, spherical volume of radius σ, in which its center can move without increasing the potential energy of the liquid as a whole. This implies among other things, that the atoms (or ions) behave as hard rigid spheres. On this assumption Wall finds a theoretical form for the shape of an isolated peak, *viz*:

$$y\equiv 4\pi r\rho_i(r)=\frac{3N_i}{5\sigma R_i}\left\{1-\frac{5(R_i-r)^2}{4\sigma^2}\times\left[1-\frac{|R_i-r|}{2\sigma}+\frac{|R_i-r|^3}{40\sigma^3}\right]\right\}. \quad (3)$$

This depends on three unknown parameters σ, N_i and R_i. σ has been defined already; N_i is the number of atoms in the coordination shell corresponding to the peak for which R_i is the mean radius. To get the complete distribution curve, $4\pi r\rho(r)$ against r, it is necessary to add together the effects of successive peaks; σ will be the same for each of them but their N's and R's are further unknown parameters. Wall determines N_0, R_0 and σ, where N_0 and R_0 appertain to the first shell, by making the left-hand side

of the first peak, $r \leqslant R_0$, coincide as closely as possible with the experimental curve. He then uses some semi-empirical calculations of Bernal[4] to find, from N_0 and R_0, the N's and R's which correspond to more distant shells. Knowing these, the complete distribution curve can be constructed, and Wall gets a curve which agrees fairly well, but by no means exactly, with the experimental one. Unfortunately, in drawing a curve through the experimental points a small, but quite definite, peak (strictly speaking the second), was smoothed out; this makes the agreement Wall has obtained (reference 2, Fig. 2) seem rather better than it really is.

Now the values of σ and N_0 found in this way are very sensitive to the precise shape of the first peak in the experimental curve. Moreover, we must not expect Wall's theoretical peaks to fit the experimental curve exactly, since that would imply that the atoms (or ions) behaved as rigid spheres. Finally it seemed to us better to try to test Bernal's formulae for N_i and R_i in terms of N_0 and R_0, rather than to assume them in the course of this theory. So to find σ and N_0, $N_1 \cdots$ we proceed rather differently.

An essential feature of Wall's theory, and indeed of any theory based on an Einstein model, is that, for any shell, N_i is proportional to $R_i Y_i$, where Y_i is the value of y in Eq. (3) which corresponds to $r=R_i$. We find the correct values of R_i and Y_i, for each peak, from our empirical resolution of the experimental distribution curve into separate peaks. We then determine N_0 and N_1 from the two conditions

$$N_0/N_1 = R_0 Y_0 / R_1 Y_1, \tag{4}$$

$$1 + N_0 + N_1/2 = 4/3 \cdot \pi \cdot R_1^3 \rho_0, \tag{5}$$

where ρ_0 is the density of the liquid in atoms per unit volume. We use the experimental value for sodium at 100°C,[8] which is $\rho_0 = 0.0247\text{A}^{-3}$. The first formula (4) is essential to Wall's theory and the second (5) is the result of assuming that if we take a small imaginary sphere of radius R_1 then it will enclose the same number of atoms wherever it be situated in the liquid. This is approximately true for a crystalline solid body, and we may suppose that it will be even more so for a liquid.

[8] E. Rinck, Ann. de Chemie **18**, 395 (1932).

We find

$$R_0 = 3.78\text{A}, \quad R_1 = 4.96\text{A},$$
$$Y_0 = 2.45, \quad Y_1 = 1.21,$$

and with these values, (4) and (5) then give

$$N_0 = 8.78, \quad N_1 = 5.69.$$

The empirical resolution of the distribution curve into peaks, as shown in Fig. 4(a), suggests that the third peak is specified by $R_2 = 6.18\text{A}$, $Y_2 = 1.74$. But when we come to use Wall's formula to construct the curve theoretically, we find that we get a much better fit if we move the third peak a little to the left, and have $R_2 = 6.06\text{A}$, $Y_2 = 1.74$. This shift of R_2 lies within the uncertainties unavoidable in any graphical separation of the peaks. The formula $N_2/N_1 = R_2 Y_2 / R_1 Y_1$ then gives $N_2 = 10$. The results, are summarized in Table I. We give Wall's values for comparison. In Fig. 4(b) we show the distribution curve obtained on using our values for the parameters in Wall's theoretical formula. σ is given by $3N_0/5R_0Y_0$ and is found to be 0.57, whereas Wall's value was 0.60. Wall's curve is shown by the broken line in Fig. 4(b).

We shall not give the details of a similar analysis of Trimble and Gingrich's experimental curve for liquid sodium at 400°C, because we do not suppose that, at that temperature, a resolution into peaks will have much meaning. The calculations give, at 400°C:

$$N_0 = 8.50, \quad N_1 = 6.81;$$
$$R_0 = 3.80, \quad R_1 = 5.14.$$

TABLE I. *Comparison of constants.*

	N_0	N_1	N_2	R_0	R_1	R_2	R_1/R_0	R_2/R_0	σ
Values; this note	8.78	5.69	10	3.78	4.96	6.06	1.31	1.60	0.57
Wall's values	9.28	6	13	3.79	5.1	6.2	1.34	1.63	0.60

Finally the entropy change on melting (ΔS) and the associated latent heat of fusion (L) are estimated as in Wall's paper; the results are shown in Table II.

§4. Discussion of the Results

We do not wish to attach any importance to the precise numerical values which we have found and given above; indeed it would be unreasonable to expect better agreement than that

TABLE II. *Melting of sodium.*

	$[\Delta S]$	L (KILOJOULES/MOL.)
Present paper	0.747 R	2.31
Wall's paper	0.906 R	2.8
Experimental	0.861 R	2.65

shown in Table II from so simple a theory, but we believe that certain conclusions can, legitimately, be drawn from them.

In the first place, at 100°C, i.e., only 2.4° above the melting point, N_0 differs quite appreciably from its value, which is 8, for sodium in the solid state. The first two shells together contain nearly the same number of atoms (14.4) as in the solid state (14). We have tried to obtain a fit with the experimental curve on the assumption that $N_0=8$, but could not obtain even reasonably good agreement. We conclude therefore that there is quite a definite change of structure on melting. Moreover N_0 (400°C) is less than N_0 (100°C) while N_1 (400°C) is greater than N_1 (100°C), so that it appears that at higher temperatures the number of atoms in the second shell increases at the expense of those in the first. The liquid, then, does not tend to become close-packed at high temperatures.

Secondly, on comparing the predictions of Bernal's paper, i.e., that for $N_0=8.78$ we shall have $N_1=8$, $N_2=12$, $R_1/R_0=1.33$ and $R_2/R_0=1.63$, with the results of Table I, we find that Bernal's values for R_1/R_0 and R_2/R_0 are in good agreement with those we have found empirically; but his values for N_1, N_2 $\cdots$ are not those which we have found. The only agreement here is that if N_0, when in the neighborhood of 8, decreases, then N_1 increases. Bernal himself states that his estimates of successive N's are less reliable than those of successive values of R/R_0.

Next we observe that using the same N's and R's as in Table I, we could have got a better, and almost perfect, fit with the experimental curve if Wall's theoretical shape for a single peak had been rather fatter at the base. This would have been so if the atoms (or ions) had not been treated as hard spheres, with sharply defined free volumes, but their repulsive interactions had been taken into account, as in Lennard-Jones' picture of a liquid.[7] This is an essential defect of Wall's theory.

Finally, since our value for the latent heat of fusion is too low, we are led to enquire whether this also is due to the essential limitations of a model in which the atoms are treated as hard spheres, or whether it is due to our having neglected a communal-entropy term (see, in particular Lennard-Jones and Devonshire, 1938). We are driven to the former conclusion and end with a discussion of this point.

§5. THE MEANING OF COMMUNAL ENTROPY

The introduction of the notion of a free-volume for each atom of a liquid, in which, effectively, it can move without influencing the other atoms, at once elicits the idea of communal entropy.[9]

Free volume may be defined in two ways. We shall say that it is defined thermodynamically if it is defined purely formally from the partition function. The partition function $F(T, V, N)$ is supposed known (though in practice only approximations to it are known) as a function of T, V and N, where T is the temperature, V the volume and N the total number of atoms of the liquid; the thermodynamic free-volume v_{th}, is then defined by the equation:

$$F(T, V, N)=(2\pi mkT/h^2)^{3N/2}\cdot v_{\text{th}}{}^N, \qquad (6)$$

where m is the atomic mass, and the other symbols have their usual meanings.

On the other hand, we shall speak of the geometrical free-volume v_{geom} when we approximate to the liquid by an Einstein model. v_{geom} is then v of Eq. (1) and replaces v_{th} in Eq. (6). It has a well-defined meaning geometrically in the simple approximation in which it is supposed that each atom may be treated as a rigid sphere imprisoned in a cell whose size is fixed by the density of the liquid; this is the approximation on which Wall's theory is based.

If we restrict ourselves to Einstein models for liquids, v_{th} is an ideal quantity to which we try to approximate by assuming suitable forms for v_{geom} as a function of T, V and N. v_{th} is an

[9] (a) O. K. Rice, J. Chem. Phys. **6**, 476 (1938); (b) R. W. Gurney and N. F. Mott, J. Chem. Phys. **6**, 222 (1938); (c) L. Tonks, Phys. Rev. **50**, 955 (1936).

average determined by all the positions of all the atoms of the liquid, though only those that are at all likely will count significantly. v_{geom}, in which each atom is confined to the neighborhood of a certain site, may then be too small, since by confining the atoms to particular regions of space, large fluctuations in the interatomic distances are ruled out; but it need not be too small because exact agreement with v_{th} may be obtained, at any one temperature, by suitable choice of the potential field ϕ. Of course it may not be possible to get a good approximation to v_{th} at all temperatures by choice of a potential field ϕ, which must depend explicitly only on the density and be otherwise independent of the temperature. For this reason an approximation to the partition function is sometimes made (e.g. Lennard-Jones and Devonshire, 1938) in which a reasonable form for ϕ is chosen, and then the resulting "Einstein" partition function is multiplied by another factor, frequently e^N, to take account of large fluctuations in the atomic distances. It is this extra factor which is called the communal entropy term and e^N is chosen because that is the difference which would be made to the partition function of a perfect gas of N molecules if its volume were to be subdivided into N equal cells and each molecule be confined to one cell. But of course the factor ought strictly to be temperature dependent and its nature must depend on the initial choice of ϕ.

Now at any temperature, the measurable properties of a liquid depend on all the possible positions of all the atoms of the liquid, and to predict them theoretically we must use a good approximation to v_{th}. If we include parameters in the potential field ϕ of v_{geom}—for example in Wall's case the radius of his spherical free volume —and so choose these that some physical properties of the liquid have their correct experimental values, then we are not at liberty still to include a communal entropy term in the partition function. If the resulting formulae do not give the correct experimental values of other measurable properties, this is because we do not have sufficient parameters in ϕ, i.e., to an essential limitation of the model used.

This is the case in the present instance. We have chosen σ in Wall's theoretical formula for an atomic distribution curve, Eq. (3), so as to get as good a fit as possible with a distribution curve found experimentally, and the fact that Wall's theory does not then give a good value for the entropy of melting is due, we suggest, not to omission of a communal entropy term—inclusion of which would mean that there were positional distributions of the atoms which affected the entropy but not the atomic distribution curve—but to the essential limitations of a model which treats the atoms (or ions) of the liquid as hard spheres.

The writers would like to acknowledge helpful discussion of the ideas in this paper with Mr. J. Corner.

Dependence of Ferromagnetic Anisotropy on the Field Strength

L. P. TARASOV
Research Laboratory, General Electric Company, Schenectady, New York
(Received August 14, 1939)

In evaluating the anisotropy constants of ferromagnetic materials a common method is to measure the torque exerted on a specimen of circular section by a uniform magnetic field, to determine the maximum torque by extrapolation to infinite field strength, and to multiply this by an appropriate number. The law of approach of the torque, T_H, to its limiting value, T_∞, is now found to be

$$T_H = T_\infty(1 - H_0/H_a)$$

for a number of disks and ellipsoids of single crystals of iron-silicon alloys containing up to 7.4 percent silicon, and for polycrystalline disks of iron and of silicon steel. Here H_a is the strength of the applied field uncorrected for demagnetizing field and H_0 is a constant which depends mostly upon the dimension-ratio of the disk. This law is discussed in relation to a similar law proposed by Schlechtweg, and to the familiar law of approach of magnetization to saturation. It is concluded that for disks the approach to saturation of the torque peaks is connected with the lack of magnetic saturation at their edges.

IT is a well-established fact that ferromagnetic single crystals generally show considerable anisotropy in their magnetic properties. The simple theory of ferromagnetic anisotropy and the several methods of measuring it have recently been reviewed by Bozorth.[1] The simplest of these methods involves the use of a magnetic torquemeter to measure the torque exerted by a strong field on a suitably held single crystal disk, the torque arising from a lack of parallelism between the direction of the magnetization intensity in the disk and the direction of the applied field. This deviation between I and H occurs because of the anisotropy of the material. If the orientation of the disk with respect to the crystal axes is known, the anisotropy constants can easily be calculated from the torque data.[2-4] It is usually preferable to have some simple crystallographic plane lying in the plane of the disk because the resulting torque curve must then be symmetrical, unless the crystal is imperfect; in this case, the degree of symmetry throws some light on the trustworthiness of the calculated anisotropy constants.

In order to calculate the anisotropy constants from the torque data, it is necessary to use an applied field strong enough to make the torque independent of it. It has generally been thought that a field of several thousand oersteds is sufficient for a disk with not too large a ratio of thickness to diameter and some evidence to this effect was found[2] when a moderately accurate torquemeter was used. On the other hand, some later work by Schlechtweg[3] indicated that the torque did not reach a saturation value in fields of the same order of magnitude. Unfortunately, his highest field strength was only 2400 oersteds, and under the conditions of the experiment this was too low to prove conclusively that the torque would not have reached a limiting value at a somewhat higher field. By using a torquemeter of very high sensitivity, the author has been able to show in the present paper that a saturation value of the torque cannot be obtained experimentally, but can be calculated by extrapolating to $1/H=0$.

APPARATUS

The torquemeter used in this work was of the familiar torsion type, but built on a larger scale than usual. The electromagnet was about the same size as the one illustrated elsewhere,[4] mounted so as to rotate around a vertical axis. With the flat faces of the pole pieces $1\frac{3}{4}$ inches apart, a field of 4000 oersteds could be obtained, but measurements ordinarily could not be made above 3500 oersteds because of overheating. The field was calibrated in terms of the magnetizing current in the usual manner with the aid of a search coil and a ballistic galvanometer. The fields could be measured with an accuracy of one-tenth of a percent relative to each other, but the uncertainty involved in reading the ammeter

[1] R. M. Bozorth, J. App. Phys. **8**, 575 (1937).
[2] R. M. Bozorth, Phys. Rev. **50**, 1076 (1936).
[3] H. Schlechtweg, Ann. d. Physik [5] **27**, 573 (1936).
[4] L. P. Tarasov and F. Bitter, Phys. Rev. **52**, 353 (1937).

during the actual use of the torquemeter brought the possible error in H to about one-half percent. The field was uniform to at least this extent over the area of the single crystal disks used in this investigation, which were mostly half an inch in diameter; however, the field probably varied somewhat more over the area of the one-inch polycrystalline disks which were also used. The uncertainty in the field was in all cases too small to affect the results appreciably. The highest fields used were too low to require any correction for the image effect described by Weiss and Forrer.[5]

The specimen was held by the pressure of a thumbscrew in an aluminum holder which was suspended between the pole pieces. Phosphor bronze wires 0.032 inch in diameter were used for the suspension. The upper wire, which was fastened securely to the frame of the torquemeter, was 10 inches long; the lower wire, held at the other end in a wire chuck attached to an accurately machined gear, was 24 inches long. This gear was meshed with a worm gear, a complete revolution of which corresponded to a 12-degree twist of the lower end of the suspension. On the same shaft with the worm gear was a large dial graduated into 100 divisions. The mechanical torque required to balance the magnetic torque exerted by the field on the specimen could be reproducibly measured to a tenth of a division, and since the torque peaks of most of the specimens examined amounted to one or two complete revolutions of the dial, an accuracy of one part in a thousand or better could be reached. A galvanometer mirror was mounted on the upper suspension wire just above the aluminum disk-holder, and the image of a cross-hair thrown on a scale clamped to the torquemeter frame showed accurately when the specimen was in its zero position, i.e., the position in which the magnetic and mechanical torques were properly balanced. To convert the arbitrary dial readings to absolute units it was found best to calibrate the suspension by means of a specimen whose torque peaks had been measured on a balance-type torquemeter, which gave the results in absolute units directly.[6] It was thus found that one dial division corresponded to 65.4 dyne-cm. In making the measurements, it was necessary to introduce a slight correction for the torque exerted by the aluminum disk-holder which probably arose from ferromagnetic impurities. Because the precision was so high it was also necessary to correct for any temperature change during a set of readings. This correction was found experimentally to be one part in 700 for 1°C, a value very close to the known temperature variation of the anisotropy constant of iron at 25°C. The temperature was read on a thermometer suspended from the frame of the torquemeter in such a way that the bulb was only a millimeter or two above the specimen and slightly to one side of it.

Measurements on Single Crystal Disks

The first set of measurements was made on a group of fourteen well-annealed single crystal disks of iron containing from 2.4 to 7.4 percent of silicon by weight,[7] as found from subsequent chemical analyses on the disks. Eleven of these had the (100) plane in the plane of the disk, the others had (110). Back-reflection Laue patterns of the disks proved that the deviations from these ideal orientations were a few degrees at most, not enough to affect the validity of the results to be described. After the measurements on these disks were complete, some of them were

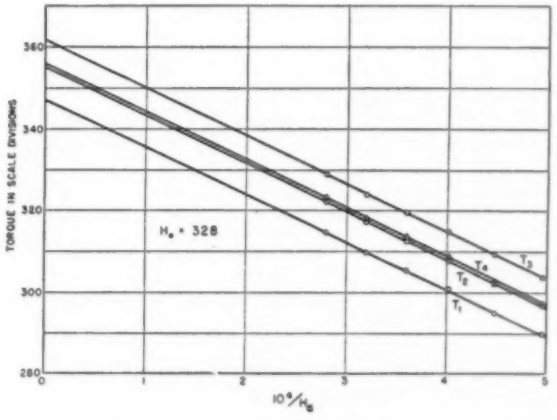

FIG. 1. Variation with $1/H_a$ of the magnetic torque peaks of a (100) disk. The successive peaks are numbered in order. H_a is the applied field.

[5] P. Weiss and R. Forrer, Ann. de physique [10] **12**, 297 (1929).

[6] This was done through the kindness of Dr. A. R. Kaufmann at the Massachusetts Institute of Technology, who used the torquemeter described in reference 4.

[7] These disks, to be described in greater detail in a subsequent paper on the anisotropy of iron-silicon alloys, were prepared several years ago by Dr. K. J. Sixtus, at that time of the General Electric Research Laboratory.

polished and etched deeply to reduce the thickness and were remeasured. There were thus available data on disks ranging from 0.37 to 0.75 inch in diameter, and from 0.008 to 0.035 inch in thickness. The ratio t/D of thickness to diameter varied from 0.015 to 0.090.

For the present the discussion will be restricted to the (100) disks, whose four torque peaks are of equal magnitude. In Fig. 1 the torque peaks found for one of these disks are plotted individually as a function of $1/H_a$, where H_a is the applied field. This was varied between 2000 and 3500 oersteds. It is clear that at least in this range the magnitude of the torque peak changes linearly with $1/H_a$ to a high degree of accuracy. The results can be expressed by the equation

$$T_H = T_\infty(1 - H_0/H_a), \qquad (1)$$

where T_H and T_∞ are the magnitudes of the torque peaks for an applied field H_a and for an infinite one, respectively, and H_0 is a constant. This linear relationship was found to hold only above 2000 oersteds or thereabouts, the curve breaking suddenly downward for lower fields. Above 2000 oersteds the law held all the way to $1/H_a = 0$, as was demonstrated by measurements on an oblate ellipsoid of revolution to be described later. For disks or ellipsoids cut parallel to the (100) plane, the anisotropy constant is given by $K_1 = 2T_\infty$.

At this point, it is desirable to mention the effect of rotational hysteresis upon the results. It is known that the two torque curves obtained by rotating the field in opposite directions are separated vertically by an amount proportional to the rotational hysteresis. The data plotted in Fig. 1 were obtained by always rotating the field in the same direction through all four peaks. Hence, two of the peaks were too small by an amount equal to the torque arising from rotational hysteresis, while the other two were large by the same amount. Since rotational hysteresis tends toward zero as magnetic saturation is approached, the error becomes less in higher fields with the result that the slope of two of the lines, such as are drawn in Fig. 1, may differ slightly from the slope of the other two lines. In some cases, as in Fig. 1, the error arising from rotational hysteresis was so small that all four lines were parallel within experimental error; in other cases, especially for polycrystalline disks, the error was large enough to give a perceptible difference in slopes. Were it not for imperfections in the specimen, such as a slight deviation between the (100) plane and the plane of the disk, the four lines of Fig. 1 would be coincident. Even where rotational hysteresis was comparatively large, it was far too small to account for the observed differences in the sizes of the supposedly equal torque peaks. To eliminate the effect of rotational hysteresis, the results were always plotted to give a single line showing the variation of the sum of the four torque peaks with $1/H_a$, for in this case the errors automatically canceled.

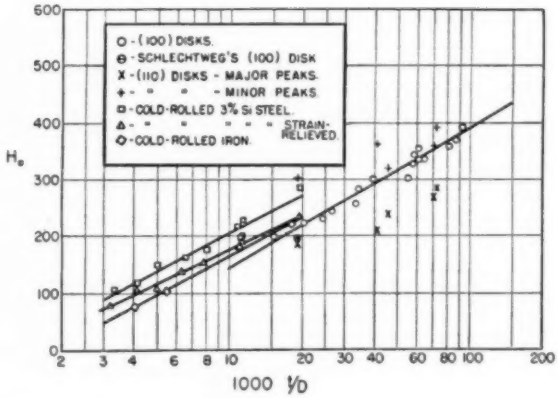

FIG. 2. H_0 as function of t/D, the ratio of the thickness of a disk to its diameter. The straight line on the right was calculated by least squares using only the circles. The three straight lines at the left, drawn in directly, connect the three sets of data for cold-rolled and strain-relieved materials.

It was noticed that H_0 increased with the ratio of the thickness of a disk to its diameter. Several ways of plotting results were tried, but the only one that gave a reasonably linear variation was the one in which H_0 was plotted against log (t/D), where t and D are the thickness and diameter. The results for all the (100) disks are indicated by circles in Fig. 2. A dashed circle shows the result calculated from similar data obtained by Schlechtweg[3] on a (100) disk. This point is in reasonably good agreement with the others.

It is obvious that there is considerable scatter in H_0, when only the points for the (100) disks are considered. An examination of the original data showed that this scatter could not be accounted for on the basis of variations in the

silicon content of the disks which, as has already been mentioned, contained from 2.4 to 7.4 percent, nor because of slight deviations from the ideal orientation. The only explanation of the scatter is that it arises from certain peculiarities of the specimens whose nature is unknown at present, for the amount of scatter is larger than can be ascribed to errors in the measurements. The straight line drawn through these points was calculated by least squares, and its equation is

$$H_0 = 637 + 246 \log_{10} (t/D), \qquad (2)$$

or in a slightly different form,

$$H_0 = 246 \log_{10} (385t/D). \qquad (2a)$$

It is obvious that this equation is valid only between certain limits of t/D; moreover, it applies only to the torque peaks of (100) single crystal disks. The line corresponding to this equation in Fig. 2 is drawn somewhat beyond the experimental points to indicate the probable range of validity.

The discrepancy between the experimental values of H_0 and those corresponding to the line was generally less than 5 percent. If it is assumed that H_0 can be calculated for a (100) single-crystal disk from its dimensions with an error not exceeding 5 percent, then the torque peaks can be extrapolated to $1/H_a = 0$ according to Eq. (1) with an error of less than 0.5 percent, using the reasonable values of $H_a = 3000$ and $H_0 = 300$. Thus this equation should be useful when experimental circumstances make impossible the accurate determination of H_0.

We now turn to the (110) disks, which have two major and two minor peaks instead of four of the same size. Similar measurements on the (110) disks showed that H_0 for the minor peaks is considerably larger than for the major ones. The two sets of points are plotted in Fig. 1 as crosses. The scatter is considerable because few disks were available and also because they were smaller than the (100) disks so that the variation of the peaks with $1/H_a$ was harder to determine accurately. There can be no doubt, however, that H_0 for the (100) disks is smaller than for the minor peaks of the (110) disks and larger than for their major peaks. At the same time, it appears that H_0 for both sets of (110) peaks does not increase as rapidly with t/D as does H_0 for the (100) peaks. More data on (110) disks are needed before it will be possible to calculate H_0 from the dimensions with any reasonable accuracy.

Measurements on Polycrystalline Disks

Some 3 percent silicon steel was cold rolled from 100 mils down to various thicknesses ranging from 20 to 3 mils. Disks one inch in diameter were punched from this material, which is described in detail elsewhere,[8] and were measured both in the cold-rolled condition and after being annealed just below the recrystallization temperature to relieve the strains as much as possible without changing the texture. The predominant texture of severely cold-rolled silicon steel is one having the (100) planes in the rolling plane or deviating by various amounts from this ideal orientation. The torque curve of this material is similar to that of a (100) single crystal disk in that the four torque peaks are of approximately the same size; furthermore, the torque curve remains practically the same after the disks have been annealed for strain relief. Some work was also done on three disks of fairly pure iron, all of which were cold rolled to a 95 percent reduction in thickness.

The three sets of results are shown, distinctively marked in Fig. 2 on the left. Although the points are very scattered, it is possible to draw three straight lines, one through each set. The same disks were used before and after the strain relief so that the decrease in H_0 following the anneal is known to be a real effect. The values of H_0 for the three iron disks are even smaller, but not enough specimens were available to make sure that this was not an accidental variation. Although the lines drawn through the three sets of points have roughly the same slope as the line for the (100) single-crystal disks, the lines themselves are all somewhat higher. One reason for this is the difference between the strain conditions in the two cases. It may also be that instead of drawing a straight line for the single-crystal disks and another one for the strain-relieved disks, there should be drawn a slightly curved line passing through both sets of points.

[8] L. P. Tarasov, Trans. A. I. M. E. **135**, 353 (1939). See Table I.

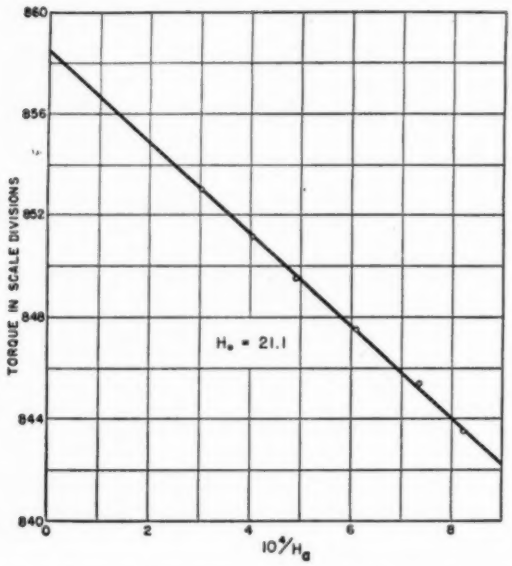

FIG. 3. Sum of four torque peaks of the (100) ellipsoid as function of $1/H_a$. This ellipsoid was filed from the (100) disk referred to in Fig. 1. The straight line is drawn to have a width of 0.1 division, the limit of accuracy in the measurements.

The considerable scatter that occurs in H_0 for polycrystalline material shows that it is best not to depend too much upon the values shown in Fig. 2.

MEASUREMENTS ON SINGLE CRYSTAL ELLIPSOIDS

After the measurements were finished on the (100) single-crystal disk for which the results are shown in Fig. 1, this disk was filed into a highly accurate oblate ellipsoid of revolution.[9] The torque peaks of this ellipsoid, which contained 2.4 percent silicon, were measured with the highest possible precision after it had been etched and annealed to remove the distorted surface.

The results, shown in Fig. 3, indicate that an ellipsoid follows the same type of law as do the disks. However, H_0 is only 21.1 as compared with 328 for the same single crystal when it was still a disk. The accuracy with which the $1/H_a$ law is followed can be seen from the thickness of the line which corresponds to 0.1 division, the limit of accuracy of a single reading. The linear relationship extends to considerably lower fields than for disks, entirely on account of the relative ease of "saturating" an ellipsoid and a disk. The deviations from linearity are so negligible that the relatively short extrapolation to $1/H_a=0$ needs no further justification.

The work on the ellipsoid made it possible to check the validity of the linear extrapolation to $1/H_a=0$ in the case of the (100) disks. The effective anisotropy constants were calculated ($K_1=2T_H$) for various fields for both the disk and the ellipsoid into which it was made, and the values were plotted as in Fig. 4. The anisotropy constant extrapolated to $1/H_a=0$ was the same within experimental error in the two cases. This establishes the validity of Eq. (1) for the (100) single crystal disks, and it is reasonable to assume that the same is true of polycrystalline disks.

A (110) disk containing 5.9 percent silicon was similarly filed into an ellipsoid and it was found that H_0 for the major peaks was very close to 20. The variation of the minor peaks with $1/H_a$, which was hard to determine with any certainty, gave H_0 equal to about 15. The validity of the linear extrapolation to $1/H_a=0$ for (110) disks was also checked and Eq. (1) was again found to be satisfactory in the extrapolated range.

TORQUE BEHAVIOR IN LOWER FIELDS

It has already been mentioned that the linear relation given by Eq. (1) was followed only for

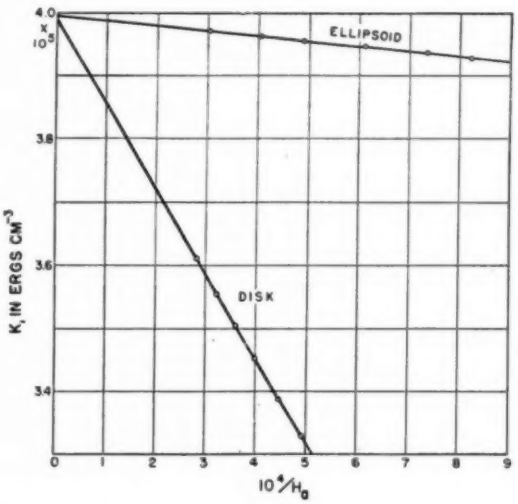

FIG. 4. Apparent anisotropy constants calculated for various fields for a (100) single crystal disk and for the ellipsoid into which it was filed. The true anisotropy constant is the value of K_1 for $1/H_a=0$.

[9] The method is essentially the one described by L. W. McKeehan, Rev. Sci. Inst. **5**, 265 (1934). This and another ellipsoid were prepared at M. I. T. through the kind cooperation of Dr. A. R. Kaufmann.

fields above a certain minimum value, which in the case of disks generally was in the neighborhood of 2000 oersteds. Disks with a high ratio of thickness to diameter required a stronger field for the $1/H_a$ law to hold than did disks with a low ratio. This behavior is clearly connected with the relative ease of approaching magnetic saturation in the disks in the two cases.

For the (100) ellipsoid, the minimum satisfactory field was considerably lower than for a disk of the same dimension ratio, as would be expected on the basis of ease of saturation. The deviations from the $1/H_a$ law were negligible down to 1100 oersteds, but just below this there was an abrupt drop in the magnitude of the torque peaks. Had the ellipsoid been thinner with respect to its diameter, the break would not have occurred until even lower fields were reached.

The major peaks of the (110) ellipsoid behaved exactly like the peaks of the (100) ellipsoid, but it was a different story for the minor peaks. The variation of a major and a minor peak of the (110) ellipsoid is shown in Fig. 5, where it can be seen that at 1000 oersteds or so the minor peak is 25 percent larger than the value it attains at much higher fields. Below 800 oersteds, the major and minor peaks are of practically the same magnitude. A satisfactory explanation of this phenomenon has not yet been given.

Discussion of the $1/H_a$ Law

The only theoretical work on the approach of torque measurements to their saturation value is that of Schlechtweg,[10] who predicted that the torque peaks of a homogeneously magnetized disk should approach saturation according to a $1/H_a$ law. The restriction to homogeneously magnetized disks is nothing more than a restriction to the use of ellipsoids instead of disks. Calculation of H_0 for the torque peaks of (100) and (110) ellipsoids according to Schlechtweg's equations gave $H_0=0$ in both cases, although for other orientations it was not zero. This indicated that the experimentally observed values of H_0 for the two ellipsoids had to be explained by a different theory than the one proposed by Schlechtweg.

It is interesting to compare the approach to saturation of the torque peaks with the similar approach to saturation found for the intensity of magnetization in the case of iron and iron-silicon alloys.[5, 11] One highly important difference between the two cases is that the *applied* field is used in connection with the torque measurements while the *effective* field is used for the magnetic intensity. The coefficient a appearing in place of H_0 in the similar equation of approach to saturation of magnetization has been measured by Fallot,[12] who found that a varied between 5 and 24 for iron-silicon alloys. The values obtained depended entirely upon some unknown property of the specimen measured and not upon the silicon content. Hence, all that can be said about H_0 and a is that they are of the same order of magnitude.

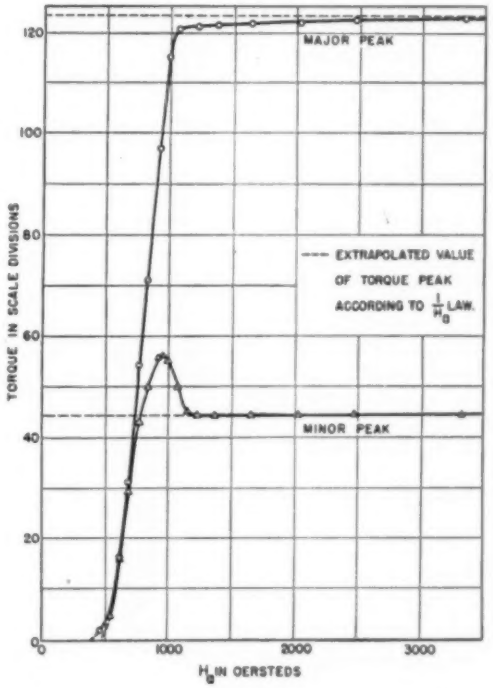

FIG. 5. Major and minor torque peaks of (110) ellipsoid plotted against magnetic field.

Before trying to reconcile this apparent similarity of the coefficients in spite of the difference

[10] Reference 3; also H. Mussmann and H. Schlechtweg, Ann. d. Physik [5] **32**, 290 (1938).

[11] A. Kussmann and E. Schoen, Physik. Zeits. **38**, 777 (1937).

[12] M. Fallot, Ann. de physique [11] **6**, 305 (1936).

between the meanings of H, an attempt was made to replot the torque data for one of the (100) disks on the basis of the effective field rather than the applied one. In order to get a linear approach to saturation using the effective field H, it was necessary to use a law of the form

$$T_H = T_\infty(1 - H_0'/H^n), \tag{3}$$

where n was very nearly equal to $\frac{1}{6}$. This equation is useless because neither n nor T_∞ can be obtained with any certainty from the data. Thus the only simple and easily obtainable equation that fits the torque data is the one involving the applied field. An examination of Fallot's data shows that it is equally hopeless to replot them on the basis of the applied field rather than the effective one and still retain a linear law; such a change, moreover, could not be justified theoretically.

The best explanation of the apparent similarity in the two laws of approach seems to be the following: The $1/H$ law for the approach to magnetic saturation holds only for polycrystalline material, where the direction of magnetization is averaged over all orientations, because it is known that the magnetization curves of a single crystal along the directions of easy magnetization do not conform to this law; instead, saturation is reached at very low fields for the [100] direction in iron, and in somewhat higher fields for the [110] direction. With the torque peaks, on the other hand, the direction of magnetization is along the same crystallographic direction within a few degrees, so that the magnetization along this direction may well approach saturation according to some other law than $1/H$. Since the magnitude of the torque peak is, among other things, proportional to the intensity of magnetization, it follows that the approach to saturation in torque will also follow this law. It seems, then, that the difference in crystallographic conditions between the two cases is accidentally balanced by the difference in the nature of the magnetic fields, i.e., applied or effective, leaving the laws formally the same and with coefficients of the same order of magnitude.

As has been mentioned, Schlechtweg's torque equations in $1/H_a$ predict a zero value for H_0 for the torque peaks of the (100) and (110) ellipsoids, and nonzero values for other orientations. For the two special orientations, H_0 was experimentally found to be in the neighborhood of 20, which appears to be an empirical constant of the material. It is probable that the torque peaks of an ellipsoid of some other orientation than (100) or (110) would have values of H_0 somewhat higher than this, the excess being given by Schlechtweg's theory.

Thus far, the discussion has been concerned only with ellipsoids. For disks, it is clear that the very much larger values of H_0 are associated with the difficulty of saturating their edges, i.e., the material outside the inscribed ellipsoid. This is in line with the results shown in Fig. 2. Probably a very small part of H_0 for a disk is to be attributed to the approach to magnetic saturation of the specimen as a whole, as in the case of the ellipsoids, but the important part is due to edge effects.

Conclusions

There are really three distinct $1/H_a$ laws for torque peaks. The first is Schlechtweg's theoretical one, which predicts an increase with field in the peaks of single crystal ellipsoids unless they are of the (100) or (110) orientation. Next, there is the experimentally determined $1/H_a$ law for (100) and (110) ellipsoids, which is attributed to the slow increase in magnetic saturation noticeable even in very high fields. And finally, there is the $1/H_a$ law observed for disks, for which H_0 is quite high because it is connected with the approach to saturation of the edges.

The usefulness of the $1/H_a$ law for disks lies in the fact that it makes possible the calculation of a unique value of the anisotropy constant, the one corresponding to $1/H_a = 0$, which does not depend upon the field used nor upon the dimensions of the specimen. The validity of the extrapolation to $1/H_a = 0$ has been satisfactorily checked by the measurements on two ellipsoids.

Ferromagnetic Anisotropy of Iron and Iron-Rich Silicon Alloys

L. P. TARASOV
Research Laboratory, General Electric Company, Schenectady, New York
(Received September 14, 1939)

The ferromagnetic anisotropy constant K_1 has been accurately measured by the magnetic torque method for a group of iron alloys containing up to 13.7 atomic percent silicon. The points fall on two intersecting straight lines given by the equations:

$$K_1\times10^{-5}=5.29-0.279A \qquad A<9.86$$

and

$$K_1\times10^{-5}=4.43-0.1915A \qquad A>9.86$$

K_1 is expressed in ergs/cm³ and A is the atomic percentage of silicon. The value for iron is considerably higher than the one due to Akulov which has often been quoted in the literature. It is shown that the latter is unreliable because it is an average value based on the highly discordant results of several investigators. Torque measurements were made on the identical ellipsoid of iron for which Piety measured the magnetization curves along the simple crystallographic directions and a large discrepancy was found between the values of K_1 calculated by these two methods. This leads to the belief that the present-day theory of ferromagnetic anisotropy is in need of some revision, possibly in connection with the higher order terms in the magnetic energy equation. When K_1 is plotted against the atomic percentage of silicon, the change in slope occurs at very nearly the same concentration as the similar change in slope found by Jette and Greiner for the lattice parameter a_0. An attempt is made to explain the occurrence of these breaks in terms of a change from a hypothetical superlattice with a silicon concentration of 3/32 to a partially formed Fe_3Si superlattice.

INTRODUCTION

A KNOWLEDGE of the ferromagnetic anisotropy of iron-silicon alloys is useful from both the practical and the theoretical points of view. The study of the preferred orientations of the grains of cold-rolled strip has its greatest importance in connection with transformer steels, which contain up to 6 percent by weight of silicon. Any thorough investigation of this texture by the magnetic torque method requires some knowledge of the anisotropy constant, to which the measured torque is directly proportional.[1]

The variation of the anisotropy constant with silicon content is also of interest in connection with the known anomalous behavior of the alloys in the α solid solution range.[2] Several investigators have measured the anisotropy of iron, the most recent work being done on material of high purity, and others have measured the anisotropy of individual iron-silicon alloys. The results on iron have been in poor agreement with each other. As for the iron-silicon alloys, all that could be said was that the anisotropy constant decreased rapidly with the addition of silicon.

Four methods of determining the anisotropy are available, three of which are described in a single article by Williams.[3] These are magnetic torque studies, the measurement of the areas between magnetization curves along various simple crystallographic directions, and the comparison of the shapes of the magnetization curves with the theoretically predicted ones. The fourth method involves the direct measurement of the normal component I_n of the magnetization by means of a suitable search coil, as was done by Honda and Kaya.[4] The derivation of the anisotropy constant from such measurements is described by Bitter.[5]

For simplicity, it has been tacitly assumed in the foregoing that there is only a single anisotropy constant. Actually, the experimental data may require more than one such constant, as has been shown by Bozorth.[6] For cubic lattices, the first two anisotropy constants, K_1 and K_2, are defined by the equation

$$E=K_0+K_1(\alpha_1^2\alpha_2^2+\alpha_2^2\alpha_3^2+\alpha_3^2\alpha_1^2)+K_2\alpha_1^2\alpha_2^2\alpha_3^2, \quad (1)$$

where E is the energy of magnetization in a given

[1] L. P. Tarasov, J. App. Phys. **9**, 192 (1938); and Trans. A. I. M. E. **135**, 353 (1939).
[2] E. R. Jette and E. S. Greiner, Trans. A. I. M. E. **105**, 259 (1933); and M. Fallot, Ann. de physique [11] **6**, 305 (1926).
[3] H. J. Williams, Phys. Rev. **52**, 747 (1937).
[4] K. Honda and S. Kaya, Sci. Rep. Tôhoku Imp. Univ. **15**, 755 (1926).
[5] F. Bitter, *Introduction to Ferromagnetism* (McGraw-Hill, 1937) p. 201.
[6] R. M. Bozorth, Phys. Rev. **50**, 1076 (1936).

direction, and the α's are the cosines of the angles between this direction and the cubic axes; along these axes, K_0 is the energy of magnetization. In the case of iron and iron-silicon alloys, it is fortunate that at room temperature the effect of K_2 upon the results is quite small compared with that of K_1. Were this not so, it would be very difficult to use torque data in studying the texture of polycrystalline material. When torque measurements are used to determine the form of the anisotropy, it is found from considerations of symmetry that for a disk having (100) lying in its plane only K_1 appears in the equation of the torque curve; but if (110) lies in the plane of the disk, K_2 also has to be taken into account. Since the measurements reported below were mostly on (100) disks, information was obtained in those cases only about K_1, which will generally be referred to as the anisotropy constant without further qualification.

The rest of this paper can be conveniently divided into three parts. The first of these describes the experimental work on iron and iron-silicon alloys done by the writer. The next part is a critical discussion of the discrepancies between these results and the ones that have been previously reported, especially for unalloyed iron. In the last part, the anisotropy data obtained for the iron-silicon alloys are compared with other types of data in an attempt to find some reasonable interpretation of certain discontinuities that have been observed in the α solid solution range.

Part I

Specimens

The specimens were single crystal disks of iron containing various percentages of silicon and cut so as to have either a (100) or a (110) plane parallel to the plane of the disk. The single crystals were prepared[7] by melting the required proportions of electrolytic iron and the 90 percent grade of ferrosilicon in small beryllia crucibles in an atmosphere of hydrogen. The ingots were made to solidify as large crystals by lowering the crucibles at a suitable rate through a vertical tube furnace. Slabs of the desired orientation, as determined by x-rays, were cut from the large crystals and from these slabs disks were ground about $\frac{1}{2}$ inch in diameter and from 0.020 to 0.035 inches in thickness. The disks were polished and slightly etched to make certain of their monocrystalline nature.

After a set of torque measurements had been made on the disks in this condition, they were etched more deeply to remove any surface material that was deformed during the grinding and polishing operations; following this, they were annealed for 2 hours at 1100°C in pure dry hydrogen and were then furnace cooled. A surface etch showed that the disks were still single crystals and did not contain any small included grains. The anisotropy data on the iron-silicon alloys were obtained, with one exception, from the torque measurements made on these annealed disks. The exception was a disk that was filed into an ellipsoid of revolution[8] and then annealed like the others. It may be mentioned here that the effect of annealing was usually, but not always, to increase K_1 by 1 or 2 percent.

When all the torque measurements had been completed, the disks were cut into several pieces which were analyzed individually for silicon with a probable error of 0.02 weight percent. This was necessary because in some instances the silicon had not diffused uniformly throughout an ingot, so that considerable variations in the silicon content existed within a single disk. Only those disks were used in the final calculation of the variation of K_1 with silicon content for which the analyses of the separate portions agreed within 0.1 percent of silicon.[9] These individual analyses were suitably averaged to give the effective composition of the specimens.

The carbon content of the original ingots varied from 0.02 to 0.04 percent, a range that can be accepted as substantially correct for the disks themselves since the only two disks that were anlyzed for carbon gave results in good agreement with those for the corresponding ingots. The 2-hour anneal at 1100°C probably

[7] The work up to and including the grinding of the properly oriented disks was done by Dr. K. J. Sixtus.

[8] This was done at the Massachusetts Institute of Technology through the kindness of Dr. A. R. Kaufmann; the same holds for the measurement of the torque peaks of this ellipsoid for the purpose of calibrating the writer's torquemeter suspension in absolute units.

[9] Unless otherwise stated, weight percent is meant throughout the paper.

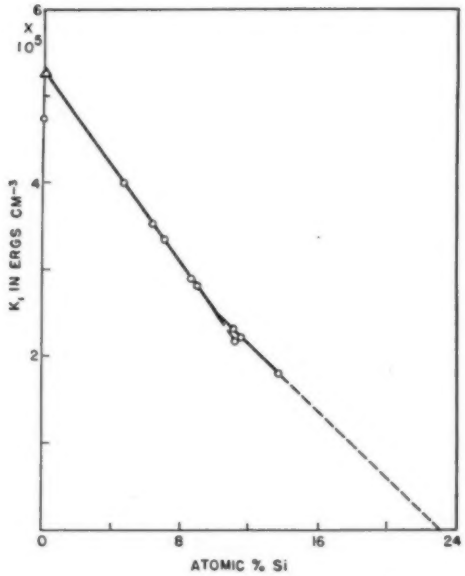

FIG. 1. Anisotropy constant K_1 plotted as a function of atomic percentage of silicon.

did not decrease the carbon that was present because the hydrogen was dry whereas moist hydrogen is required for the reduction of the last traces of carbon. In addition to carbon, other impurities must have been present since the 90 percent ferrosilicon from which the alloys were made is known to contain 1 to 3 percent of total impurities other than iron, mostly aluminum together with some calcium and a little titanium.[10] Unfortunately, these impurities were not analyzed for and all that can be said is that the disks contained these additional impurities to the extent of 1 to 3 percent of the silicon content.

Besides these iron-silicon disks, two ellipsoids of high purity iron were measured on the magnetic torquemeter. They were the identical ellipsoids used by Piety[11] in 1936 in studying the anisotropy constants of iron at several temperatures, and were measured in the condition in which they were left at the conclusion of his work.

[10] According to Table 4, p. 19, *Alloys of Iron and Silicon* by E. S. Greiner, J. S. Marsh and Bradley Stoughton (McGraw-Hill, 1932).

[11] R. G. Piety, Phys. Rev. **50**, 1173 (1936). One of the ellipsoids measured by the writer was the one identified as *P*10, having (110) in the equatorial plane; the other one was the (100) ellipsoid, which Dr. Piety did not test sufficiently to enable him to calculate K_1. The second (110) ellipsoid used by Dr. Piety, *P*12, had been destroyed prior to the present investigation.

Magnetic torque measurements

The magnetic torque curves from which the anisotropy constants were calculated were obtained on the torsion-type torquemeter described elsewhere by the writer.[12] The measurements consisted of the four peaks of the torque curve, each taken at six different values of the applied magnetic field H_a, which were suitably spaced between 2000 and 3500 oersteds. The peaks were plotted against $1/H_a$ and extrapolated to $1/H_a=0$, for it has been established[12] that the correct values of the anisotropy constants are obtained in this manner, regardless of whether the specimen investigated is an ellipsoid or a disk. The calibration of the torquemeter suspension in absolute units and the necessary corrections to the measured values of the peaks are described in this same reference; and the curves there shown for the variation of torque with $1/H_a$ are representative of the ones from which the anisotropy data were derived. When the iron ellipsoids were measured, it was necessary to replace the usual 32-mil phosphor bronze suspension wire with one 20 mils in diameter, in order to increase the sensitivity sufficiently to compensate for the extremely small size of the specimens.

The torque peaks were accurately reproducible and the values obtained by a linear extrapolation to $1/H_a=0$ are unlikely to be in error by more than 0.5 percent. When K_1 is plotted as a function of the silicon content as in Fig. 1, the possible errors in the two coordinates are of the same size.

Calculation of anisotropy constants

It should be mentioned here that the specimens were not all perfectly oriented, i.e., the (100) or (110) plane did not lie exactly in the plane of the disk. Since the orientation was known to within a degree from x-ray pictures obtained by the back-reflection Laue method, it was possible in each case to calculate the corresponding change in the magnitude of the torque peaks by using the equations for the coefficients of the torque equation as given by Tarasov and Bitter.[13]

[12] L. P. Tarasov, Phys. Rev., this issue, preceding paper. ("Dependence of Ferromagnetic Anisotropy on the Field Strength.")

[13] L. P. Tarasov and F. Bitter, Phys. Rev. **52**, 353 (1937).

The torque equation for disks which are nearly of the (100) type reads in the notation of this reference,

$$T=(K_1/2)(A_1 \sin 2\theta+A_2 \sin 4\theta), \qquad (2)$$

the term in K_2 being negligibly small, as are the coefficients B_1 and B_2 of the cosine terms. A_1 is zero for the perfect (100) orientation and quite small for orientations close to it. In the latter case its only effect is to increase slightly two of the four torque peaks and decrease the other two, so that the average of the four peaks remains exactly equal to $\frac{1}{2}K_1A_2$. The error introduced by the uncertainty in A_2 is negligible in comparison with other errors.

The situation is considerably more complicated for disks of the (110) type because K_2 affects the torque curve most for just this orientation, and lengthy computations are necessary if the disks deviate from this ideal orientation. It is experimentally impracticable to extrapolate the whole torque curve to $1/H_a=0$ because the nature of the extrapolation has been determined only for the peaks. For this reason, instead of finding the values of K_1 and K_2 to give the best fit for the entire curve, they were chosen to agree with the extrapolated values of the peaks. The results in the two cases would be the same only if the anisotropy can be represented sufficiently well by two constants; otherwise, a slight difference in K_1, and a considerable one in K_2, could arise. These constants were calculated from the extrapolated values of the torque peaks with the help of these equations:

$$K_1=1.155C_1-0.693C_2$$

and

$$K_2=-2.553C_1+6.795C_2. \qquad (3)$$

Here C_1 is the sum of the *magnitudes* of the two major peaks and C_2 of the two minor peaks. Eq. (3) is valid only for K_1 positive and K_2 not too large; with certain changes of sign, it would hold for K_1 negative.

The volumes of the disks, required for expressing the anisotropy in the customary ergs/cm³, could not be determined with sufficient accuracy by direct measurement; instead, they were obtained from the weights and densities of the disks, the latter having been calculated from the lattice parameters of the iron-silicon alloys. The

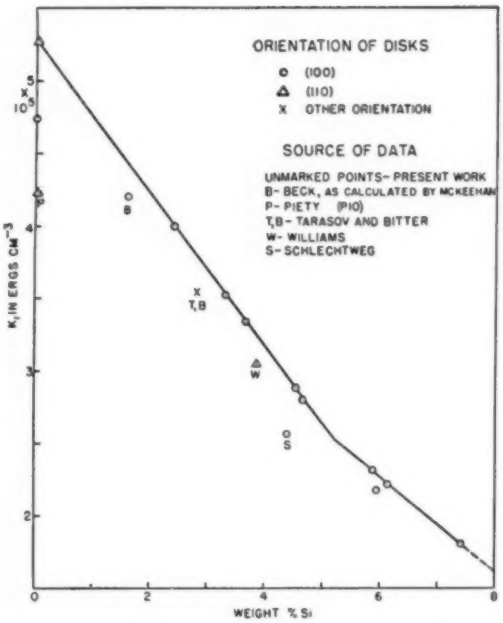

FIG. 2. Same points as in Fig. 1, replotted against the weight percentage. Results of previous investigations are included.

reason for not using measured densities was the possibility of fairly large errors arising from voids and imperfections likely to occur in cast material that had never been subjected to any mechanical treatment. The lattice parameters as given by Jette and Greimer[2] fall quite well on two intersecting straight lines when plotted against the atomic percentages A of silicon. The equations of the two lines as calculated by least squares are:

$$a_0=2.8610-0.000723A, \quad A<9.55,$$

and

$$a_0=2.8744-0.002130A, \quad A>9.55, \qquad (4)$$

where a_0 is the lattice parameter in angstrom units. When 28.06 and 55.84 are taken as the gram-atomic weights of Si and Fe, the densities are also found to fall on two intersecting straight lines, which are given by

$$\rho=7.864-0.0332A, \quad A<9.55,$$

and

$$\rho=7.767-0.0232A, \quad A>9.55. \qquad (5)$$

The volumes of the disks were derived according to Eq. (5) from the densities corresponding to the proper compositions.

Variation of K_1 with silicon content

The anisotropy constants of a number of iron-silicon single crystal specimens and of two high purity iron ellipsoids were calculated in the foregoing manner. The values of K_1 at 25°C are plotted in Fig. 1 against the atomic percentage of silicon. Of the fourteen disks originally available, five were rejected for too great a variation in silicon content, for too great a deviation from the ideal orientation, or for surface or edge defects. Including the two ellipsoids of iron, there are eleven experimental points, of which six fall on one straight line, three on an intersecting one, while the other two points fall below the solid lines. The equations of the two lines, as calculated by least squares, are:

$$K_1\times10^{-5}=5.29-0.279A, \quad A<9.86,$$

and

$$K_1\times10^{-5}=4.43-0.1915A, \quad A>9.86. \quad (6)$$

The atomic rather than the weight percentage is theoretically preferable for the usual physicochemical reasons when dealing with solutions. A linear extrapolation, not to be taken too seriously, shows that K_1 becomes zero at 23.1 atomic percent or 13.1 weight percent of silicon.

For general use, it is more convenient to plot K_1 against weight percent, as is done in Fig. 2. It happens that the points still lie on two straight lines because of the near-linearity existing between the atomic and weight percentages in the two ranges of composition separated by the intersection of the straight lines. The equations of the lines in terms of the weight percentage W are:

$$K_1\times10^{-5}=5.29-0.532W, \quad W<5.20,$$

and

$$K_1\times10^{-5}=4.21-0.324W, \quad W>5.20. \quad (7)$$

Returning to Fig. 1, it is important to note that the break in slope there shown cannot be ascribed to the break which occurs in the density curve at about the same composition. If the original torque data are used to get the anisotropy constant in terms of ergs/g so that density values are not required, the results still plot as two intersecting straight lines and the break is of very nearly the same magnitude as that shown in Fig. 1. This, of course, arises from the very much slower decrease of density than of anisotropy with increasing silicon content.

Those points in Fig. 2 which were measured in the present investigation are only for the etched and annealed specimens since the results obtained before such treatment were not as consistent. The two points (unmarked circles) that do not fall on the curve are shown because there was no experimentally justifiable reason for rejecting them. The higher of the two points for iron is thought to be more likely the correct one since it lies exactly on the extrapolated portion of the straight line passing through the other points. The definitely lower value for the (100) ellipsoid of iron must be attributed to some unknown factor and not to experimental error, and the same is probably true of the other point, for which the discrepancy is much less.

The anisotropy of iron has been investigated by others much more thoroughly than that of the iron-silicon alloys, and it will be discussed in considerable detail in Part II of this paper. This is necessary because the values in the literature differ greatly among themselves and the generally quoted value of 4.3×10^5 ergs/cm^3 for K_1 does not agree at all with 5.29×10^5 as found in the present study.

Part II

Previous work on iron

The first work from which ferromagnetic anisotropy can be calculated was that by Beck,[14] whose experiments were carried out on iron containing 1.62 percent silicon. Webster[15] made torque measurements on (100) single-crystal disks whose composition approached a little closer to that of pure iron. Sufficient amounts of C, S, Si, Mn and P were present to classify the specimens as low-carbon steel rather than iron. Disk *A* contained 0.220 percent P, an abnormally high amount; while disk *B*, which was annealed in hydrogen so that the carbon was reduced to a small but unknown percentage, had a typical low-carbon steel composition, containing about 0.4 percent Mn. Shortly afterward, Honda and

[14] K. Beck, Vierteljahrsschrift der naturforschenden Gesellschaft in Zürich **63**, 116 (1918). The data are discussed in a more available publication by L. W. McKeehan, Trans. A. I. M. E. **111**, 11 (1934).

[15] W. L. Webster, Proc. Roy. Soc. **A107**, 496 (1925).

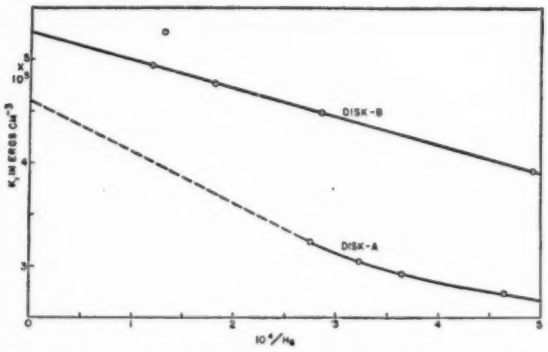

FIG. 3. Webster's original data for single crystals of iron plotted against $1/H_a$ to show the extent to which his results can be reliably used in deriving the value of K_1.

co-workers[4, 16] prepared specimens of iron of somewhat greater purity, the analysis being 0.40 percent Mn, 0.021 S, 0.021 P and a trace of Si. Carbon was practically eliminated by decarburizing four days in moist hydrogen. The ellipsoids prepared by Piety[11] were of very much greater purity than any of the preceding, containing less than 0.1 percent of total impurities. The provisional limit of 0.03 percent Si given by Piety was used in plotting the points for iron in Figs. 1 and 2.

Let us first consider the data obtained by Webster using the torque method. These data are listed by Mahajani,[17] who averaged the results to get $K_1=4.66\times10^5$ for disk B and 2.98×10^5 for disk A. If the same points are plotted against $1/H_a$ as in Fig. 3, it is evident that disk B obeys the $1/H_a$ law[12] to a high degree of precision except for one point which is clearly in error. On the other hand, disk A does not follow this law, possibly on account of its abnormal phosphorus content. The values of K_1 obtained by extrapolating to $1/H_a=0$ are 5.26×10^5 for B and 4.60×10^5 for A. The extrapolation for the latter is, of course, merely suggestive and it is possible that the broken line should rise even higher. The curves of Fig. 3 prove beyond question that Mahajani's averaging process leads to low values of K_1. The good agreement between the recalculated value of K_1 for disk B and the value found by the author for the (110) ellipsoid of iron is probably fortuitous, in view of the differences in composition. Still, this agreement is of interest in that it furnishes evidence for a considerably higher value of K_1 than has generally been assumed to occur.

A value calculated by Akulov,[18] 4.28×10^5, has been repeatedly cited in the literature. Taking the magnetization curve data published by Honda and Kaya,[4] Akulov obtained five separate values of K_1, varying from 4.84 to 3.34 and whose average was 4.22. (For convenience, a factor of 10^5 has been omitted.) In a separate calculation, some data from the same source involving the maximum value of I_n, the normal component of magnetization, gave values of 4.94 and 4.48; and when these were combined with the previously mentioned calculations by Mahajani[17] (which have been shown to be much too low), the much quoted value of 4.28 was obtained. The large discrepancies between individual values, the experimental uncertainties inherent in much of the original data, and the error introduced by using Mahajani's average values are the factors that make these values given by Akulov unacceptable. But the fact that some of the individual values are quite high compared to the averages again shows that the value of K_1 found in the present investigation should not be considered unusually high.

K_1 as measured by two methods

Piety[11] made some very careful measurements of the magnetization curves of two (110) ellipsoids and from these calculated K_1 to be 4.23 and 4.38×10^5 ergs/cm³ for specimens $P10$ and $P12$, respectively. (His original results have been corrected slightly to bring them to the standard temperature of 25°C used in this paper.) The previously described torque measurements on $P10$ showed that K_1 was 5.27 instead of 4.23, a difference far greater than could be attributed to any experimental errors. $P12$ was not available for a similar comparative study.

A comparison of the two methods of evaluating K_1 was also made with the (100) iron ellipsoid, for which K_1 was 4.74 according to torque measurements and 4.66 ± 0.30 when derived from the area between the magnetization curves.[19] The

[16] K. Honda, H. Masumoto and S. Kaya, Sci. Rep. Tôhoku Imp. Univ. **17**, 111 (1928).
[17] G. S. Mahajani, Phil. Trans. Roy. Soc. **A228**, 63 (1928).
[18] N. S. Akulov, Zeits. f. Physik **57**, 249 (1929).
[19] These magnetization curves were measured by Dr. E. M. Grabbe at Yale University in the same manner as Dr. Piety had previously measured the (110) ellipsoids. The considerable uncertainty in K_1 was due to the instability of the magnetic field at high intensities in the apparatus used by Dr. Grabbe.

large probable error unfortunately makes it impossible to say whether or not the two values of K_1 are in good agreement.

The only other work in which K_1 has been determined with satisfactory accuracy by more than one method on a single material is that reported by Williams,[3] who worked with iron containing 3.85 percent Si. He obtained 2.72 and 2.80×10^5 for K_1 by two different methods of utilizing magnetization curve data. The torque data for a (110) disk gave 2.87, but this value is raised to 3.05 by a rough extrapolation to $1/H_a=0$. Here again K_1 is appreciably higher when obtained from torque measurements instead of from magnetization curves.

This suggests that the present-day theory of ferromagnetic anisotropy is in need of some revision because the magnitude of K_1 seems to depend upon the method by which it has been determined. One possibility is that the discrepancies would disappear if higher order energy terms were used in Eq. (1).

In one respect, it seems quite reasonable that K_1 should be at least slightly different in the two cases. When it is deduced from the area between the magnetization curves along the ⟨100⟩ and ⟨110⟩ directions, the two curves come together for an applied field of perhaps 2000 oersteds, taking the case of the iron ellipsoids used by Piety. The area from which K_1 is determined is thus definitely fixed. The torque data taken on the same specimen at this field strength must be increased by about one percent to take care of the necessary extrapolation to $1/H_a=0$, so that a discrepancy of this amount can be expected between the values obtained by the two methods. This increase in the torque for an ellipsoid, which is probably connected with the observed slow increase of the saturation intensity of magnetization,[12] cannot explain the much larger discrepancies that have been mentioned.

K_1 for iron-silicon alloys

The values of K_1 for four iron-silicon alloys that have been recorded in the literature[3, 13, 14, 20] are included in Fig. 2. Where necessary, the values have been extrapolated as well as possible to $1/H_a=0$. Although Beck[14] made torque measurements on disks, these data were not available in suitable form for the calculation of K_1, and the point shown is that calculated by McKeehan from Beck's magnetization curves. The other three points were derived from magnetic torque studies. These points fall from 5 to 13 percent below the straight line representing the results of the present work. In view of the discrepancies between the present results and the previous ones, it appears that although the anisotropy constants depend mostly upon the composition, certain unknown factors have an appreciable influence. The very good linear relationship that was found to hold for the iron-silicon alloys should be ascribed to the identical history of the specimens involved.

It may be well to mention here Zaimovskii's[21] indirect determination of K_1 for a group of iron-silicon alloys, since this reference is the only one listed in *Gmelins Handbuch*.[22] His values are very much lower than those shown in Fig. 2, but they can be omitted from consideration because his indirect method was later shown[23] to be without foundation.

Significance of K_2

A few scattered values of K_2 were available from torque measurements on (110) specimens and some results have been reported in the literature. They are tabulated in Table I, and it is clear that no relationship can be set up between K_2 and the composition. The lack of any regularity either is a further indication that the form of the correction to the fourth power term of the anisotropy is more complicated than has been assumed, or it shows that K_2 is very sensitive to the condition of the specimen.

TABLE I. *Values of K_2 from torque measurements.*

PERCENT Si	$K_2\times10^{-6}$	COMMENTS
None	1.4	*P*12, measured by Piety.
None	−1.7	*P*10, measured by Piety.
None	−3.0	*P*10, torque data.
3.0	−0.13	Si content in doubt.
3.85	1.0	As measured by Williams.
4.6	−0.9	Not exactly a (110) disk.
5.9	−0.3	Defective edge, Si only approximate.

[20] H. Schlechtweg, Ann. d. Physik [5] **27**, 573 (1936).

[21] A. S. Zaimovskii, Katchestvennaia Stal **1**, No. 6, p. 35 (1935).

[22] *Gmelins Handbuch* (8th ed., 1936), Eisen, Part D, p. 15.

[23] W. S. Messkin and B. E. Somin, Zeits. f. Physik **98**, 610 (1936).

Conclusions

The results show that under carefully controlled experimental conditions it is possible to obtain values of K_1 which vary in a regular manner with silicon content, but at the same time occasional discrepancies are to be expected, whose cause is unknown at present. Measurements of the anisotropy using two different methods on the same specimen indicate that the theory may require some revision, and until this is done, it may be necessary to distinguish between the anisotropy constants obtained from torque studies and those obtained from magnetization curves.

Part III

Discontinuities in properties in the α-phase iron-silicon alloys

Although the phase diagram of the iron-silicon system shows that the α solid solution phase extends at room temperature to about 26 atomic percent of silicon, a number of puzzling discontinuities in physical properties have been observed in this range which are difficult to interpret in terms of a single phase.

The discontinuity in the slope of the lattice parameter curve at 9.55 atomic percent of silicon and the similar change in slope for K_1 at 9.86 atomic percent have already been described. Fallot[2] made a comprehensive study of the variation with silicon content of certain magnetic properties and correlated his discontinuities with various superlattices which he proposed. He found that the curve of magnetic moment against atomic percentage showed sudden changes in slope at fractional silicon concentrations of $\frac{1}{16}$, $\frac{1}{8}$ and $\frac{1}{4}$; that the same was true of the Curie temperature; while the curve of σ_0/σ_{290}, σ being the saturation intensity corresponding to the absolute temperature indicated by the subscript, consisted of two distinctly separated parallel parts, with the break occurring at 12.5 atomic percent. However, the Curie temperature can just as well be replotted to show other discontinuities and hence cannot be used as the basis of any argument. Finally, from a practical point of view, it has long been known that silicon steels containing more than 5 weight percent Si are brittle and that discontinuities in other mechanical properties are observed at lower percentages,[24] but so many variables are always present that a really satisfactory explanation has never been developed.

As to the relative trustworthiness of the various phenomena, the most dependable discontinuities are those shown by a_0 and by σ_0/σ_{290}, but to make matters difficult, each of these has only one discontinuity between 0 and 25 atomic percent and these occur at unmistakably different concentrations. The break observed in the slope of the K_1 curve is pronounced enough to corroborate the existence of some peculiarity in the iron-silicon system in the neighborhood of 9.5 atomic percent.

Since the behavior of a_0 is accurately known to the limit of solid solubility at 26 atomic percent while K_1 has been studied only half as far, and because it is easier to picture changes in a_0 than in K_1 when changes occur in atomic distribution, the subsequent discussion will center on the lattice parameter. In view of the very nearly identical compositions at which the discontinuities occur in a_0 and K_1, it appears reasonable to assume that the same explanation holds for both. A more detailed interpretation of the observed behavior of K_1 must wait until more is known both about the atomic arrangements in this range and about their possible effect upon the anisotropy.

Interpretations of the discontinuities in a_0

Phragmén[25] found that the silicon atoms in a thoroughly homogenized alloy containing 25 atomic percent silicon were substituted in a regular manner for the iron atoms in the body-centered cubic lattice of the latter. The superlattice cell is a cube, $2a_0$ on the side, where a_0 always refers to the size of the unit cell of the iron lattice. The silicon atoms are arranged tetrahedrally at the alternate corners of a small cube, as shown in Fig. 4, reproduced from Jette and Greiner's paper.[2] The superlattice has been detected by x-rays in alloys containing as little as 13 atomic percent silicon. Jette and Greiner interpret the data as showing that at 12.5 atomic percent every superlattice cell has two of the

[24] E. S. Greiner, J. S. Marsh and Bradley Stoughton, *Alloys of Iron and Silicon* (McGraw-Hill, 1932), p. 75.
[25] G. Phragmén, J. Iron and Steel Inst. **114**, 397 (1926).

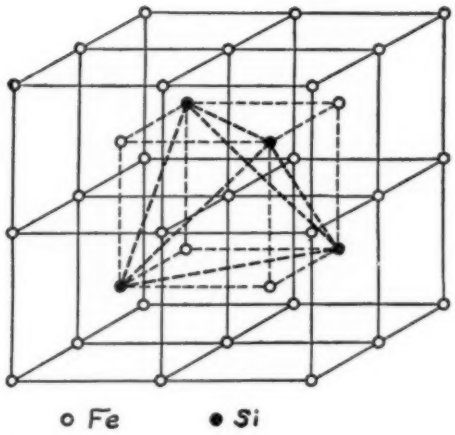

FIG. 4. Fe_3Si superlattice. (Jette and Greiner, reference 2).

tetrahedron corners occupied by the available silicon atoms, and that as the concentration increases, the iron atoms at the other corners of the Fe_3Si tetrahedron are progressively replaced by the silicon atoms.

Below 12.5 atomic percent, they offer two related hypotheses in an attempt to account for the sudden change of slope in their lattice parameter data. According to hypothesis *A*, up to 6 atomic percent the alloy would be a solid solution of silicon in iron; from 9 to 25 atomic percent, it would be a solid solution of iron in Fe_3Si; and in between, it would be a mixture of the two solid solutions. According to hypothesis *B*, there is only a single phase in the whole range, the alloys being disordered below 9 atomic percent and ordered above. The original article must be referred to for a complete discussion of the two hypotheses, neither of which could be proved or disproved. The important thing is that according to either hypothesis, the break in the vicinity of 9 atomic percent is associated with the formation of a superlattice. The picture that is offered is that at a silicon concentration of $\frac{3}{32}$, i.e., 9.375 atomic percent, one-half of the eventual superlattice cells have only one corner of the tetrahedron occupied by a silicon atom, and the other half have two corners thus occupied. For lower concentrations, not enough silicon atoms are present to create this partial superlattice. This picture is not very convincing because it is assumed that two forms of an incomplete superlattice can coexist; moreover, this picture does not even attempt to "explain" why the superlattice should first appear at such an unorthodox concentration.

An alternative interpretation

Since a superlattice has to be admitted into any discussion of the α solid solution range, a somewhat different hypothesis was developed to serve not only as a picture, but also as an "explanation" of the breaks in a_0 and K_1. Although this hypothesis, like those already described, is of an admittedly *ad hoc* nature, it is offered because it seems plausible and can perhaps be subjected to experimental check.

It is first necessary to describe the superlattice which is supposed to exist at a silicon concentration of $\frac{3}{32}$. There is no x-ray evidence for such an atomic arrangement, but that can be overlooked for the present since the other hypotheses were built on an equally weak foundation. We first consider the usual body-centered arrangement of iron atoms and take as the unit a cube $2a_0$ on a side. If the iron atom at the center of this unit is replaced by a silicon, and the same is done with respect to the iron atoms at the *alternate* corners of the unit, the silicon concentration will be $\frac{3}{32}$ and the silicon atoms will be arranged in a large tetrahedron with a silicon atom at its center. The closest Si−Si distance is $\sqrt{3}a_0$ and the next closest $2a_0$. Eight such units are required for a complete unit cell of the superlattice, which thus contains 116 Fe and 12 Si atoms and is a cube $4a_0$ on a side. The projection of this superlattice cell on a cube plane is shown schematically in Fig. 5.

The observed breaks in the slopes of a_0 and K_1 are then explained in the following manner: For lower concentrations than $\frac{3}{32}$, the silicon atoms are assumed to be arranged at random, but as their concentration is increased the lattice positions taken by the silicon atoms tend to approximate more and more the $\frac{3}{32}$ superlattice just described. At $\frac{3}{32}$, the superlattice is completely formed, but at a higher concentration too many silicon atoms are present for this superlattice. Possibly the interatomic forces between the silicon atoms become great enough, on account of the excess of such atoms, to bring them closer together than $\sqrt{3}a_0$ allowed by the large tetrahedron. The atoms then go into lattice positions consistent with the Fe_3Si superlattice shown in

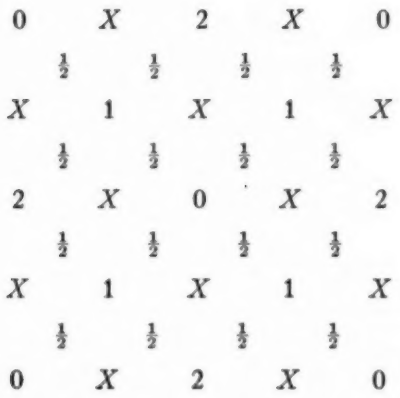

FIG. 5. Projection on cube plane of unit cell of superlattice, proposed to account for sudden changes in slope of the curves of lattice parameter and of K_1 occurring near a $\frac{3}{32}$ atomic concentration of silicon in iron. The unit cell of this superlattice, whose edge is four times that of the iron lattice, contains 12 atoms of silicon and 116 of iron. z is the third coordinate, expressed in units of a_0, the lattice parameter of iron.

Symbol	*Interpretation*
½	$z=\frac{1}{2}, \frac{3}{2}, \frac{5}{2} \cdots$; always Fe.
X	$z=0, 1, 2 \cdots$; always Fe.
0	Si if $z=0, 4, 8 \cdots$; otherwise Fe.
1	Si if z is odd; otherwise Fe.
2	Si if $z=2, 6, 10, \cdots$; otherwise Fe.

Fig. 4. In other words, the large tetrahedron of silicon atoms containing a silicon at its center collapses into a much smaller and incomplete tetrahedron, the shortest Si−Si distance changing from $\sqrt{3}a_0$ to $\sqrt{2}a_0$.

This picture, although artificial, is quite consistent with the observed variation in the lattice parameter. Up to a concentration of $\frac{3}{32}$, or possibly slightly higher, a_0 decreases slowly with the addition of silicon since the silicon atoms, which are somewhat smaller than the iron ones, are far apart. Above this concentration, the shortest Si−Si distance suddenly drops and the small Si atoms become much more effective in reducing a_0.

The objection to this picture, that a superlattice has not been detected by x-rays for alloys containing less than 13 atomic percent silicon, can now be briefly considered. Since at such low concentrations as $\frac{3}{32}$ the silicon atoms are spaced fairly far apart and since the unit cell of the superlattice is $4a_0$ on a side, it is easily conceivable that only short-distance order exists, such as cannot be detected by x-rays. A similar statement would hold for concentrations between $\frac{3}{32}$ and $\frac{1}{8}$, where only the beginnings of a Fe_3Si superlattice are supposed to exist. Another possible objection to the hypothetical $\frac{3}{32}$ superlattice is that the arrangement of the silicon atoms is not in accord with the accepted ideas of the silicon bonding. In answer to this, it should be pointed out that silicon in a metal lattice may behave entirely differently than when in a different type of compound. Incidentally, the same objection was unsuccessfully raised to the Fe_3Si tetrahedron when it was proposed.

As has already been pointed out, Fallot's results are irreconcilable with the ones obtained for a_0 and K_1. Since nothing is known about any relationship between superlattices and the magnetic properties reported by him, Fallot's results cannot at present be considered as contradicting the explanation offered for the sudden changes in slope in the case of the lattice parameter and the anisotropy constant.

ACKNOWLEDGMENTS

The writer wishes to express his appreciation to Professor L. W. McKeehan for making available the iron ellipsoids, and to the others mentioned in the body of the paper for the material assistance they rendered.

LETTERS TO THE EDITOR

Prompt publication of brief reports of important discoveries in physics may be secured by addressing them to this department. Closing dates for this department are, for the first issue of the month, the eighteenth of the preceding month, for the second issue, the third of the month. Because of the late closing dates for the section no proof can be shown to authors. The Board of Editors does not hold itself responsible for the opinions expressed by the correspondents.

Communications should not in general exceed 600 words in length.

Fast Neutron Measurements with Recoil Counters

For certain purposes it is convenient to have counters which respond to fast neutrons only. Proportional counters,[1] with gases other than BF_3, may be used to count recoil nuclei. A fast neutron may collide with one of the nuclei of the gas in the counter, and will then produce a recoil nucleus which will in general ionize heavily along a comparatively short range. If the counter be operated at a voltage below its threshold then the size of the pulse arriving on the central wire will be proportional to the number of ions formed in the counter by the passage of the ionizing particle. By adjusting the amplifier to discriminate against pulses below a certain size, or by adjusting the voltage applied to the counter and hence the amount of additional ionization produced by each ion as it travels toward the central wire, it is possible to count only particles producing more than a certain number of ions. In this way a counter may discriminate against pulses produced by beta- or gamma-rays. Such a counter will have a background due to the alpha-rays emitted by the natural contamination, which can easily be measured and allowed for.

The counting rate, n counts per second, of a fast neutron recoil counter will be a measure of the current $i(v)$ of fast neutrons per cm² per sec. of velocity v passing through the counter, as given by:

$$n = VNMp\int_{v_{\min}}^{\infty} i(v)\sigma_r(v)dv, \qquad (1)$$

where N is the Loschmidt number, p is the gas pressure in the counter in atmospheres, M is the number of nuclei per molecule, V is the volume of the counter, σ_r is the cross section of the nuclei of the gas in the counter for the production of recoils of energy $E > E_{\min}$, where $E_{\min}$ is the smallest amount of energy which, if liberated as ionization in the counter, will produce a count, and $v_{\min}$ is the velocity corresponding to $E_{\min}$. This latter quantity can be determined experimentally for a given counter at a given voltage by observing the response to rays of different known ionizing powers. The above relation neglects wall effects and end corrections, which for certain cases can be shown to be unimportant.

In a specific example, Fig. 1 shows the counting rate of such a counter, with a hydrogen-methane filling when operated in the presence of a Ra-Be neutron source. It will be seen that at low voltages (1450 volts) the most heavily ionizing of the recoils produces pulses just big enough to record. As the voltage is increased the number of additional ions produced in the counter is increased, and recoils of less and less energy are counted, until at 1770 volts the largest of the pulses produced by beta-rays is big enough to be counted. At still higher voltages (1850 volts), the counting rate rises rapidly as all the beta- and gamma-rays are counted.

It will be noted that this counter has no plateau, but that the counting rate rises steadily with the voltage. This absence of plateau is due to the continuous distribution of energies of the recoiling nuclei, and is to be contrasted with the behavior of the BF_3 counters[1] in the presence of slow neutrons. The latter exhibit a plateau since the pulses produced by the alpha-particles resulting from the boron disintegration are all greater than a given size.

This type of counter has been used in studying the neutrons in the cosmic radiation. A preliminary balloon flight has been made with such a counter. The data were transmitted by short wave radio to the ground station. Interpretation of the results in terms of a neutron flux, by use of Eq. (1), is difficult, because of our lack of knowledge of the energy distribution. However, by making a simplifying assumption, a rough calculation can be made. Let us assume that protons are the only recoiling particles, and further, that σ_r is a constant and about 2×10^{-24} cm². (This corresponds[2] to 4-Mev neutrons; at lower energies σ is larger and at higher energies smaller.) The observed n was 6×10^{-3} per sec. (at 1 meter of water), V was 60 cc, MNp was 8×10^{18}, and hence i was 6.9 neutrons per cm² per sec. This may be compared with a current of 1.5 reported by v. Halban, Kowarski and Magat[3] at a lower

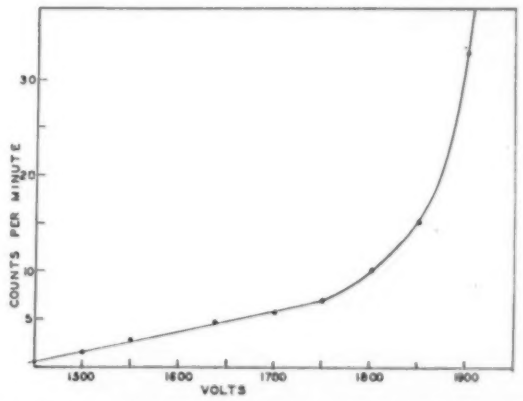

FIG. 1. Counting rate of recoil counter in presence of Ra-Be neutron source, as a function of voltage. No beta- or gamma-rays are counted below about 1770 volts.

elevation (3 m water). It must be remembered that this estimate is very rough. Further experiments and calculations are in progress.

This work has been partly supported by the Carnegie Institution of Washington. The author is indebted to M. D. Whitaker and New York University for the loan of the neutron source, and to E. T. Clarke for assistance with the observations.

S. A. KORFF

Bartol Research Foundation of the Franklin Institute,
Swarthmore, Pennsylvania,
October 30, 1939.

[1] S. A. Korff and W. E. Danforth, Phys. Rev. **55**, 980 (1939).
[2] C. Kittel and G. Breit, Phys. Rev. **56**, 747 (1939).
[3] H. v. Halban, L. Kowarski and M. Magat, Comptes rendus **208**, 572 (1939).

The Absorption of Mesotrons in Air and in Condensed Materials*

It has been pointed out by several authors that the absorption of mesotrons in air is considerably larger than the absorption by equal masses of condensed materials. This fact has been interpreted as evidence for a spontaneous decay of the mesotron. A lifetime of about 2×10^{-6} sec. is required in order to account for the difference.

The great theoretical importance of this conclusion justifies a careful investigation of possible alternative explanations of the observed difference in absorption. I have therefore considered the following effect which seems to explain the observations, at least to some extent, without assuming a decay of the mesotron.

The ionization loss of energy by a fast particle passing through matter is partly due, as is well known, to close impacts between the particle and the material electrons; a large fraction of the loss, however, is due to impacts at distances greater than the atomic radius. For a mesotron with energy of the order of some billions of ev the ionizing effects of the particle can reach to distances of over 10^4 times the interatomic distances.

In a rarefied gas the action of the field of the passing particle on every molecule is independent of the perturbation due to the surrounding molecules. This is no longer true for a condensed material in which the electric field of the passing particle is largely affected by the reaction of the electric polarization of the substance. A calculation of this effect based on the classical theory of the ionization loss shows that it is by no means negligible.

Simple formulas can be obtained if the dielectric properties of the medium are schematized by assuming all the electrons (n per unit volume) to be elastically bound with the same frequency ν_0. The dielectric constant for low frequencies would then be $\epsilon=1+ne^2/\pi m\nu_0^2$. With these assumptions it can be proved that the energy loss per unit path for a particle moving with velocity v is less than the loss calculated with the ordinary theory by the following amount:

$$\frac{2\pi ne^4}{mv^2}\log\epsilon \quad \text{for} \quad v<c/\sqrt{\epsilon},$$

$$\frac{2\pi ne^4}{mv^2}\left[\log\frac{\epsilon-1}{1-v^2/c^2}+\frac{1-\epsilon v^2/c^2}{\epsilon-1}\right] \quad \text{for} \quad v>c/\sqrt{\epsilon}.$$

The result is not essentially dependent on the special assumption as to the dielectric properties of the substance.

While these formulas give a relatively unimportant change in the stopping power of gases and solids for slow particles like protons or α-particles, the difference in behavior becomes rather large when the velocity approaches that of light. Let us consider for example the energy loss of a mesotron of 3×10^9 ev in two different media: A condensed material for which we take $\epsilon=2$; and air for which we take $\epsilon=1.00054$. Neglecting the present effect one would expect the energy loss to be approximately 2.3 Mev·cm²/g for both media. The reduction of loss due to the interaction is negligible in the case of air; it is instead about 0.5 Mev·cm²/g for the condensed substance. This reduces the loss in the latter case to only 1.8 Mev·cm²/g.

The effect of this difference on the absorption of cosmic rays can be estimated if we assume the number of mesotrons with energy $>W$ to vary as $W^{-1.9}$. The ratio of the mesotron intensity observed under equal amounts of air and of condensed materials should then be $(2.3/1.8)^{1.9}=1.6$. According to Ehmert the experimental value of the ratio is about 2.

It seems therefore that the theory accounts for the order of magnitude of the effect even without any contribution from the decay of the mesotron.

Whether all the effects, and especially the somewhat greater differences of absorption reported as results of observations with relatively thin absorbers, can be interpreted on the outlined basis is doubtful. Indeed the theoretical result seems to be near one-half of the experimental difference. But in any case the interactions between atoms represent an important factor to be taken into account in the interpretation of experiments of this type.

I hope to be able to give soon the details of the theory and of its applications in a more extensive publication.

ENRICO FERMI

Pupin Physics Laboratories,
Columbia University,
New York, New York,
October 1, 1939.

* Publication assisted by the Ernest Kempton Adams Fund for Physical Research of Columbia University.

Helium of Mass Three as an Agent in Nuclear Reactions

Recently Alvarez and Cornog[1] have demonstrated the existence of stable He^3. It seems worth while to call attention to the important applications this isotope may have in extending the scope of nuclear physics to the study of nuclear types not previously obtainable.

One observes first that the average binding energy per particle in He^3 is very low (2.72 mMU), so that as a general rule processes induced by it will be exothermic. In addition, with large cyclotrons it is convenient to obtain beams of He^{3++} ions having exceedingly high energies so that the penetration of Coulomb potential barriers up to large atomic numbers is possible.

Recent work at Princeton[2] on the systematic production and study of light odd nuclei having one more proton than neutron was undertaken because of the usefulness of these

TABLE I. *Some* (He^3, n) *reactions. Energy release in thousandths of a mass unit.*

TARGET	PRODUCT	Q	TARGET	PRODUCT	Q
H^2	Li^{6*}	−4.1	Al^{27}	P^{29}	6.1
Li^6	B^{9*}	−2.4	Si^{28}	S^{30}	0.3
Li^7	B^{9*}	9.7	Si^{29}	S^{31}	5.5
B^{10}	N^{12}	0.8	P^{31}	Cl^{33}	5.1
C^{12}	O^{14}	−1.5	S^{32}	A^{34}	0.6
N^{14}	F^{16}	−1.9	S^{33}	A^{35}	4.6
O^{16}	Ne^{18}	−3.3	Cl^{35}	K^{37}	5.4
Ne^{20}	Mg^{22}	0.7	A^{36}	Ca^{38}	0.1
Mg^{24}	Si^{26}	1.2			

* These nuclei are probably unstable against disintegration into heavy particles. The masses have been estimated by H. A. Bethe, Phys. Rev. **55**, 434 (1939).

nuclei in the understanding of the beta-decay process,[3] and for the accurate estimate of the Coulomb energy difference between isobars. The available reactions leading to members of this series (the second column of Table IV in reference 4) are severely limited by the proton energies available. The use of He^3, however, would seem to offer the possibility of extending the work far beyond the present limit.

Of probably even greater interest is the feasibility of making members of the series of even nuclei having two more protons than neutrons (listed in the first column of Table IV of reference 4). No nucleus of this type has as yet been reported, although the sequence of these nuclei, along with the two isobaric series having, respectively, equal numbers of protons and neutrons, and two more neutrons than protons, is of the greatest importance in the study of the finer details of the like and unlike particle interactions.

Of the possible reactions (He^3, n), (He^3, H^1) (He^3, He^4), (He^3, H^2) and (He^3, γ), the first three types may with considerable probability be expected to occur. Of these the most useful for the production of nuclei at present not known is (He^3, n). It has been rather well established from the reactions (He^4, n), (H^2, n), (H^1, n), (γ, n) and (n, $2n$) that when sufficient energy is available for the emission of a neutron from the compound nucleus, the probability of this process will be large. It is difficult therefore to think of a reason why reactions of the type (He^3, n) should not be highly probable. In Table I are listed some of the more interesting of such reactions together with the anticipated[4] release of energy. Many of these product nuclei cannot be formed by any other process.

It may be pointed out, too, that the reaction $H^2(He^3, H^1)He^4$ is expected to yield protons of extraordinary energy since the "Q" for this reaction is 19.73 mMU.

It is of course unfortunate that the light isotope of helium exists with only a small abundance, but presumably the methods of isotope concentration now in use will help to increase the obtainable beam intensities.

WALTER H. BARKAS

Institute for Advanced Study,
Princeton, New Jersey,
December 1, 1939.

[1] L. W. Alvarez and R. Cornog, Phys. Rev. **56**, 379 (1939); **56**, 613 (1939).
[2] White, Delsasso, Fox and Creutz, Phys. Rev. **56**, 512 (1939).
[3] E. P. Wigner, Phys. Rev. **56**, 519 (1939).
[4] W. H. Barkas, Phys. Rev. **55**, 691 (1939).

The Use of Radioactive Elements as Tracers in Physiology

In a Letter to the Editor of *The Physical Review*[1] Dr. A. Barnett has raised a question as to whether the radiation from a radioactive tracer may exert a disturbing influence upon the physiological process which is being studied. In particular he refers to the measurement of permeability of the red blood cell, by means of radiosodium. Fortunately there exist some data on the effects of radiation on permeability, and an estimate of the magnitude of the effect can be made. It hardly need be remarked that it is unnecessary to consider the *local* effect of a particular radioactive atom upon a cell which happens to be close to it, first because the range of the beta-ray (or gamma-ray) is much greater than the size of the cell; second because if the atom emits radiation before entering the cell it is thereafter "dead" as far as detection is concerned. The effect upon permeability will therefore be the result of the generalized dose of ionization which is delivered to the material throughout its volume, and this may be spoken of in terms of r units. A large number of experiments upon induced changes in permeability by exposure to gamma-rays and x-rays have been summarized in a review article by Heilbrunn and Mazia.[2] Although the results vary considerably, it is to be noticed that in general no clear-cut effect occurs for doses less than a few hundred r units. What concentration of radiosodium will give a dose of, say, 500 r in 10 hours? If it is assumed that the beta-rays alone are absorbed in the material, the answer is about 10^6 disintegrations per cc per second, or the equivalent of about 10^{-3} milligram of radium per cc, in terms of gamma-ray strength. It is ordinarily not necessary to use tracers in such high concentration as this. However, in exceptional cases a correction may have to be applied for the effect of volume irradiation of the material.

As to the ability of biological material to discriminate between the radioactive and nonradioactive isotopes of a given element, a remark may be made. In the case of hydrogen it is quite clear that the isotopes behave differently, chemically, and this is best illustrated by the fact that they can be separated by chemical means in the laboratory. Obviously this is the extreme case, in that the isotopes differ in weight by a factor two, or even three, if radiohydrogen is included. For the heavier elements the isotopic difference in chemical behavior is agreed to be negligible, as far as any simple reaction is concerned, but biochemists might not allow us to generalize this to include the complicated and delicately balanced systems of reactions which occur in living material. One way in which we may hope to find a rather conclusive answer to this question is as follows. So far as the author is aware, no appreciable difference has been noted in the behavior of biological material toward the various *stable* isotopes of any element, with the possible exception of hydrogen. If such a difference does exist, a variation in the isotopic ratio in an element should be found in going from one compound of biological origin to another. An accurate test of this point is possible by means of the mass spectrograph. It follows, of course, that the difference, biochemically, between radioactive and nonradioactive isotopes will

certainly not be greater than the difference between the stable isotopes of a given element. Finally, it may be pointed out that the use of radioactive isomers as tracers would be free even from the above question, since they differ neither in weight nor in charge. It is almost certain that the number of known isomers will grow, and they may find a unique application in certain tracer problems.

H. R. CRANE

University of Michigan,
Ann Arbor, Michigan,
November 27, 1939.

[1] A. Barnett, Phys. Rev. **56**, 963 (1939).
[2] L. V. Heilbrunn and Daniel Mazia, *Biological Effects of Radiation*, edited by B. J. Duggar (New York, 1936).

Vitrification of Water

The main reason for the general failure of attempts to obtain water in the vitreous (amorphous) state by a rapid cooling from the liquid state, seems to be the high rate of formation of crystallization nuclei and the high velocity of growth of the ice crystals. With the idea that a sufficiently rapid cooling would finally prevent the formation of ice, we tried various procedures which consisted essentially in immersing suddenly in liquid air preparations in which droplets of water were either sprayed with an atomizer on thin glass or mica sheets or deposited on glass plates by the condensation of steam. An examination of these droplets between crossed Nicols revealed a crystalline structure. The cooling velocity had evidently not been high enough.

We finally succeeded in obtaining amorphous solid water by flattening small quantities of liquid water between two metal plates, cooled in liquid air, one of which was thrown toward the other at a high speed. A cylindrical stream of water 1 mm in diameter was made to flow vertically from a pipette. A brass disk 12 mm in diameter and 2 mm thick, mounted on a rod perpendicular to the plane of the disk, and cooled in liquid air immediately before being used, was fastened about 2 mm behind the stream, the direction of the latter being parallel to the plane of the disk. Another brass disk of the same size, mounted on a rod 12 cm long, and cooled in liquid air, was thrown against the first disk by the propelling action of the spring of a toy pistol. The pistol had previously been fastened in a steady position and adjusted so that the disk that it was to throw was parallel to the other disk and about 13 mm away from it. The disk thrown by the pistol was, then, at a distance of 1 cm from the stream.

The water flattened between the two disks takes the shape of a film a few microns thick. Pieces of this film, which sometimes have an area of 10 mm^2, were transported on a cooled glass slide into a specially built desiccated chamber placed on the stage of a polarizing microscope. These pieces are dark between crossed Nicols and stay dark for about 30 seconds. Then, with the rise in temperature, one can observe a gradual reestablishment of light and, finally, when the temperature approaches the melting point of ice, the preparation is full of crystals large enough to be well observed under the microscope. Water has evidently undergone vitrification and devitrification.

This experiment, of course, does not allow one to conclude anything as to the possible formation of crystalline nuclei smaller than the wave-length of the light used to detect them.

B. J. LUYET

Department of Biology,
Saint Louis University,
Saint Louis, Missouri,
November 16, 1939.

Radioactive Isotopes in Biology

In a recent note[1] it has been suggested that the general body of biological work with artificially radioactive indicators, which is currently appearing in journals, is subject to the criticism that apparently no one has made any measurements of the effects of these radioactive isotopes on biological materials. As regards the general systemic effects of radioactive isotopes, Hamilton and Alles[2] have data to show that at the concentrations with which they worked, there was no effect on electrocardiographic tracings, respiratory rate, pulse, and blood pressure. Greenberg and Glazko[3] also found no difference between active and inactive salts when used on isolated hearts, *in vitro*. Work from this laboratory[4] has shown that in the case of the unicellular alga *Nitella*, high activities (1–50 millicuries/liter) of radioactive Na will produce a decrease in the rate of uptake of sodium by the cell. This rate of penetration is inversely proportional to the logarithm of the millicurie dose, and is almost certainly due to the radiation from the artificial isotope $_{11}Na^{24}$ and not due to some differential penetration of inactive Na rather than active Na. That this is so is shown by the fact that the above results could be quantitatively duplicated with x-rays as a radiant source. Radioactive $_{19}K^{42}$ could also be shown to produce the effect as stated above.

When doses of below 1 millicurie per liter of radioactive Na were used, there was no longer any change in the rate of penetration with dosage, and it was concluded that below this value there was no effect. In most of the published experiments so far done the dosage has been below this limit, although it is true that there are papers describing work in which undoubtedly the radiation was producing an effect. In the case of the experiments of Cohn and Cohn[5] who used radioactive Na, the writer is acquainted with the dosage used and it is certainly below the activity to produce any so far known biological effect. In regard to the criticism in the previous note[1] it appears there are several points on membrane structure and permeability in which more recent work has shown him to be in error. Limited space does not permit of their discussion. In concluding it seems desirable to emphasize that the radiations emitted from the various radioactive isotopes important in biology vary so markedly in their character that a different limit of biological effect will have to be made for each one.

LORIN J. MULLINS

Department of Zoology,
University of California,
Berkeley, California,
November 17, 1939.

[1] A. Barnett, Phys. Rev. **56**, 963 (1939).
[2] J. G. Hamilton and G. Alles, Am. J. Physiol. **125**, 2 (1939).
[3] A. J. Glazko and D. M. Greenberg, Am. J. Physiol. **125**, 2 (1939).
[4] L. J. Mullins, J. Cell. Comp. Physiol. **14**, 3 (1939).
[5] W. E. Cohn, and E. T. Cohn, Proc. Soc. Exp. Biol. Med. **41**, 445–49 (1939).

On Explosion Showers

Let us consider a high energy collision between two particles of initial impulses $|p_1| \cong |p_2| \gg p_0 = hc/l$ (where p_1, p_2 are referred to a barycentric frame: $p_1+p_2=0$, and l is a universal length $\sim 10^{-13}$ cm).

Heisenberg,[1] starting from a half-classical theory of explosion showers, showed that the number of particles created by collision must be sensibly proportional to the initial energy $E=2|p_1|c \sim nhc/l$.

Our purpose is to examine whether it is permissible to apply the second quantization method and to assume the existence of a suitable relativistic interaction-operator in order to obtain some additional information about this kind of shower. We arrive at the same description of showers obtained by Heisenberg, and this seems to support the consistency of our assumption. Moreover our method leads to the result that the cross section for explosion showers decreases for $n>1$ and tends to 0 when $E \to \infty$.

In analogy to Heisenberg's Lagrangian we shall consider here, as a plausible and typical example, an interaction-operator $G(\xi)$ which is a function of

$$\xi = l^2 \Box.$$

We suppose also that this operator corresponds to some kind of short range forces, e.g. we consider $G(\xi)$ of the type $\exp[-|\xi|]$ or $(\xi+1)^{-1}$ (for Yukawa forces), or other types used for "cutting off" purposes.

The general term of interaction, which in the formalism of second quantization, corresponds to an explosion shower, is:

$$b_{k_1}^* b_{k_2}^* \cdots b_{k_n}^* a_{p_1} a_{p_2} \int_\Omega \varphi_{k_1}^*(x,t) \cdots \varphi_{k_n}^* G(\xi) \psi_{p_1} \psi_{p_2}(x,t) dx,$$

where $\varphi_{k_s} \psi_{p_s}$ represent plane waves with impulses $k_s p_s$ and $b_{k_s}^* a_{p_s}$ are the usual operators representing the creation and the annihilation of particles. $\varphi_{k_s} \psi_{p_s}$ are normalized in a volume Ω, and thus assume the form:

$$\Omega^{-\frac{1}{2}} u_p \exp(i/\hbar)(px - Et),$$

where u_p are only spin dependent factors. We have:[2]

$$G(\xi)\psi_{p_1}\psi_{p_2} = G\{-p_0^{-2}[(p_1+p_2)^2 - c^{-2}(E_1+E_2)^2]\} \times u_{p_1} u_{p_2} \exp(i/\hbar)[(p_1+p_2)x - (E_1+E_2)t].$$

Applying the usual perturbation method in order to obtain the Fourier coefficients of the function χ which represents a state:

$$\chi(N k_1 N k_2 \cdots N p_1 \cdots t) = \Sigma c(N k_1 \cdots N p_1 \cdots t) \exp[-(i/\hbar)(N k_1 E_1 + \cdots)t]$$

(with obvious signification of the symbols) we obtain:

$$|c(1 k_1 \cdots 1 k_n 0 p_1 0 p_2 t)|^2 = t \frac{2\pi}{\hbar} \frac{1}{\Delta E} \left| \int_\Omega \varphi_{k_1}^* \cdots \varphi_{k_n}^* G \psi_{p_1} \psi_{p_2} dx \right|^2_{(t=0)},$$

where

$$\frac{1}{\Delta E} = \left(\frac{\delta \pi \Omega}{h^3}\right)^n \left(\frac{k_1^2}{v_1}\right) \cdots \left(\frac{k_n^2}{v_n}\right)$$

is the number of quantum states referred to unit energy interval. In a barycentric frame we have $p_1+p_2=0 = k_1+k_2+\cdots+k_n$. An easy calculation shows that: $|c|^2$ results independent of Ω and proportional to:

$$k_1^2 k_2^2 \cdots k_n^2 G\left[\left(\frac{E_{p_1}+E_{p_2}}{cp_0}\right)^2\right].$$

In order to study how this probability varies with n and with the spatial distribution of vectors k_s, we make use of the conservation law:

$$E_{p_1}+E_{p_2} = E_{k_1}+E_{k_2}+\cdots+E_{k_n}$$

and find that this probability is the maximum in the case:[3] $|k_1| \sim |k_2| \sim \cdots \sim |k_n| \sim p_0$.

Thus n is proportional to the initial energy and the frequency of explosion showers results reduced by the factor G for incident energies greater than cp_0.

GLEB WATAGHIN

Department of Physics,
Sao Paulo University,
Brazil.
November 16, 1939.

[1] W. Heisenberg, Zeits. f. Physik **110**, 251 (1938); **113**, 61 (1939).
[2] Following a remark of Mario Schönberg, the operators of the type $\exp(\Delta/K_0^2)$ applied to a function give in the corresponding Fourier-development a cut-off factor.
[3] G. Wataghin, Nature **142**, 393 (1938); Comptes rendus, August (1938).

Ferromagnetic Anisotropy of Low Nickel Alloys of Iron

Although the ferromagnetic anisotropy constant K_1 has been determined accurately for iron-nickel alloys containing 50 percent or more of nickel, nothing at all is known about the low nickel alloys. The marked discontinuity in magnetic properties of 30 percent nickel makes it impossible to interpolate between iron and the high nickel alloys. Until the time when suitable low nickel single crystals of iron are grown, the only way of obtaining any idea as to the behavior of the anisotropy constant K_1 in the low nickel range is to make use of cold-rolled material. This is possible because the texture of cold-rolled iron-nickel alloys has been carefully investigated by McLachlan and Davey,[1] using standard x-ray diffraction technique. They found that for a given total percentage of cold reduction in thickness, the texture was independent of the composition up to at least 20 percent nickel.

The magnetic torque curve of cold-rolled iron is similar to that of an iron single crystal disk having (100) in its plane.[2] The exact shape and the amplitude of the polycrystalline torque curve depend upon the nature of the deviations from the ideal (100) orientation and upon the fraction of material having a random texture. It is convenient to speak of a texture factor, which is defined as the ratio of the amplitude of the predominant 40 term in the torque curve of the cold-rolled material to the corresponding amplitude for a single crystal of the same composition and volume For all practical purposes, the texture factor can be taken as the ratio of the average of the torque peaks of the polycrystalline material to that of the single crystal. In view of the work of McLachlan and Davey, it can be assumed that if iron and iron-nickel alloys are cold-rolled in the same manner, their texture factor will be the same, at least as a first approximation. The average values of the torque peaks will then be directly proportional to the corresponding values of K_1.

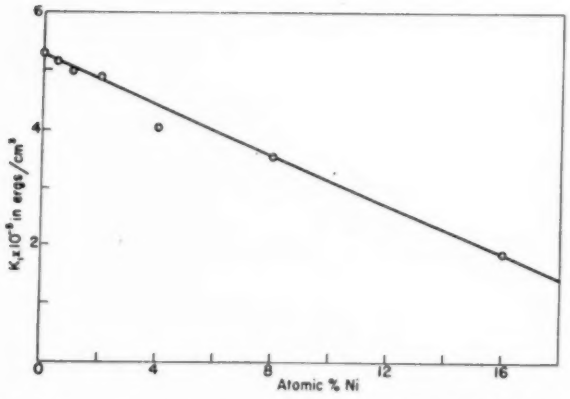

FIG. 1. Ferromagnetic anisotropy constant for various low nickel alloys of iron.

Pressed powder ingots of iron containing various amounts of nickel were hot-rolled from a thickness of 1 in. to 0.60 in., and then cold-rolled 97 percent to 0.020 in. Several 1-in. disks were stamped from each strip for the magnetic torque measurements. The torque peaks were measured at several different fields to permit of extrapolating them to their limiting values.[3] The results, calculated on the assumption that for iron $K_1 = 5.29 \times 10^5$ ergs/cm³ and that the texture factor is constant for all the compositions studied, are shown in Fig. 1. A texture factor of 0.335 was found for the iron specimens.

The probable accuracy of the results depends entirely upon the constancy of the texture factor. It is reasonable to assume that if this factor varies by 20 percent or thereabouts, the texture must have changed enough to affect the x-ray diffraction patterns. Since no such effect was found by McLachlan and Davey, a conservative estimate of the probable error of K_1 for the higher nickel range is not more than 20 percent. The error should be proportionately less for the alloys poorer in nickel, if we assume that, as the nickel content increases, the texture factor departs in a uniform manner from its value for iron. According to the straight line drawn through the points of Fig. 1, the anisotropy constant of iron containing 12 atomic percent of nickel is half that of pure iron.

L. P. TARASOV

Research Laboratory,
General Electric Company,
Schenectady, New York,
December 1, 1939.

[1] D. McLachlan, Jr., and W. P. Davey, Trans. Am. Soc. for Metals **25**, 1084 (1937).
[2] R. M. Bozorth, Phys. Rev. **50**, 1076 (1936).
[3] L. P. Tarasov, Phys. Rev. **56**, 1231 (1939).

Author Index to Volume 56

References with (A) are to abstracts of papers presented at meetings of the American Physical Society; references with (L) are to Letters to the Editor and those with (T) designate title only.

Abbott, F. R. and Joseph E. Henderson. Range and validity of the field current equation—113

——— **and Joseph E. Henderson.** Validity of the field current equation—853(A)

Abelson, Philip H. Identification of characteristic x-rays associated with radioactive decay—753

——— Investigation of the products of the disintegration of uranium by neutrons—1

Aebersold, Paul C. Production of a beam of fast neutrons—714

Alfvén, Hannes. On the origin of cosmic radiation—1060(L)

Allison, Samuel K., Lester S. Skaggs and Nicholas M. Smith, Jr. Experimental studies of energy releases in reactions of light nuclei—860

——— **Lester S. Skaggs and Nicholas M. Smith, Jr.** Remeasurement of the energies released in the reactions Li^7 (p,α) He^4 and Li^6 (d,α) He^4—288(L)

Alvarez, Luis W. (see Lawrence, Ernest O.)—124(L)

——— **and Robert Cornog.** He^3 in helium—379(L)

——— **and Robert Cornog.** Helium and hydrogen of mass 3—613(L)

Amaldi, E., D. Bocciarelli, F. Rasetti and G. C. Trabacchi. On the scattering of neutrons from the C+D reaction—881

Anderson, H. L., E. Fermi and Leo Szilard. Neutron production and absorption in uranium—284

Anderson, Paul A. Contact difference of potential between silver films on glass and on rocksalt—850(A)

——— (see Johnson, G. W.)—852(A)

Archdeacon, Bruce (see McCay, Myron)—847(A)

Archibald, William J. Specific heat of a monatomic liquid—926

Bacher, R. F. Erratum: The interaction of configurations: sd—p^2—385(L)

——— **and D. C. Swanson.** On the collimation of fast neutrons—483(L)

Bacon, R. H., E. N. Grisewood and C. W. Van der Merwe. Radioactivity of Mn^{56}—1168(L)

Bagley, Dale. Effect of cloud chamber expansion ratio on drop count determination of specific ionization of cosmic rays—851(A)

——— (see Brode, Robert B.)—209(A)

Bainbridge, K. T. and H. G. Vogt. Performance of a system of modified Hertz pumps—213(A)

Baltzer, O. J. and G. E. M. Jauncey. X-ray fluorescing coefficient and the orientation of a zinc crystal—289(L)

Band, William. Klein's fifth dimension as spin angle—204(L)

Barkas, Walter H. Helium of mass three as an agent in nuclear reactions—1242(L)

——— Some new reactions in light nuclei with high energy protons—287(L)

——— (see Weil, George L.)—485(L)

——— **and Milton G. White.** Disintegration of deuterium by protons and p-n reactions in light gaseous elements—288(L)

Barker, E. F. and H. Y. Sheng. Further resolution of 10μ and 16μ ammonia bands—854(A)

Barnes, S. W. Proton activation of indium and cadmium—414

——— Proton activation of $_{48}Cd$ and $_{49}In$—859(A)

Barnett, A. Use of radioactive forms of the common elements in physiology—963(L)

Barr, E. S. and C. H. Chrisman. Near infra-red absorption spectra of some sugars—845(A)

Barry, J. Griffiths (see Johnson, Thomas H.)—219

Barschall, H. (see Ladenburg, R.)—168

Bartlett, J. H. and R. E. Watson. Elastic scattering of fast electrons by heavy elements—612(L)

Bath, Jean (see Ellis, Joseph W.)—859(A)

Bayley, D. S. (see Van Allen, J. A.)—383(L)

Beams, J. W. and R. E. Fox. Analytical centrifuge—848(A)

——— **and C. Skarstrom.** Concentration of isotopes by the evaporative centrifuge method—266

Bearden, J. A. Precision determination of the viscosity of air—1023

Becker, R. A. (see McLean, W. B.)—859(A)

——— **and E. R. Gaerttner.** Half-life of B^{12}—854(A)

Beeman, W. W. and H. Friedman. X-ray K absorption edges of the elements Fe (26) to Ge (32)—392

Beth, Richard A. Multiple nomogram for the atomic constants—208(A)

Bethe, H. A. (see Marshak, R. E.)—210(A)

——— **and W. J. Henderson.** Evidence for incorrect assignment of the supposed Si^{27} radioactivity of 6.7-minute half-life—1060(L)

Bidwell, Charles C. Precise method of measuring heat conductivity applicable to either molten or solid metals. Thermal conductivity of zinc—594

Bitter, F. and A. R. Kaufman. Magnetic studies of solid solutions. I. Methods of observations and preliminary results on the precipitation of iron from copper—1044

Bleakney, Walker (see Delfosse, J.)—208(A), 256

Bocciarelli, D. (see Amaldi, E.)—881

Bohn, J. Lloyd (see Nadig, Francis H.)—216(A)

Bohr, Niels and John A. Wheeler. Fission of protactinium—1065(L)

——— **and John Archibald Wheeler.** Mechanism of nuclear fission—426

Bonner, T. W. Neutrons from the disintegration of fluorine by deuterons—207(A)

Boorse, H. A. Hydrogen liquefaction plant at Columbia University—1068(T)

Booth, E. T. (see Grosse, A. v.)—382(L)

Bosch, Walter C. and Barremore B. Brown. Linearity of wide range galvanometer response in a photoelectric spectrophotometer utilizing a balanced amplifier circuit—846(A)

Boynton, W. P. Quenched primary spark of an induction coil—853(A)
Bozorth, R. M. (see Williams, H. J.)—837(L)
——— **and H. J. Williams.** Directional magnetic properties of nickel at liquid hydrogen temperature—1068(T)
Bradbury, N. E. Initial recombination—849(A)
Brady, James J. and John D. Todd. Photoconductivity of tartaric acid crystals—859(A)
Breazeale, Francis. Remarks on the study of structural viscosity and an example of the technique for a cellulosic "solution"—845(A)
Breit, G. (see Hoisington, L. E.)—884
——— (see Kittel, C.)—744
Brobeck, William M. (see Lawrence, Ernest O.)—124(L)
Brode, Robert B. and G. Dale Bagley. Specific ionization measurements and sign preference for condensation in a Wilson cloud chamber—209(A)
Brody, I. and F. de Kőrösy. Convection and conduction of heat in gases—217(A)
Brown, Barremore B. (see Bosch, Walter C.)—846(A)
Brown, Frederick W. Binding energy of H^3—1107
——— **and Milton S. Plesset.** On the equality of the proton-proton and proton-neutron interactions—841(L)
Brown, G. H. Velocity of radio waves in air—385(L)
Brubaker, Gordon. Scattering of alpha-particles by nitrogen—207(A), 1181
Buehl, R. C. and A. von Hippel. Electrical breakdown strength of ionic crystals as a function of temperature—941
Burbank, Cecil J. New x-ray lines in the *L* series resulting from *K* auger transitions—142
Burch, John C., E. T. Ellison and N. Underwood. Physical factors involved in blood volume determination—844(A)
Burton, E. F., J. Hillier and A. Prebus. Report on the development of the electron supermicroscope at Toronto—1171(L)

Cady, Walter G. Transitions between glow and arc discharges—123(L)
Cernuschi, Félix. On the behavior of matter at extremely high temperatures and pressures—450
——— Super-novae and the neutron-core stars—120(L)
——— Tentative theory of the origin of cosmic rays—120(L)
Chao, Kuang-Tseng (see Duffendack, O. S.)—176
——— (see Oleson, N. L.)—482(L), 1171(L)
Chodorow, Marvin I. (see Manning, Millard F.)—787
Chrisman, C. H. (see Barr, E. S.)—845(A)
Christy, R. F. and J. M. Keller. X-ray spin doublet splittings—856(A)
Chu, L. J. (see Stratton, J. A.)—99, 316
Clarke, E. T. (see Korff, S. A.)—704(L)
Clogston, Albert M. (see Goldberg, Leo)—696
Cloud, R. W. (see Trump, J. G.)—215(A)
Cohen, V. W. (see Zinn, W. H.)—260
Cohn, Bryon E. Luminescence of synthetic halite crystals—856(A)
Collins, E. Hobart. Zeeman effect of the hyperfine structure of optically excited mercury resonance radiation—48
Collins, George B., Bernhard Waldman and Eugene Guth. Disintegration of beryllium by electrons—876
Colwell, R. C. (see Thomas, C. D.)—1214
Combes, Lewis S., Royal M. Frye and Norton A. Kent. Interferometer wave-lengths of certain lines in the secondary spectrum of hydrogen—678
Constant, F. W. and J. M. Formwalt. Investigations of ferromagnetic impurities. I—373
——— **and J. M. Formwalt.** Surface effects in testing for ferromagnetic impurities—846(A)
Cooksey, Donald. (see Lawrence, Ernest O.)—124(L)
Cooper, F. S. (see Pollock, H. C.)—170
Cork, J. M. and J. L. Lawson. Induced radioactivity in cadmium and indium—291
Cornog, Robert (see Alvarez, Luis W.)—379(L), 613(L)
Corson, Dale R. (see Lawrence, Ernest O.)—124(L)
——— (see Wilson, Robert R.)—851(A)
Coulson, C. A. and G. S. Rushbrooke. On the interpretation of atomic distribution curves for liquids—1216
Cowie, D. H. (see Montgomery, C. G.)—635
Crane, H. R. Use of radioactive elements as tracers in physiology—1243(L)
——— (see Oleson, N. L.)—482(L), 1171(L)
——— (see Slawsky, M. M.)—1203
——— **and J. Halpern.** Further experiments on the recoil of the nucleus in beta-decay—232
Crenshaw, C. M. (see Myers, F. E.)—1104
Creutz, E. Analysis of proton-proton scattering data—893
——— (see White, M. G.)—512
———, **M. G. White, L. A. Delsasso and J. G. Fox.** Proton induced radioactivity in fluorine and sodium—207(A)
Critchfield, Charles L. Spin-dependence in the electron-positron theory of nuclear forces—540
——— (see Wigner, Eugene P.)—530
Crittenden, E. C., Jr. Beta-ray spectra of Mg^{27}, Cu^{62} and the nuclear isomers of Rh^{104}—709

Dancoff, S. M. Virtual state of He^5 and meson forces—384(L)
——— Virtual level of He^5 and meson forces—852(A)
Davidson, William L., Jr. Study of the protons from calcium under deuteron bombardment—1061(L)
——— Study of the protons from V, Cu, Mn, and Sc under bombardment by deuterons—1062(L)
——— (see Pollard, Ernest)—206(A)
Davis, Leverett, Jr. Change of resistance in a magnetic field—93
——— Note on the wave functions of the relativistic hydrogenic atom—186, 851(A)
Davis, Thomas. Statistical treatment of the ultracentrifugation of a bacteriophage—845(A)
Decherd, Loraine (see Williams, Dudley)—847(A)
Delfosse, J. and Walker Bleakney. Dissociation of hydrocarbons by electron impact—208(A)
——— **and Walker Bleakney.** Dissociation of propane, propylene and allene by electron impact—256
Delsasso, L. A. (see Creutz, E. C.)—207(A)
——— (see White, M. G.)—512

Dember, A. (see Goetz, A.)—857(A)
——— **and A. Goetz.** Measurement of intensity profiles of Bragg reflections from calcite between 300° and 4.2°K—857(A)
Deming, Lola S. (see Deming, W. Edwards)—108
Deming, W. Edwards and Lola S. Deming. Some physical properties of compressed gases. VI. The fugacity of carbon dioxide—108
Dennison, D. M. (see Fuson, Nelson)—982
Derieux, J. B. Mileage of gasoline at different speeds, and of different grades—845(A)
Dixon, A. A. Change of the viscosity of liquids produced by an electric field—847(A)
Doran, R. L. (see Henderson, W. J.)—123(L)
Dow, R. B. Some interesting biochemical and physical effects at high pressure—215(A)
Drill, Harry T. Search for an electrostatic analog to the gravitational red shift—184
DuBridge, L. A. and John Marshall. Radioactive isomer of Sr^{87}—706(L)
Duffendack, O. S. and Kuang-Tseng Chao. Temperature parameters from negative bands of nitrogen under excitation by electron impact—176
DuMond, Jesse W. M. Our present dilemma regarding the values of the natural constants e, m and h. A new graphical method of presentation—153
Dunning, J. R. (see Grosse, A. v.)—382(L)

Eichelberger, J. F. (see Green, J. B.)—51
Eisenbud, L. (see Wigner, E.)—214(A)
Ellett, A. (see Van Allen, J. A.)—383(L)
Ellis, Joseph W. and Jean Bath. Infra-red pleochroism and Fermi resonance associated with CH_2 groups in crystals—859(A)
Ellison, E. T. (see Burch, John C.)—844(A)
Elmore, W. C. Magnetic structure of electrolytically polished silicon-iron crystals—210(A)
Elsasser, Walter M. Far infra-red water bands and heat transfer in the atmosphere—855(A)
Enns, T. Radioactivities produced by proton bombardment of palladium—872
Eyster, Eugene H. (see Gillette, R. H.)—1113

Fajans, Kasimir and David W. Stewart. Induced radioactivity in europium—625
Farnsworth, H. E. and Ralph P. Winch. Work functions of different faces of silver single crystals—1067(L)
Fenn, W. H. Generation of square-wave voltages at high frequencies—850(A)
Fermi, Enrico. Absorption of mesotrons in air and in condensed materials—1242(L)
Fermi, E. (see Anderson, H. L.)—284
Feynman, R. P. Forces in molecules—340
Findlay, J. C., A. Pitt, H. Grayson Smith and J. O. Wilhelm. Velocity of sound in liquid helium under pressure—122(L)
Fine, Paul Charles. Normal modes of vibration of a body-centered cubic lattice—355, 852(A)
Fisher, Russell A. (see Fry, Arthur S.)—669
——— **and Arthur S. Fry.** Hollow cathode source for the Zeeman effect—675
Fisk, J. B. Emission of electrons from "cold" metallic targets under high energy positive ion bombardment—846(A)
——— (see Getting, I. A.)—213(A), 1098
Fleming, G. M. and Joseph E. Henderson. Thermoelectric method for the determination of work functions—853(A)
Focke, Alfred B. Twinning in bismuth crystals—854(A)
——— (see Hartmann, G. K.)—217(A)
——— (see Shear, Sidney K.)—217(A)
Formwalt, J. M. (see Constant, F. W.)—373, 846(A)
Foster, M. G. and A. Goetz. Conduction and mobility of thin lead films—849(A)
Fountain, C. R. Dental fluoroscope and shield—844(A)
Fowler, W. A. (see Lauritsen, C. C.)—858(A)
——— (see Sheppard, C. W.)—849(A)
——— **and C. C. Lauritsen.** Low energy gamma-radiation from lithium bombarded with protons—841(L)
——— **and C. C. Lauritsen.** Pair emission from fluorine bombarded with protons—840(L)
——— **and C. W. Sheppard.** Production of secondary electrons by high energy electrons—859(A)
Fox, Gerald W. and Alden H. Ryan. Dielectric constant of ammonia, nitrogen and carbon dioxide at ultra-high frequency—1132
Fox, J. G. (see Creutz, E. C.)—207(A)
——— (see White, M. G.)—512
Fox, R. E. (see Beams, J. W.)—848(A)
Friedman, H. (see Beeman, W. W.)—392
Fröhlich, H. Dielectric breakdown in ionic crystals—349
——— **W. Heitler and B. Kahn.** Deviation from the Coulomb law for a proton—961(L)
Fry, Arthur S. (see Fisher, Russell A.)—675
——— **and Russell A. Fisher.** Zeeman effect in the hyperfine structure of iodine. II—669
Frye, Royal M. (see Combes, Lewis S.)—678
Furry, W. H. On transition probabilities in double beta-disintegration—1184
Fuson, Nelson, H. M. Randall and D. M. Dennison. Far infra-red absorption spectrum and the rotational structure of the heavy water vapor molecule—982

Gaerttner, E. R. (see Becker, R. A.)—854(A)
——— (see Pardue, Louis A.)—855(A)
——— **Louis A. Pardue and J. F. Streib.** Experiments on the scattering of fast neutrons—856(A)
Gast, Paul (see Loughridge, Donald H.)—1169(L)
Gautier, T. N. and Dudley Williams. Effects of alkali halides on the 5.7μ water band—616(L)
Germer, L. H. Electron diffraction studies of thin films. I. Structure of very thin films—58
——— **and F. E. Haworth.** Order in the copper-gold alloy system—212(A)
Getting, I. A., J. B. Fisk and H. Vogt. Some features of an electrostatic generator and ion source for high voltage research—1098
——— **H. G. Vogt and J. B. Fisk.** Design and operation of a high voltage unit for nuclear investigations—213(A)
Giarratana, Joseph (see MacPhail, Malcolm)—207(A)

Gill, Piara S. Time distribution of cosmic-ray bursts—632
Gillette, R. H. and Eugene H. Eyster. Fundamental rotation-vibration band of nitric oxide—1113
Gingrich, Newell S. and C. N. Wall. Structure of liquid potassium—336
Githens, Sherwood, Jr. Influence of discharge chamber geometry upon the striking potential of the h.f. discharge —845(A)
Goble, A. T. Energies in the d^9p configuration of the nickel-like and palladium-like spectra—209(A)
Godart, O. World-wide variations of the earth's magnetic field and the intensity of cosmic radiation—1074
Goetz, A. (see Dember, A.)—857(A)
——— (see Fowler, M. G.)—849(A)
——— (see Gould, W. O.)—850(A)
——— **and A. Dember.** Recording Bragg spectrometer for use between room temperature and helium temperature —857(A)
Goldberg, Leo and Albert M. Clogston. Variational atomic wave functions—696
Goloborodko, T. and A. Leipunski. Scattering of photo-neutrons from deuterium by the nuclei of atoms of light elements—891
Good, W. E. and R. D. Hill. Investigation of boron by slow neutrons—288(L)
Good, W. M. and J. D. Stranathan. Improved method of making permanent electrets and factors which affect their behavior—810
Gordy, Walter (see Nielsen, Alvin H.)—781
Goss, Wilbur H. and Joseph E. Henderson. New method for the measurement of work functions—857(A)
Goudsmit, S. and J. L. Saunderson. Multiple scattering of charged particles—122(L)
Gould, W. O. and A. Goetz. About the physical nature of the graininess of photographic emulsions—850(A)
Green, J. B. and J. F. Eichelberger. Paschen-Back effect. V. Theory of the effect for intermediate coupling—51
——— **and J. A. Peoples, Jr.** Paschen-Back effect. VI. The spectrum of neon—54; Erratum—385(L)
Grisewood, E. N. (see Bacon, R. H.)—1168(L)
Grönblom, B. O. β-decay and spin of light nuclei—508
Grosse, A. v., E. T. Booth and J. R. Dunning. Fission of protactinium—382(L)
Grover, Horace and John Hutzenlaub. Specific heat of nickel-chromium alloys—212(A)
Guth, Eugene (see Collins, George B.)—876

Hafstad, L. R. (see Heydenburg, N. P.)—1078
Hale, Donald H. Second townsend ionization coefficient for nickel cathodes in pure hydrogen—858(A)
——— Townsend ionization coefficients for Ni and Al cathodes in an atmosphere of hydrogen—1199
Halpern, J. (see Crane, H. R.)—232
——— (see Oleson, N. L.)—482(L), 1171(L)
Halpern, O. Some new aspects of neutron scattering. Theoretical—1068(T)
Hamilton, Donald R. Atomic beam study of the hyperfine structure of the metastable $^2P_{3/2}$ state of $In^{115}I$. The electric quadrupole moment of In^{115}—30
Hane, W. A. (see Johnson, G. W.)—852(A)
Harris, W. T. (see Kanner, M. H.)—207(A); 839(L)
Hartmann, G. K. and Alfred B. Focke. Absorption of supersonic waves in water and in aqueous suspensions—217(A)
Harvey, G. G. On alleged discontinuities in the diffuse scattering of x-rays from crystals at small angles—247
——— On the total scattering of x-rays from crystals—242
Haupt, R. F. and E. Teller. Specific heat and the double minima problem of the NH_3 molecule—208(A)
Haworth, F. E. Superstructure in Fe Ni_3—289(L)
——— (see Germer, L. H.)—212(A)
Haxby, R. O. (see Stephens, W. E.)—209(A)
Hebb, M. H. (see Nordheim, L. W.)—494
Heck, C. M. Measurement of radiation of the sky—848(A)
Heitler, W. (see Frölich, H.)—961(L)
Hellund, E. J. and E. A. Uehling. Transport phenomena in mixtures of gases—818, 851(A)
Henderson, Joseph E. (see Abbott, F. R.)—113, 853(A)
——— (see Fleming, G. M.)—853(A)
——— (see Goss, Wilbur H.)—857(A)
——— (see Rubens, R. M.)—854(A)
——— **and K. V. MacKenzie.** Fields involved in field emission—857(A)
Henderson, Malcolm C. Beryllium targets for nuclear research—207(A)
——— Heat fission of uranium—703(L)
Henderson, W. J. (see Bethe, H. A.)—1060(L)
——— (see King, L. D. P.)—1169(L)
——— **and R. L. Doran.** Existence of radioactive Al^{29}—123(L)
Herman, R. C. (see Hofstadter, R.)—212(A)
Hershey, Allen V. Measurements of the mobility of potassium ions at high field intensity and low pressure—908
——— Ridges in a liquid surface due to the temperate dependence of surface tension—204(L)
——— Theory for the mobility of ions of high velocity—916
Heydenburg, N. P. and R. B. Roberts. Deuteron-deuteron, proton-helium, and deuteron-helium scattering—1092
———, **L. R. Hafstad and M. A. Tuve.** Scattering of protons by protons. III—1078
Hilberry, H. Van Norman (see Rossi, Bruno)—837(L)
Hill, R. D. (see Good, W. E.)—288(L)
Hillier, J. (see Burton, E. F.)—1171(L)
Hinton, Benjamin (see Williams, Dudley)—844(A)
Hippel, A. von (see Buehl, R. C.)—941
Hoag, J. Barton (see Rossi, Bruno)—837(L)
Hofstadter, R. and R. C. Herman. Photoconductivity of crystalline willemite at low temperatures—212(A)
Hoisington, L. E. (see Thaxton, H. M.)—1194
———, **S. S. Share and G. Breit.** Effects of shape of potential energy wells detectable by experiments on proton-proton scattering—884
Holden, A. N., G. T. Kohman, W. P. Mason and S. O. Morgan. Heavy water rochelle salt—378(L)
Hole, W. L. and R. W. Wright. Emissive and thermionic characteristics of uranium—785
Holloway, M. G. and B. L. Moore. Disintegration of N^{14} and N^{15} produced by deuteron bombardment—705(L)
Holmes, F. T. Graphical evaluation of the statistical significance of rate differences—844(A)

Hooley, J. G. (see Stephenson, C. C.)—121(L)
Horvay, Gabriel. Generalization of Weinstein's theorem—214(A)
Houston, W. V. and S. Rubin. Adsorbed films on interferometer mirrors—852(A)
Hulburt, E. O. Suggested observation of the zodiacal light during a total solar eclipse—960(L)
Hull, A. W. Dispenser cathode. A new type of thermionic cathode for gaseous discharge tubes—86
Humphreys, Richard F. Separation of bromine isotopes by centrifugation—684
Huntoon, R. D. (see Myers, F. E.)—1104
Hurst, William. Recording sensitive differential manometer—846(A)
Hustrulid, Andrew, Marvin M. Mann and John T. Tate. Dissociation of H_2O vapor by electron impact—208(A)
Hutzenlaub, John (see Grover, Horace)—212(A)

Inglis, D. R. Spin-orbit coupling in the alpha-model of light nuclei—1175
——— Viscous force between almost-coaxial cylinders—1040
Ives, Herbert E. Theory of the double Fizeau toothed wheel—215(A)

Jacobs, Robert Byron. X-ray measurements of compressibility—211(A)
Jahn, H. A. Note on coriolis coupling terms in polyatomic molecules—680
James, Hubert M. and Vivian A. Johnson. Electron distribution in ZnO crystals—119(L)
Jauncey, G. E. M. Theory of the diffuse scattering of x-rays by crystals in the region of the *K* critical absorption wave-length—644
——— (see Baltzer, O. J.)—289(L)
Jesse, W. P. (see Schein, Marcel)—613(L)
Johnson, G. W., W. A. Hane and P. A. Anderson. Quantitative study of the clean-up of hydrogen by barium—852(A)
Johnson, R. P. Note on the hole theory of diffusion—814
——— Zone theory and the properties of sulfide phosphors—213(A)
Johnson, Thomas H. Angular dispersion of the cosmic radiation in the upper atmosphere resulting from the deflection of low energy particles in the earth's magnetic field—210(A), 226
——— **and J. Griffiths Barry.** East-west symmetry of the cosmic radiation at very high elevations near the equator and evidence that protons constitute the primary particles of the hard component—219
Johnson, Vivian A. (see James, Hubert M.)—119(L)

Kahn, B. (see Frölich, H.)—961(L)
Kanner, M. H. (see Ladenburg, R.)—168
——— **and W. T. Harris.** Search for β and delayed γ-radiation from the *d*-*d*-reaction—207(A), 839(L)
Kaplan, Joseph. Forbidden transitions in nitrogen—858(A)
Kaufmann, A. R. (see Bitter, F.)—1044
Keen, Richard C. Unit cell and space group of potassium bicarbonate—847(A)
Keller, J. M. (see Christy, R. F.)—856(A)
Kellogg, J. M. B., I. I. Rabi, N. F. Ramsey, Jr. and J. R. Zacharias. Magnetic moments of the proton and deutron. The radiofrequency spectrum of H_2 in various magnetic fields—728
———, **I. I. Rabi, N. F. Ramsey, Jr. and J. R. Zacharias.** Radiofrequency spectrum of the HD molecule in magnetic fields—213(A)
Kemble, Edwin C. Fluctuations, thermodynamic equilibrium and entropy—1013
——— Quantum-mechanical basis of statistical mechanics—1146
Kennedy, G. W., G. T. Seaborg and E. Segrè. Nuclear isomerism in zinc—1095
Kenrick, G. W. and P. J. Sammon. Fluctuations in intensity of static—203(L)
Kent, Norton A. (see Combes, Lewis S.)—678
Kenty, Carl. Quartz membrane manometer of small volume and its use in the study of pressure and temperature in high intensity mercury lamps—215(A)
King, Allen. New method for measuring Young's modulus—216(A)
King, G. W. and J. H. Van Vleck. Relative intensities of singlet and singlet-triplet transitions—464
King, L. D. P. and W. J. Henderson. Radioactive isotopes of indium from alpha-bombardment of silver—1169(L)
Kingdon, K. H. and E. J. Lawton. Velocity of mercury ions in mercury vapor—215(A)
Kirby-Smith, J. S. Apparatus for the excitation of Raman spectra of gases—844(A)
Kirkham, Don. Streamline flow of water from an artesian basin into horizontal drains: theory compared with experiment—852(A)
Kirkpatrick, Paul (see Veith, Werner)—705(L)
Kittel, C. and G. Breit. Note on the scattering of neutrons by protons—744
Kliever, W. H. Intensities of the *K*-series x-ray lines of tungsten and platinum—387
Knauss, Harold P. (see McCay, Myron)—847(A)
Kohman, G. T. (see Holden, A. N.)—378(L)
Korff, S. A. Evidence for neutrons in the cosmic radiation—210(A)
——— Fast neutron measurements with recoil counters—1241(L)
——— **and E. T. Clarke.** Upward radiation produced by cosmic rays at high altitudes—704(L)
Kőrösy, F. de (see Brody, I.)—217(A)
Kruger, P. Gerald, F. W. Stallmann and W. E. Schoupp. Nuclear energy levels in B^{10}—297
Kuerti, G. and S. N. Van Voorhis. Induced radioactivity produced by bombarding aluminum with protons—614(L)
Kusch, P. (see Millman, S.)—165, 214(A), 303
——— **and S. Millman.** Nuclear magnetic moments of $_5B^{10}$ and $_5B^{11}$—213(A)
——— **and S. Millman.** On the nuclear magnetic moments of the isotopes of rubidium and chlorine—527

Kyropoulos, S. Contact electric phenomena in the flow of oil—853(A)

Ladenburg, R., M. H. Kanner, H. Barschall and C. C. Van Voorhis. Study of uranium and thorium fission produced by fast neutrons of nearly homogeneous energy—168
Lamb, W. E., Jr. Deviation from the Coulomb law for a proton—384(L)
Landé, Alfred. Sommerfeld's fine structure constant and Born's reciprocity—482(L)
——— Structure of electric particles and the number 137—486(L)
Landsverk, O. G. $^1\Sigma \rightarrow {}^1\Sigma$ transition of the C_2 molecule—769
Lang, R. J. Regularities in the third spectrum of thorium—272
Langer, Lawrence M., Allan C. G. Mitchell and Paul W. McDaniel. Coincidences between beta- and gamma-rays in indium—380(L)
———, **Allan C. G. Mitchell and Paul W. McDaniel.** Coincidences between beta- and gamma-rays in manganese—422
——— **Allan C. G. Mitchell and Paul W. McDaniel.** Coincidences between beta- and gamma-rays in Na^{24}—962(L)
Langer, R. M. Growth of droplets in an expansion chamber—851(A)
Langsdorf, Alexander, Jr. Fission products of thorium—205(L)
Latimer, W. M. and H. A. Young. Nature of visual observations at low light intensities—963(L)
Lauritsen, C. C. (see Fowler, W. A.)—840(L), 841(L)
———, **W. A. Fowler and T. Lauritsen.** Gamma-radiation from fluorine plus protons—858(A)
Lauritsen, T. (see Lauritsen, C. C.)—858(A)
Lawrence, Ernest O., Luis W. Alvarez, William M. Brobeck, Donald Cooksey, Dale R. Corson, Edwin M. McMillan, W. W. Salisbury and Robert L. Thornton. Initial performance of the 60-inch cyclotron of the William H. Crocker Radiation Laboratory, University of California—124(L)
Lawson, A. W. and R. Scheib. Variation of the adiabatic elastic moduli of ammonium chloride with temperature between 200°K and 273°K—211(A)
Lawson, J. L. Beta-ray spectra of phosphorous, sodium and cobalt—131
——— (see Cork, J. M.)—291
Lawton, E. J. (see Kingdon, K. H.)—215(A)
Lewis, Arthur B. Effect of humidity and sphere material on the sparkover voltage of the 2-centimeter sphere gap—846(A)
Leipunski, A. (see Goloborodko, T.)—891
Libby, W. F. Natural radioactivity of leutecium—21
Loughridge, Donald H. and Paul Gast. Air mass effect on cosmic intensity—1169(L)
Luyet, B. J. Vitrification of water—1244(L)
Lyman, Elisabeth Reed. Elementary processes in the sensitized fluorescence of OH molecules—466

MacColl, L. A. Numerical calculations of the reflection of electrons by metals—699
MacKenzie, K. V. (see Henderson, Joseph E.)—857(A)
MacPhail, Malcolm and Joseph Giarratana. Total cross sections of carbon, nitrogen, sodium, magnesium and aluminum—207(A)
Mann, Marvin M. (see Hustrulid, Andrew)—208(A)
Manning, Millard F. and Marvin I. Chodorow. Electronic energy bands in metallic tungsten—787
Margenau, H. Van der Waals potential in helium—1000
Marshak, R. E. and H. A. Bethe. Energy production in the sun—210(A)
Marshall, John (see DuBridge, L. A.)—706(L)
Martin, S. T. On the thermionic and adsorptive properties of the surfaces of a tungsten single crystal—947
Marton, L. On the sensitivity of photographic emulsions for electrons between 50 and 100 kev—290(L)
Mason, W. P. (see Holden, A. N.)—378(L)
McCay, Myron S., Harold P. Knauss and Bruce Archdeacon. Effective rotation temperatures of CO in the electrodeless discharge—847(A)
McCreary, R. L. (see Valley, G. E.)—863
McDaniel, Paul W. (see Langer, Lawrence M.)—380(L), 422, 962(L)
McGrath, James W. Differences between the M_5 and M_4 absorption edges of gold in the pure metal and in a gold-copper alloy—137
——— M_1 and M_2 x-ray absorption edges of lead—765; Erratum—1068(L)
McLean, W. B. and R. A. Becker. Resonance in the production of short range alpha-particles from $F^{19}+H^1$—859(A)
McMillan, Edwin M. (see Lawrence, Ernest O.)—124(L)
——— **and W. W. Salisbury.** Modified arc source for the cyclotron—836(L)
McNatt, E. M. X-ray dispersion and atomic electron cloud distortion in zinc crystals—406
Miller, Franklin, Jr. On the single crystal x-ray diffraction pattern of calcite—757
Millikan, R. A. and H. V. Neher. New evidence for a change with time of the total energy brought into the earth by cosmic rays—491
———, **H. V. Neher and D. O. Smith.** Seasonal cosmic-ray effects at sea level—487
Millman, S. (see Kusch, P.)—213(A), 527
——— **and P. Kusch.** Nuclear magnetic moment of $_{13}Al^{27}$—214(A)
——— **and P. Kusch.** Nuclear spin and magnetic moment of $_{13}Al^{27}$—303
———, **P. Kusch and I. I. Rabi.** On the nuclear magnetic moments of the boron isotopes—165
Mitchell, Allan C. G. (see Langer, Lawrence M.)—380(L), 422, 962(L)
Monroe, A. M. (see Thaxton, Hubert M.)—616(L)
——— **and Hubert M. Thaxton.** Phase shifts (K_1) for the square well—616(L)
Montgomery, C. G. and D. D. Montgomery. Intensity of neutrons of thermal energy in the atmosphere at sea level—10
——— **and D. D. Montgomery.** Transition effect for large bursts of cosmic-ray ionization and the number of primary electrons of very high energy—640
———, **W. E. Ramsey, D. H. Cowie and D. D. Montgomery.** Slow mesons in the cosmic radiation—635

Montgomery, D. D. (see Montgomery, C. G.)—10, 635, 640
Moore, B. L. (see Holloway, M. G.)—705(L)
Morgan, S. O. (see Holden, A. N.)—378(L)
Morrison, P. Energy fluctuations in the electromagnetic field—849(A), 937
Morton, G. A. and E. G. Ramberg. Point projector electron microscope—705(L)
Mott-Smith, H. M. Periodic deviation from the Schottky line—668
Mouzon, J. C. Apparatus for nuclear physics—846(A)
——— **and R. D. Park.** Delayed gamma-rays from uranium activated by neutrons—238
Mueller, Hans and B. W. Sakmann. New electro-optical effect—615(L)
Mulliken, Robert S. Note on electronic states of diatomic carbon, and the carbon-carbon bond—778
Mullins, Lorin J. Radioactive isotopes in biology—1244(L)
Myers, F. E., R. D. Huntoon, C. G. Shull and C. M. Crenshaw. Search for a short range group of protons in the D-D reaction—1104

Nadig, Francis H. and J. Lloyd Bohn. Wide range high voltage electrostatic voltmeter—216(A)
Neher, H. V. (see Millikan, R. A.)—487, 491
Nielsen, Alvin H. and Walter Gordy. Infra-red spectrum and molecular constants of nitric oxide—781
——— **and Harald H. Nielsen.** 7.4μ fundamental vibration of methyl chloride—274
——— **and Harald H. Nielsen.** 7.5μ fundamental vibration of CH_3Cl—847(A)
Nielsen, Carl E. Phase control circuit and mercury arc illumination of cloud chamber—855(A)
Nielsen, Harald H. (see Nielsen, Alvin H.)—274, 847(A)
——— (see Shaffer, Wave H.)—188, 895, 1051
Nier, Alfred O. Coefficient of thermal diffusion of methane —1009
Nix, F. C. (see Steigman, J.)—13
Nordheim, L. W. On the production of the hard component of the cosmic radiation. II. Protons or neutral particles as primaries—502
——— **and M. H. Hebb.** On the production of the hard component of the cosmic radiation. I. Photon hypothesis —494

Oleson, N. L., K. T. Chao, J. Halpern and H. R. Crane. Multiple scattering of fast electrons—482(L); correction —1171(L)
Olson, N. Kermit. Magnetic field effect upon photoelectric properties of iron—210(A)
Onsager, L. and William W. Watson. Turbulence in convection in gases between concentric vertical cylinders—474
Oppenheimer, F. and E. P. Tomlinson. The positron spectra of N^{13} and Na^{22}—858(A)
Oppenheimer, J. R. and J. S. Schwinger. On pair emission in the proton bombardment of fluorine—1066(L)
——— **and H. Snyder.** On continued gravitational contraction—455

Pan, S. T. Magnetic test for superstructure in permalloy—933
Pardue, Louis A. and E. R. Gaerttner. Gamma-radiation from nitrogen bombarded by deuterons—855(A)
——— (see Gaerttner, E. R.)—856(A)
Park, R. D. (see Mouzon, J. C.)—238
Parker, E. R. (see Tarasov, L. P.)—379(L)
Parratt, Lyman G. X-ray resonance absorption lines in the argon K spectrum—295
Pasternack, Simon. Transition probabilities of forbidden lines—854(A)
Patterson, A. L. Diffraction of x-rays by small crystalline particles—972
——— Sherrer formula for x-ray particle size determination—978
Paul, Fred W. Observation of the spectrum of Ne V—1067(L)
——— **and W. A. Rense.** Spectra of Y V and Zr VI—1110
Pearson, G. L. Formation of metallic bridges between separated contacts—471
Peoples, J. A., Jr. (see Green, J. B.)—54, 385(L)
Phipps, T. E. (see Seifert, R. L. E.)—652
——— (see Turnbull, D.)—663
Pitt, A. (see Findlay, J. C.)—122(L)
Pittman, M. A. Skin temperature measurements—844(A)
Plesset, Milton S. (see Brown, Frederick W.)—841(L)
Plyler, E. K. (see Shearin, P. E.)—845(A)
Pollard, Ernest. Mass and energy levels of S^{33}—961(L)
——— Mass and stability of C^{14}—1168(L)
———, **W. L. Davidson, Jr. and Howard Schultz.** Transmutation of boron by deuterons—206(A)
Pollard, W. G. Use of surface states to explain activated adsorption—324
Pollock, H. C. and F. S. Cooper. Effect of pressure on the positive point-to-plane discharge in N_2, O_2, CO_2, SO_2, SF_6, CCl_2F_2, A, He and H_2—170
Potter, James G. Temperature dependence of the work function of tungsten—216(A)
Prebus, A. (see Burton, E. F.)—1171(L)
Purks, J. H., Jr. (see Stipe, Gordon, Jr.)—843(A)

Rabi, I. I. (see Kellogg, J. M. B.)—213(A), 728
——— (see Millman, S.)—165
Raines, Barbara. Accommodation coefficient of helium on nickel—691
Ramberg, E. G. (see Morton, G. A.)—705(L)
Ramo, Simon. Space charge and field waves in an electron beam—276
Ramsey, N. F., Jr. (see Kellogg, J. M. B.)—213(A), 728
Ramsey, W. E. (see Montgomery, C. G.)—635
——— (see Swann, W. F. G.)—378(L)
Randall, H. M. (see Fuson, Nelson)—982
Randall, R. H., F. C. Rose and C. Zener. Intercrystalline thermal currents as a source of internal friction—343
Rasetti, F. (see Amaldi, E.)—881
Read, T. A. Internal friction of zinc crystals—211(A)
Rense, W. A. (see Paul, F. W.)—1110
Ribner, H. S. Experimental test of Schremp's theory of cosmic-ray fine structure—1069
Richtmyer, R. D. Theory of the x-ray lines LL-LM—146
——— Theory of x-ray lines resulting from double ionization of the L-shell—857(A)

Roberts, R. B. (see Heydenburg, N. P.)—1092
Rochester, George D. Absorption spectrum of aluminum fluoride (AlF)—305
Rose, F. C. (see Randall, R. H.)—343
Rose, M. E. Electric quadrupole and magnetic dipole moments of Li^6 and N^{14}—1064(L)
Rossi, Bruno, H. Van Norman Hilberry and J. Barton Hoag. Disintegration of mesotrons—837(L)
Ruark, Arthur. Time distribution of so-called random events—1165
Rubens, S. M. and J. E. Henderson. Function of anode spots in the glow discharge—854(A)
Rubin, S. (see Houston, W. V.)—852(A)
Rushbrooke, G. S. (see Coulson, C. A.)—1216
Ryan, Alden H. (see Fox, Gerald W.)—1132

Sakmann, B. W. (see Mueller, Hans)—615(L)
Salisbury, W. W. (see Lawrence, Ernest O.)—124(L)
——— (see McMillan, Edwin)—836(L)
Sammon, P. J. (see Kenrick, G. W.)—203(L)
Saunderson, J. L. (see Goudsmit, S.)—122(L)
Scheib, R. (see Lawson, A. W.)—211(A)
Schein, Marcel, W. P. Jesse and E. O. Wollan. Intensity and rate of production of mesotrons as a function of altitude—613(L)
Schelkunoff, S. A. On diffraction and radiation of electromagnetic waves—308
Schiff, L. I. Question in general relativity—850(A)
Schönberg, Mario. β-ray selection rules and the meson theory—612(L)
Schoupp, W. E. (see Kruger, P. Gerald)—297
Schultz, Howard. (see Pollard, Ernest)—206
Schwinger, J. S. (see Oppenheimer, J. R.)—1066(L)
Seaborg, G. T. (see Kennedy, G. W.)—1095
Seeger, R. J. and E. Teller. Remarks on the dielectric breakdown—352
Seely, S. (see Zinn, W. H.)—260
Segrè, E. (see Kennedy, G. W.)—1095
Seifert, R. L. E. and T. E. Phipps. Evidence of a periodic deviation from the Schottky line. I—652
Seitz, Frederick. Lattice defects in silver halide crystals—1063(L)
Selényi, P. Wide-angle interferences and the nature of the elementary light sources—477
Serber, Robert. Beta-decay and mesotron lifetime—1065(L)
Shaffer, Wave H. and Harald H. Nielsen. Vibration-rotation energies of the nonlinear triatomic XY_2 type of molecule—188
———, **Harald H. Nielsen and L. H. Thomas.** Rotation-vibration energies of tetrahedrally symmetric pentatomic molecules. I—895, II—1051
Share, S. S. (see Hoisington, L. E.)—884
Sharp, D. Gordon. Lethal effect of 2537A radiation on bacteria—846(A)
Shear, G. M. and H. D. Ussery. Spectrographic differentiation of thallium toxicity and frenching of tobacco plants—844(A)
Shear, Sidney K. and Alfred B. Focke. Dispersion of supersonic waves in cylindrical rods of polycrystalline silver, nickel and magnesium—217(A)
Shearin, P. E. and E. K. Plyler. Infra-red absorption of mixtures containing D_2O—845(A)
Sheng, H. Y. (see Barker, E. F.)—854(A)
Shenstone, A. G. Additions to the arc spectrum of silver—209(A)
Sheppard, C. W. (see Fowler, W. A.)—859(A)
——— **and W. A. Fowler.** Experiments on the multiple scattering of electrons and positrons—849(A)
Shive, John N. Practice and theory of the modulation of Geiger counters—579
Shockley, William. On the surface states associated with a periodic potential—317
——— Relationship between surface states and energy bands in crystals—212(A)
——— (see Steigman, J.)—13
Shoupp, W. E. (see Kruger, P. Gerald)—297
——— (see Stephens, W. E.)—209(A)
Shull, C. G. (see Myers, F. E.)—1104
Sibaiya, L. Structure of iridium lines—768
——— **and H. S. Venkataramiah.** Raman effect in samarium nitrate solutions—381(L)
Siegel, Sidney. Elastic constants of single crystals of the alloy Cu_3Au—211(A)
Siegert, A. J. F. On the derivation of the dispersion formula for nuclear reactions—750
Simmons, J. W. Study of dielectric absorption—848(A)
Skaggs, Lester S. Precise determination of the energy released in the production of deuterium from beryllium under proton bombardment—24
——— (see Allison, Samuel K.)—288(L), 860(A)
Skarstrom, C. (see Beams, J. W.)—266
Slawsky, M. M. and H. R. Crane. Absorption of high energy electrons. IV—1203
Smith, D. O. (see Millikan, R. A.)—487
Smith, H. Grayson. (see Findlay, J. C.)—122(L)
Smith, Nicholas M., Jr. Energies released in the reactions Li^7 $(p,\alpha)He^4$ and Li^6 $(d,\alpha)He^4$, and the masses of the light atoms—548
——— (see Allison, Samuel K.)—288(L), 860(A)
Smythe, W. R. (see Townes, C. H.)—1210
Snyder, H. Limiting solutions for collapsing masses—857(A)
——— (see Oppenheimer, J. R.)—455
Spitzer, Lyman, Jr. Stark-effect broadening of hydrogen lines. II. Observable profiles—39
Squire, Charles F. Antiferromagnetism in some manganous compounds—922
——— Electrical conductivity as a function of temperature of some manganous compounds—960(L)
——— Low temperature transition phenomena in some paramagnetic salts—211(A)
Stallmann, F. W. (see Kruger, P. Gerald)—297
Starr, Chauncey. Cathode sputtering—216(A)
Steigman, J., W. Shockley and F. C. Nix. Self-diffusion of copper—13
Stephens, W. E., W. E. Shoupp, R. O. Haxby and W. H. Wells. High pressure cloud chamber—209(A)

Stephenson, C. C. and J. G. Hooley. Heat capacity of potassium dihydrogen phosphate at the Curie point—121(L)
Stephenson, S. T. Fine structure in the absorption and emission spectra of x-rays—856(A)
Stevenson, A. F. Method for improved calculation of energies of two-electron configurations from Hartree functions. Application to $2p^2$ terms in O III—586
Stewart, David W. Induced radioactivity in strontium and yttrium; nuclear isomers in strontium—629
——— (see Fajans, Kasimir)—625
Stipe, Gordon, Jr., and J. H. Purks, Jr. Method of measuring electrolytic conductivity at high frequencies—843(A)
Strait, Louis A. Quantitative analysis of rubidium in plant sap by spectrographic means—855(A)
Stranathan, J. D. (see Good, Wilfred M.)—810
Stratton, J. A. and L. J. Chu. Diffraction theory of electromagnetic waves—99
——— **and L. J. Chu.** Note on diffraction and radiation of electromagnetic waves—316
Streib, J. F. (see Gaerttner, E. R.)—856(A)
Suits, C. G. Arcing phenomena in mercury switches—215(A)
Sutherland, G. B. B. M. High frequency perpendicular fundamental vibration of the ammonia molecule—836(L)
Swann, W. F. G. Nature of cosmic-ray phenomena at high altitudes—209(A)
——— **and W. E. Ramsey.** Showers produced by penetrating rays—378(L)
Swanson, D. C. (see Bacher, R. F.)—483(L)
Szilard, Leo. (see Anderson, H. L.)—284
——— (see Zinn, W. H.)—619

Talley, J. L. Light plane hypothesis—848(T)
Tape, G. F. Beta-spectra of iodine—965
Tarasov, L. P. Dependence of ferromagnetic anisotropy on the field strength—1224
——— Ferromagnetic anisotropy of iron and iron-rich silicon alloys—1231
——— Ferromagnetic anisotropy of low-nickel alloys of iron—1245(L)
——— Rotational and alternating hysteresis losses in electrical sheet steel—1170(L)
——— **and E. R. Parker.** Ferromagnetism in austenite—379(L)
Tate, John T. (see Hustrulid, Andrew)—208(A)
Taub, A. H. Spinor equations for the meson and their solution when no field is present—799, 853(A)
Teller, E. (see Haupt, R. F.)—208(A)
——— (see Seeger, R. J.)—352
——— (see Wigner, Eugene P.)—530
Thaxton, Hubert M. (see Monroe, A. M.)—616(L)
——— **and L. E. Hoisington.** Phase shift calculations for proton-proton scattering at high energies—1194
——— **and A. M. Monroe.** (K_1) phase shifts for the error well—616(L)
Thode, Harry G. Vapor pressures, heats of vaporization and melting points of N^{14} and N^{15} ammonia—214(A)
Thomas, C. D. and R. C. Colwell. Wave reflections from diffuse boundaries—1214
Thomas, L. H. (see Shaffer, Wave H.)—895, 1051
——— **and S. E. Whitcomb.** Normal modes of oscillation of the long chain paraffin hydrocarbons—383(L)
Thornton, Robert L. (see Lawrence, Ernest O.)—124(L)
Todd, John D. (see Brady, James J.)—859(A)
Tomlinson, E. P. (see Oppenheimer, F.)—858(A)
Tonks, L. Theory of magnetic effects in the plasma of an arc—360
Townes, Charles H. Concentration of C^{13} and measurements of its nuclear spin—850(A)
——— **and W. R. Smythe.** Spin of carbon thirteen—1210
Trabacchi, G. C. (see Amaldi, E.)—881
Tregidga, Angus C. Dielectric constant of water vapor at a frequency of 42 megacycles—856(A)
Trump, J. R., R. J. Van de Graaff and R. W. Cloud. Preliminary investigation of cathode rays—215(A)
Turnbull, D. and T. E. Phipps. Evidence of a periodic deviation from the Schottky line. II—663
Tuve, M. A. (see Heydenburg, N. P.)—1078
Tyler, A. W. Beta- and gamma-radiations from copper^{64} and europium^{152}—125
Tyrrell, Warren A., Jr. Nuclear five-body problem—250

Uehling, E. A. (see Hellund, E. J.)—818, 851(A)
Underwood, N. (see Burch, John C.)—844(A)
Ussery, H. D. (see Shear, G. M. O.—844(A)

Valley, G. E. Magnetic spectrograph investigation of N^{13} gamma-radiation—838(L)
——— **and R. L. McCreary.** Internally converted gamma-rays of several radioactive elements—863
Van Allen, J. A., A. Ellett and D. S. Bayley. Cross section for the reaction of $H^2+H^2 \rightarrow H^1+H^3$ with a gas target—383(L)
Van de Graaff, R. J. (see Trump, J. G.)—215(A)
Van der Merwe, C. W. (see Bacon, R. H.)—1168(L)
Van Vleck, J. H. (see King, G. W.)—464
Van Voorhis, C. C. (see Ladenburg, R.)—168
Van Voorhis, S. N. (see Kuerti, G.)—614(L)
Vargus, J. A., Jr. Angular distribution of cosmic-ray particles scattered in 1 cm of platinum—480
Veith, Werner and Paul Kirkpatrick. Search for weak lines in the molybdenum L spectrum—705(L)
Venkataramiah, H. S. (see Sibaiya, L.)—381(L)
Vinti, John P. Isotope shift in magnesium—1120
Vogt, H. G. (see Bainbridge, K. T.)—213(A)
——— (see Getting, I. A.)—213(A), 1098
Volkoff, G. M. On the proper energy of the electron—858(A)

Waldman, Bernard (see Collins, George B.)—876
Wall, C. N. (see Gingrich, Newell S.)—336
Wataghin, Gleb. On explosion showers—1245(L)
Watson, R. E. (see Bartlett, J. H.)—612(L)
Watson, William W. Concentration of heavy carbon by thermal diffusion—703(L)
——— (see Onsager, L.)—474
Way, Katharine. Simple picture of the binding energies of H^3 and He^5—556
Weil, George L. and Walter H. Barkas Beta-radiation of As^{76}—485(L)

Weisskopf, V. F. On the self-energy and the electromagnetic field of the electron—72
Weller, R. New method for photoelasticity in three dimensions—216(A)
Wells, W. H. (see Stephens, W. E.)—209(A)
Wheeler, John Archibald (see Bohr, Niels)—426, 1065(L)
Wheeler, Mary A. Paramagnetic susceptibility of copper-nickel and zinc-nickel alloys—1137
Whitaker, M. D. Some new aspects of neutron scattering. Experimental—1068(T)
Whitcomb, S. E. (see Thomas, L. H.)—383(L)
White, John U. Absorption spectrum of CN—853(A)
White, Milton G. (see Barkas, Walter H.)—288(L)
——— (see Creutz, E. C.)—207(A)
———, **L. A. Delsasso, J. G. Fox and E. C. Creutz.** Short-lived radioactivities induced in fluorine, sodium and magnesium by high energy protons—512
Wigner, E. P. On the coupling conditions in light nuclei and the lifetimes of β-radioactivities—519
——— **and L. Eisenbud.** On the saturation of forces derived from the meson theory—214(A)
———, **Charles L. Critchfield and Edward Teller.** Electron-positron field theory of nuclear forces—530
Wilhelm, J. O. (see Findlay, J. C.)—122(L)
Williams, Dudley. (see Gautier, T. N.)—616(L)
——— **and Loraine Decherd.** Force constants of NO_2 groups—847(A)
——— **and Benjamin Hinton.** Determination of melting points by transmitted light—844(A)
Williams, H. J. (see Bozorth, R. M.)—1068(T)
——— **and R. M. Bozorth.** Magnetic anisotropy of nickel at 20°K—837(L)
Williamson, R. C. Displacements of Raman frequencies of some aliphatic molecules in water solution—848(A)
Wilson, Robert R. Formation of ions in the cyclotron—459
——— **and Dale R. Corson.** Low-background electron counter—851(A)
Wilson, Thomas C. Effect of high pressure on the order-disorder transformations in alloys—598
Winch, Ralph P. (see Farnsworth, H. E.)—1067(L)
Witmer, Enos E., Masses and magnetic moments of the proton, neutron and deuteron—214(A)
——— Regularity in nuclear magnetic moments—203
Wollan, E. O. (see Schein, Marcel)—613(L)
Wood, R. W. Lecture demonstration of resonance radiation of sodium—1172(L)
Wooldridge, D. E. Secondary emission from evaporated nickel and cobalt—1062(L)
——— Theory of secondary emission—562
Wright, R. W. (see Hole, W. L.)—785

Young, H. A. (see Latimer, W. H.)—963(L)
Yunker, E. A. Mobility spectrum of atmospheric ions—855(A)

Zacharias, J. R. (see Kellogg, J. M. B.)—213(A), 728
Zener, C. (see Randall, R. H.)—343
Zinn, W. H. and Leo Szilard. Emission of neutrons by uranium—619
———, **S. Seely and V. W. Cohen.** Collision cross sections for D-D neutrons—260
Zlotowski, I. Nuclear disintegration induced by the cosmic radiation—484(L)

Analytic Subject Index to Volume 56

References with (A) are to abstracts of papers presented at meetings of the American Physical Society.
References with (L) are to Letters to the Editor.

Accommodation coefficient
Of He on Ni, B. Raines—691

Acoustics
Absorption of supersonic waves, G. K. Hartmann, A. B. Focke—217(A)
Dispersion of supersonic waves, S. K. Shear, A. B. Focke—217(A)
Velocity of sound in liquid He, J. C. Findlay, A. Pitt, H. Grayson Smith, J. O. Wilhelm—122(L)

Adsorption
Activated adsorption, theory of, W. G. Pollard—324

Astrophysics
Energy production in sun, R. E. Marshak, H. A. Bethe—210(A)
Gravitational contraction, J. R. Oppenheimer, H. Snyder—455
Limiting solutions, collapsing masses, H. Snyder—857(A)
Matter at extremely high temperatures and pressures, F. Cernuschi—450
Super-novae and neutron-core stars, F. Cernuschi—120(L)

Atomic mass (see **Isotopes**)

Atomic structure (see also **Spectra**)
Calculation of two-electron configurations, A. F. Stevenson—586
Variational atomic wave functions, L. Goldberg, A. M. Clogston—696

Biophysics
Absorption of 1500-kev cathode rays, J. G. Trump, R. J. Van de Graaff, R. W. Cloud—215(A)
Analysis of Rb in plant sap, L. A. Strait—855(A)
Biochemical and physical effects at high pressure, R. B. Dow—215(A)
Blood volume determination, J. C. Burch, E. T. Ellison, N. Underwood—844(A)
Lethal effect of radiation on bacteria, D. G. Sharp—846(A)
Radioactive tracers, A. Barnett—961(L); H. R. Crane—1243(L); L. J. Mullins—1244(L)
Skin temperature measurements, M. A. Pittman—844(A)
Statistical significance of rate differences, F. T. Holmes—844(A)
Thallium toxicity and frenching of tobacco plants, G. M. Shear, H. D. Ussery—844(A)

Conductivity, electrical (see **Electrical conductivity; Discharge of electricity in gases**)

Constants, physical, standards
Fine structure constant, A. Landé—482(L), 486(L)
Nomogram for atomic constants, R. A. Beth—208(A)
Values of e, m, and h, J. W. M. DuMond—153

Contact potentials
Phenomena in oils, S. Kyropoulos—853(A)
Between silver films on glass and on rocksalt, P. A. Anderson—850(A)

Cosmic radiation
Angular dispersion in upper atmosphere, T. H. Johnson—210(A), 226
Angular distribution of particles scattered in Pt, J. A. Vargus, Jr.—480
Change of energy with time, R. A. Millikan, H. V. Neher—491
Cloud chamber expansion ratio and drop count determination, D. Bagley—851(A)
East-west symmetry at high elevations, T. H. Johnson, J. G. Barry—219
Explosion showers, G. Wataghin—1245(L)
Effect of air masses, D. H. Loughridge, P. Gast—1169(L)
Fine structure, Schremp's theory, H. S. Ribner—1069
Nature at high altitudes, W. F. G. Swann—209(A)
Neutrons in radiation, S. A. Korff—210(A), 1241(L)
Neutrons of thermal energy at sea level, C. G. Montgomery, D. D. Montgomery—10
Nuclear disintegration induced by cosmic radiation, I. Zlotowski—484(L)
Origin of, H. Alfvén—1060(L)
Production of hard component, photon hypothesis, L. W. Nordheim, M. H. Hebb—494
Protons or neutrons as primaries, L. W. Nordheim—502
Seasonal effects at sea level, R. A. Millikan, H. V. Neher, D. O. Smith—487
Showers from penetrating rays, W. F. G. Swann, W. E. Ramsey—378(L)
Slow mesotrons, C. G. Montgomery, W. E. Ramsey, D. H. Cowie, D. D. Montgomery—635
Specific ionization measurements, R. B. Brode, G. D. Bagley—209(A)
Theory of origin, F. Cernuschi—120(L)
Time distribution of bursts, P. S. Gill—632
Transition effect for large bursts, C. G. Montgomery, D. D. Montgomery—640
Upward radiation at high altitudes, S. A. Korff, E. T. Clarke—704(L)
Variations of earth's magnetic field, effect of, O. Godart—1074

Crystal structure
Space group of $KH(CO_3)$, R. C. Keen—847(A)

Crystalline state
Diffusion in solid state, R. P. Johnson—814
Effect of pressure on order-disorder transformation, T. C. Wilson—598
Electrical breakdown of ionic crystals, R. C. Buehl, A. v. Hippel—941
Electron distribution in ZnO crystals, H. M. James, V. A. Johnson—119(L)

Crystalline state (continued)
Electronic energy bands in tungsten, M. F. Manning, M. I. Chodorow—787
Heat capacity at Curie point, C. C. Stephenson, J. G. Hooley—121(L)
Internal friction; intercrystalline thermal currents, R. H. Randall, F. C. Rose, C. Zener—343
Lattice defects in Ag halide crystals, F. Seitz—1063(L)
Modes of vibration of body-centered cubic lattice, P. C. Fine—355, 852(A)
Order in Cu-Au system, L. H. Germer, F. E. Haworth—212(A)
Periodic potential, associated surface states, W. Shockley—317
Photoconductivity of crystals, J. J. Brady, J. D. Todd—859(A)
Rochelle salt, properties of, A. N. Holden, G. T. Kohman, W. P. Mason, S. O. Morgan—378(L)
Self-diffusion of Cu, J. Steigman, W. Shockley, F. C. Nix—13
Superstructure in $FeNi_3$, F. E. Haworth—289(L)
Superstructure in permalloy, S. T. Pan—933
Surface states and energy bands in crystals, W. Shockley—212(A)
Susceptibility of Cu-Ni and Zn-Ni alloys, M. A. Wheeler—1137
Twinning in Bi crystals, A. B. Focke—854(A)
Vitreous state of water, B. J. Luyet—1244(L)
Zone theory, R. P. Johnson—213(A)

Dielectric constants (see **Dielectrics and dielectric properties**)
Dielectrics and dielectric properties
Absorption of charge, J. W. Simmons—848(A)
Of NH_3, N_2 and CO_2 at high frequency, G. W. Fox, A. H. Ryan—1132
Breakdown in ionic crystals, H. Fröhlich—349; R. J. Seeger, E. Teller—352; R. C. Buehl, A. v. Hippel—941
Permanent electrets, behavior of, W. M. Good, J. D. Stranathan—810
Of Rochelle salt with D_2O, A. N. Holden, G. T. Kohman, W. P. Mason, S. O. Morgan—378(L)
Of water vapor at 42 megacycles, A. C. Tregidga—856(A)
Diffusion
Coefficient of thermal diffusion, A. O. Nier—1009
Self-diffusion of Cu, J. Steigman, W. Shockley, F. C. Nix—13
In solid state, R. P. Johnson—814
Discharge of electricity in gases
Anode spots in glow discharge, S. M. Rubens, J. E. Henderson—854(A)
Arcing phenomena in Hg switches, C. G. Suits—215(A)
Cathode sputtering, C. Starr—216(A)
Chamber geometry; h. f. discharge, S. Githens, Jr.—845(A)
Effect of pressure on positive point-to-plane discharge, H. C. Pollock, F. S. Cooper—170
Formation of ions in cyclotron, R. R. Wilson—459
Humidity and sparkover voltage of sphere gap, A. B. Lewis—846(A)
Initial recombination, N. E. Bradbury—849(A)
Magnetic effects in plasma, L. Tonks—360
Temperatures in electrodeless discharge, M. S. McCay, H. P. Knauss, B. Archdeacon—847(A)
Townsend coefficients for H_2, D. H. Hale—858(A), 1199
Transitions between glow and arc, W. G. Cady—123(L)
Discharge of electricity in high vacua (see **Thermionic emission**)
Disintegration of nucleus (see also **Radioactivity**)
Of Be by electrons, G. B. Collins, B. Waldman, E. Guth—876
Of B by deuterons, E. Pollard, W. L. Davidson, Jr., H. Schultz—206(A)
Cross section for reaction $H^2+H^2 \rightarrow H^1+H^3$; gas target, J. A. Van Allen, A. Ellett, D. S. Bayley—383(L)
Delayed gamma-rays from U, J. C. Mouzon, R. D. Park—238
Of deuterium by protons and p-n reactions, W. H. Barkas, M. G. White—288(L)
Disintegration induced by cosmic radiation, I. Zlotowski—484(L)
Dispersion formula for nuclear reactions, A. J. F. Siegert—750
Energies released in Li^7 $(p,\alpha)He^4$ and $Li^6(d,\alpha)He^4$, S. K. Allison, L. S. Skaggs, N. M. Smith, Jr.—288(L), 860(A); N. M. Smith, Jr.—548
Energy released in $Be^9(p,d)Be^8$, L. S. Skaggs—24
Fission products of Th, A. Langsdorf, Jr.—205(L)
Fission of protactinium, A. v. Grosse, E. T. Booth, J. R. Dunning—382(L)
γ-radiation from F+H, C. C. Lauritsen, W. A. Fowler, T. Lauritsen—858(A)
γ-radiation from Li, W. A. Fowler, C. C. Lauritsen—841(L)
γ-radiation from $N+H^2$, L. A. Pardue, E. R. Gaerttner—855(A)
Heat of fission of U, M. C. Henderson—703(L)
Mechanism of nuclear fission, N. Bohr, J. A. Wheeler—426
Neutron production and absorption in U, H. L. Anderson, E. Fermi, L. Szilard—284
Neutrons from F by deuterons, T. W. Bonner—207(A)
Of N^{14} and N^{15} by deuterons, M. G. Holloway, B. L. Moore—705(L)
Pair emission from F, W. A. Fowler, C. C. Lauritsen—840(L)
Of protactinium, N. Bohr, J. A. Wheeler—1065(L)
Protons from V, Cu, Mn and Sc, W. L. Davidson, Jr.—1061(L); 1062(L)
Radiation from deuteron-deuteron reaction, M. H. Kanner, W. T. Harris—839(L)
Reactions involving He^3, W. H. Barkas—1242(L)
Recoil of nucleus in beta-decay, H. R. Crane, J. Halpern—232
Resonance in α-particles from $F^{19}+H^1$, W. B. McLean, R. A. Becker—859(A)
Short range protons in D-D reaction, F. E. Myers, R. D. Huntoon, C. G. Shull, C. M. Crenshaw—1104

Symmetrical distribution in $B^{10}(n,\alpha)$, W. E. Good, R. D. Hill—288(L)
Of U by neutrons; products, P. Abelson—1
U and Th fission by fast neutrons, R. Ladenburg, M. H. Kanner, H. Barschall, C. C. Van Voorhis—168
Dissociation
Of hydrocarbons by electron impact, J. Delfosse, W. Bleakney—208(A), 256
Of H_2O vapor by electron impact, A. Hustrulid, M. M. Mann, J. T. Tate—208(A)

Elasticity
Adiabatic elastic moduli of NH_3Cl, A. W. Lawson, R. Scheib—211(A)
Compressibility of Al+Cu by x-ray measurements, R. B. Jacobs—211(A)
Constants of single crystals of Cu_3Au, S. Siegel—211(A)
Internal friction; intercrystalline thermal currents, R. H. Randall, F. C. Rose, C. Zener—343
Internal friction of Zn crystals, T. A. Read—211(A)
Photoelasticity in three dimensions, R. Weller—216(A)
Young's modulus; new method, A. King—216(A)
Electrical circuits
Quenched primary of induction coil, W. P. Boynton—853(A)
Electrical conductivity and resistance
Change in a magnetic field, L. Davis, Jr.—93
Of Mn compounds; effect of temperature, C. F. Squire—960(L)
Metallic bridges between separated contacts, G. L. Pearson—471
Of thin Pb films, M. G. Foster, A. Goetz—849(A)
Electromagnetic theory
Diffraction and radiation, S. A. Schelkunoff—308; J. A. Stratton, L. J. Chu—99, 316
Energy fluctuations in field, P. Morrison—937
Reflections from diffuse boundaries, C. D. Thomas, R. C. Colwell—1214
Space charge and field waves in electron beam, S. Ramo—276
Wide-angle interference; nature of elementary light sources, P. Selényi—477
Electrons
Proper energy of electron G. M. Volkoff—858(A)
Structure of electric particles and the number 137; Born's reciprocity, A. Landé—486(L)
Electrons, scattering of (see **Scattering of electrons, neutrons and ions**)
Electrons, secondary
By high energy electrons, W. A. Fowler, C. W. Sheppard—859(A)
From metals; positive ion bombardment, J. B. Fisk—846(A)
From Ni and Co, D. E. Wooldridge—1062(L)
Theory of, D. E. Wooldridge—562
Electro-optical effects (see also **Photoelectric effect and properties**)
New effect, H. Mueller, B. W. Sakmann—615(L)
Energy states of atoms (see **Atomic structure**)
Energy states of nucleus (see **Nuclear structure**)
Errata
Interaction of configurations: sd-p^2, R. F. Bacher—385(L)
M_1 and M_2 x-ray absorption edges of lead, J. W. McGrath—1068(L)
Paschen-Back effect. VI. The spectrum of neon, J. B. Green, J. A. Peoples, Jr.—385(L)
Velocity of radio waves in air, G. H. Brown—385(L)

Field currents
Fields involved, J. E. Henderson, K. V. MacKenzie—857(A)
Range and validity of equation, F. R. Abbott, J. E. Henderson—113, 853(A)
Field theory
Self-energy and electromagnetic field of electron, V. F. Weisskopf—72
Films, properties of
Conductivity of thin Pb films, M. G. Foster, A. Goetz—849(A)
Structure of very thin films, L. H. Germer—58
Fine structure (see **Spectra,** etc. and **Hyperfine structure**)
Fluorescence
Of OH molecules, E. R. Lyman—466

Gravitation
Continued gravitational contraction, J. R. Oppenheimer, H. Snyder—455

Heat of combustion
Mileage of gasoline of different grades, J. B. Derieux—845(A)
High voltage tubes and machines (see **Methods and instruments**)
Hydrodynamics
Streamline flow, D. Kirkham—852(A)
Hyperfine structure (see also **Nuclear moments and spin**)
Of iridium lines, L. Sibaiya—768
Metastable $^2P_{3/2}$ state of In^{115}, D. R. Hamilton—30

Instruments (see **Methods and instruments**)
Ions, mobility
Of atmospheric ions, E. A. Yunker—855(A)
Hg ions in Hg vapor, K. H. Kingdon, E. J. Lawton—215(A)
Of K ions at high fields, A. V. Hershey—908
Theory of; for high velocity ions, A. V. Hershey—916
Isomers, nuclear (see **Radioactivity**)
Isotopes
Concentration of C^{13} by thermal diffusion, W. W. Watson—703(L); A. O. Nier—1009
Concentration by centrifuge, J. W. Beams, C. Skarstrom—266
He^3 and H^3, L. W. Alvarez, R. Cornog—379(L), 613(L)
Mass of Li^6, Li^7, Be^8, Be^9, N. M. Smith, Jr.—548

Isotopes (continued)
Separation of Br isotopes by centrifugation, R. F. Humphreys—684
Vapor pressures, heats of vaporization and melting points of N^{14} and N^{15} ammonia, H. G. Thode—214(A)

Kinetic theory of gases
Convection and conduction, I. Brody, F. de Kőrösy—217(A)
Fugacity of CO_2, W. E. Deming, L. S. Deming—108
Transport phenomena in mixture of gases, E. J. Hellund, E. A. Uehling—818, 851(A)
Turbulence in convection between concentric cylinders, L. Onsager, W. W. Watson—474

Liquids (see also **Hydrodynamics**)
Atomic distribution curves, C. A. Coulson, G. S. Rushbrooke—1216
Contact electric phenomena in oils, S. Kyropoulos—853(A)
Structure of liquid K, N. S. Gingrich, C. N. Wall—336
Velocity of sound in liquid He, J. C. Findlay, A. Pitt, H. Grayson Smith, J. O. Wilhelm—122(L)

Luminescence
Of sulfide phosphors, R. P. Johnson—213(A)
Of synthetic halite crystals, B. E. Cohn—856(A)

Magnetic properties
Anisotropy of Fe and Fe-Si alloys, L. P. Tarasov—1231
Anisotropy of Ni, H. J. Williams, R. M. Bozorth—837(L)
Anisotropy of Ni-Fe alloys, L. P. Tarasov—1245(L)
Antiferromagnetism in manganous compounds, C. F. Squire—922
Of electrolytically polished silicon-iron crystals, W. C. Elmore—210(A)
Ferromagnetic anisotropy, L. P. Tarasov—1224
Ferromagnetism in austenite, L. P. Tarasov, E. R. Parker—379(L)
Hysteresis losses in steel, L. P. Tarasov—1170(L)
Of solid solutions, F. Bitter, A. R. Kaufmann—1044
Surface effects of impurities, F. W. Constant, J. M. Formwalt—846(A)
Susceptibility of Cu-Ni and Zn-Ni alloys, M. A. Wheeler—1137
Test for superstructure in permalloy, S. T. Pan—933
Transition in paramagnetic salts, C. F. Squire—211(A)

Magneto-optical effects
Observations at low light intensities, W. N. Latimer, H. A. Young—963(L)

Mass defects (see **Isotopes**)

Mechanics, quantum-atomic structure and spectra
Wave functions of relativistic hydrogenic atom, L. Davis, Jr.—851(A)

Mechanics, quantum—general
Dispersion formula for nuclear reactions, A. J. F. Siegert—750
Double beta-disintegration, W. H. Furry—1184
Fluctuations in electromagnetic field, P. Morrison—849(A), 937
Klein's fifth dimension, W. Band—204(L)
Proper energy of electron, G. M. Volkoff—858(A)
Weinstein's theorem, G. Horvay—214(A)

Mechanics, statistical
Fluctuations and entropy, E. C. Kemble—1013
Quantum-mechanical basis, E. C. Kemble—1146

Mesotrons
Absorption in matter, E. Fermi—1242(L)
β-ray selection rules; theory of mesotron, M. Schönberg—612(L)
Disintegration of, B. Rossi, H. Van N. Hilberry, J. B. Hoag—837(L)
Intensity of mesotrons; function of altitude, M. Schein, W. P. Jesse, E. O. Wollan—613(L)
Lifetime and β-decay, R. Serber—1065(L)
Saturation of forces, E. Wigner, L. Eisenbud—214(A)
Slow mesotrons in cosmic radiation, C. G. Montgomery, W. E. Ramsey, D. H. Cowie, D. D. Montgomery—635
Spinor equations for mesotron, A. H. Taub—799, 853(A); H. Fröhlich, W. Heitler, B. Kahn—961(L)
Theory; Coulomb law for proton, W. E. Lamb, Jr.—384(L)

Metals (see **Crystalline state**)

Meteorology
Heat transfer in the atmosphere, W. M. Elsasser—855(A)
Radiation from sky, C. M. Heck—848(A)
Zodiacal light during solar eclipse, E. O. Hulburt—960(L)

Methods and instruments
Analysis of Rb in plant sap, L. A. Strait—855(A)
Arc source for cyclotron, E. McMillan, W. W. Salisbury—836(L)
Bent rocksalt crystal spectrograph, P. H. Abelson—753
Be targets for nuclear research, M. C. Henderson—207(A)
Bragg spectrometer for low temperature, A. Goetz, A. Dember—857(A)
Cathode sputtering, C. Starr—216(A)
Centrifuge; analytical, J. W. Beams, R. E. Fox—848(A)
Clean-up of H_2 by Ba, G. W. Johnson, W. A. Hane, P. A. Anderson—852(A)
Cloud chamber expansion ratio and drop count determination, D. Bagley—851(A)
Concentration of isotopes by centrifuge method, J. W. Beams, C. Skarstrom—266
Dental fluoroscope and shield, C. R. Fountain—844(A)
Differential manometer, W. Hurst—846(A)
Dispenser cathode; cathode for gaseous discharge tubes, A. W. Hull—86
Double Fizeau toothed wheel, H. E. Ives—215(A)
Droplets in expansion chamber, growth of, R. M. Langer—851(A)
Electrolytic conductivity at high frequencies, G. Stipe, Jr., J. H. Purks, Jr.—843(A)
Electron counter, R. R. Wilson, D. R. Corson—851(A)
Electron microscope, G. A. Morton, E. G. Ramberg—705(L); E. F. Burton, J. Hillier, A. Prebus—1171(L)
Electrostatic generator and ion source, I. A. Getting, J. B. Fisk, H. Vogt—213(A), 1098

Electrostatic voltmeter, F. H. Nadig, J. L. Bohn—216(A)
Fast neutron counters, S. A. Korff—1241(L)
Fast neutrons, beam of, P. C. Aebersold—714
Ferromagnetic impurities; method for detecting, F. W. Constant, J. M. Formwalt—373
Films on interferometer mirrors, W. V. Houston, S. Rubin—852(A)
Geiger counter, modulation of, J. N. Shive—579
Heat conductivity measurements, C. C. Bidwell—594
Hertz pumps, modified, K. T. Bainbridge, H. G. Vogt—213(A)
High pressure cloud chamber, W. E. Stephens, W. E. Shoupp, R. O. Haxby, W. H. Wells—209(A)
Illumination of cloud chamber, C. E. Nielsen—855(A)
Initial performance of 60-inch cyclotron, E. O. Lawrence, L. W. Alvarez, W. M. Brobeck, D. Cooksey, D. R. Corson, E. M. McMillan, W. W. Salisbury, R. L. Thornton—124(L)
Ions in cyclotron, R. R. Wilson—459
Low light intensities, observations of, W. N. Latimer, H. A. Young—963(L)
Manometer of small volume, C. Kenty—215(A)
Melting points by transmitted light, D. Williams, B. Hinton—844(A)
Nomogram for atomic constants, R. A. Beth—208(A)
Nuclear physics, apparatus for, J. C. Mouzon—846(A)
Photoelasticity in three dimensions, R. Weller—216(A)
Photoelectric spectrophotometer, W. C. Bosch, B. B. Brown—846(A)
Raman spectra, excitation of, J. S. Kirby-Smith—844(A)
Resistance voltmeter for high voltages, W. B. McLean, R. A. Becker—859(A)
Resonance radiation, demonstration of, R. W. Wood—1172(L)
Square-wave voltages at high frequencies, W. H. Fenn—850(A)
Statistical significance of rate differences, F. T. Holmes—844(A)
Temperature from nitrogen bands, O. S. Duffendack, Kuang-Tseng Chao—176
Time distribution of random events, A. Ruark—1165
Ultracentrifugation of a bacteriophage, T. Davis—845(A)
Use of radioactive tracers, A. Barnett—963(L); H. R. Crane—1243(L); L. J. Mullins—1244(L)
Viscosity measurements, D. R. Inglis—1040
Work functions, determination of, G. M. Fleming, J. E. Henderson—853(A)
Work functions, measurement of, W. H. Goss, J. E. Henderson—857(A)
Young's modulus; new method, A. King—216(A)

Mobility of ions (see **Ions, mobility**)

Molecular structure and constants (see also **Spectra, molecular and Raman spectra**)
Coriolis coupling terms in polyatomic molecules, H. A. Jahn—680
Double minima problem of NH_3 molecule, R. F. Haupt, E. Teller—208(A)
Electronic states of diatomic carbon, R. S. Mulliken—778
Energies of pentatomic molecules, W. H. Shaffer, H. H. Nielsen, L. H. Thomas—895
Force constants of NO_2 groups, D. Williams, L. Decherd—847(A)
Forces in molecules; formulas for, R. P. Feynman—340
Fundamental vibration of NH_3, G. B. B. M. Sutherland—836(L)
Vibration of CH_3Cl at 7.5μ, A. H. Nielsen, H. H. Nielsen—847(A)
Vibration-rotation energies of nonlinear triatomic molecule, W. H. Shaffer, H. H. Nielsen—188

Neutrons
Collimation of fast neutrons, R. F. Bacher, D. C. Swanson—483(L)
Fast neutrons, beam of, P. C. Aebersold—714
Production and absorption in U, H. L. Anderson, E. Fermi, L. Szilard—284
Recoil of nucleus in β-decay, H. R. Crane, J. Halpern—232

Nuclear moments and spin (see also **Hyperfine structure**)
Of $_{13}Al^{27}$, S. Millman, P. Kusch—214(A), 303
Of B isotopes, S. Millman, P. Kusch, I. I. Rabi—165
Of C^{13}, C. H. Townes—850(A); C. H. Townes, W. R. Smythe—1210
Electric and magnetic moments of Li^6 and N^{14}, M. E. Rose—1064(L)
Electric quadrupole moment of In^{115}, D. R. Hamilton—30
Of $_5B^{10}$ and $_5B^{11}$, P. Kusch, S. Millman—213(A)
Of Ir, L. Sibaiya—768
Of proton and deuteron, J. M. B. Kellogg, I. I. Rabi, N. F. Ramsey, Jr., J. R. Zacharias—213(A), 728
Of the proton, neutron and deuteron, E. E. Witmer—214(A)
Regularity in moments, E. E. Witmer—203(L)
Of Rb and Cl isotopes, P. Kusch, S. Millman—527

Nuclear structure (see also **Disintegration of nucleus; Energy states of nucleus**)
Binding energies of H^3 and He^5, K. Way—556
Binding energy of H^3, F. W. Brown—1107
Coupling conditions in light nuclei, E. P. Wigner—519
Deviation from Coulomb law, W. E. Lamb, Jr.—384(L); H. Fröhlich, W. Heitler, B. Kahn—961(L)
Levels in B^{10}, P. G. Kruger, F. W. Stallmann, W. E. Schoupp—297
Mesotron forces; state of He^5, S. M. Dancoff—384(L)
Nuclear five-body problem, W. A. Tyrrell, Jr.—250
Pair emission from Ne^{20}, J. R. Oppenheimer, J. S. Schwinger—1066(L)
Phase shifts for error well, H. M. Thaxton, A. M. Monroe—616(L)
Phase shifts for square well, A. M. Monroe, H. M. Thaxton—616(L)
Probabilities in double β-disintegration, W. H. Furry—1184
Spin-dependence of nuclear forces, C. L. Critchfield—540
Spin-orbit coupling in light nuclei, D. R. Inglis—1175

Nuclear structure (continued)
Of S^{33}, E. Pollard—961(L)
Theory of nuclear forces, E. P. Wigner, C. L. Critchfield, E. Teller—530
Virtual level of He^5, S. M. Dancoff—852(A)

Optical constants and properties
Infra-red pleochroism in CH_2 groups, J. W. Ellis, J. Bath —859(A)
Optical instruments (see **Methods and instruments**)

Paschen-Back effect
In Ne, J. B. Green, J. A. Peoples, Jr.—54
Theory for intermediate coupling, J. B. Green, J. F. Eichelberger—51
Photoconductivity
Of tartaric crystals, J. J. Brady, J. D. Todd—859(A)
Of willemite at low temperatures, R. Hofstadter, R. C. Herman—212(A)
Photoelectric effect and properties; cells
Magnetic field effect, N. K. Olson—210(A)
Of U, W. L. Hole, R. W. Wright—785
Work functions, measurement of, W. H. Goss, J. E. Henderson—857(A)
Work functions Ag crystal faces, H. E. Farnsworth, R. P. Winch—1067(L)
Photography
Graininess of photographic emulsions, W. O. Gould, A. Goetz—850(A)
Sensitivity of emulsions for electrons, L. Marton—290(L)
Photometry
Photoelectric spectrophotometer, W. C. Bosch, B. B. Brown—846(A)
Proceedings of the American Physical Society
Metropolitan Section, Meeting, October 27, 1939—1068
Princeton, New Jersey, Meeting, June 23–4, 1939—206
Southeastern Section: University of Georgia Meeting, March 31–April 1, 1939—843
Stanford, California, Meeting, June 28–July 1, 1939—849

Radio
Fluctuations in intensity of static, G. W. Kenrick, P. J. Sammon—203(L)
Radioactivity (see also **Disintegration of nucleus**)
Of Al bombarded by H′, G. Kuerti, S. N. Van Voorhis—614(L)
β-decay of light nuclei, B. O. Grönblom—508
β- and γ-rays from Cu^{64} and Eu^{152}, A. W. Tyler—125
β- and γ-rays, coincidences from indium, L. M. Langer, A. C. G. Mitchell, P. W. McDaniel—380(L)
β-radiation of As^{76}, G. L. Weil, W. H. Barkas—485(L)
β-ray spectra of Mg^{27}, Cu^{62}; isomers of Rh^{104}, E. C. Crittenden, Jr.—709
β-ray spectra of P, Na and Co, J. L. Lawson—131
Coincidences between β- and γ-rays, L. M. Langer, A. C. G. Mitchell, P. W. McDaniel—422, 962(L)
Delayed γ-radiation from the *d-d* reaction, M. H. Kanner, W. T. Harris—207(A)
Double β-disintegration, W. H. Furry—1184
Emission of neutrons by U, W. H. Zinn, L. Szilard—619
In Eu, K. Fajans, D. W. Stewart—625
γ-radiation from N^{13}, G. E. Valley—838(L)
Half-life of B^{12}, R. A. Becker, E. R. Gaerttner—854(A)
Of In, L. D. P. King, W. J. Henderson—1169(L)
Of Cd and In, J. M. Cork, J. L. Lawson—291; S. W. Barnes—414, 859(A)
Of In, E. Pollard—1168(L)
Internally converted γ-rays, G. E. Valley, R. L. McCreary—863
Of I, β-spectra, G. F. Tape—965
Isomer of Sr^{87}, L. A. DuBridge, J. Marshall—706(L)
Isomerism in Zn, J. W. Kennedy, G. T. Seaborg, E. Segrè—1095
Lifetimes of β-activities, E. P. Wigner—519
Of Lu, W. F. Libby—21
Of Mn^{56}, R. H. Bacon, E. N. Grisewood, C. W. Van der Merwe—1168(L)
Of Pd by proton bombardment, T. Enns—872
Positron spectra of N^{13} and Na^{22}, F. Oppenheimer, E. P. Tomlinson—858(A)
Products of disintegration of U by neutrons, P. Abelson—1
Reactions in light nuclei with protons, W. H. Barkas—287(L)
Short-lived activities in F, Na and Mg, M. G. White, L. A. Delsasso, J. G. Fox, E. C. Creutz—207(A), 512
Of Si^{27} incorrectly assigned, H. A. Bethe, W. J. Henderson—1060(L)
In Sr and Y, D. W. Stewart—629
Test for $Mg^{26}(\alpha,p)\,Al^{29}$, W. J. Henderson, R. L. Doran—123(L)
Time distribution of random events, A. Ruark—1165
Use of "tracers," A. Barnett—963(L); H. R. Crane—1243(L); L. J. Mullins—1244(L)
X-rays associated with radioactive decay, P. H. Abelson —753
Raman spectra
Of aliphatic molecules in water solution, R. C. Williamson—848(A)
In samarium nitrate, L. Sibaiya, H. S. Venkataramiah—381(L)
Relativity
Electrostatic analog to gravitational red shift, H. T Drill—184
Rotating charged concentric spheres, L. I. Schiff—850(A)
Wave functions of relativistic hydrogenic atom, L. Davis, Jr.—186
Resonance radiation
Demonstration of, R. W. Wood—1172(L)

Scattering of electrons, neutrons, and ions (see also **Electrons, scattering of; Electron diffraction**)
Of α-particles by N, G. Brubaker—207(A), 1181
Of cathode rays, J. G. Trump, R. J. Van de Graaff, R. W. Cloud—215(A)
Collision cross sections for D-D neutrons, W. H. Zinn, S. Seely, V. W. Cohen—260
Cross sections of C, N, Na, Mg, and Al for neutrons, M. MacPhail, J. Giarratana—207(A)

D-D, H-He, D-He scattering, N. P. Heydenburg, R. B. Roberts—1092
Of electrons in Pb and Al; energy losses, M. M. Slawsky, H. R. Crane—1203
Of fast electrons, N. L. Oleson, K. T. Chao, J. Halpern, H. R. Crane—482(L), 1171(L)
Of fast electrons by heavy elements, J. H. Bartlett, R. E. Watson—612(L)
Of fast neutrons, E. R. Gaerttner, L. A. Pardue, J. F. Streib—856(A)
Multiple scattering of charged particles, S. Goudsmit, J. L. Saunderson—122(L)
Multiple scattering of electrons and positrons, C. W. Sheppard, W. A. Fowler—849(A)
Of neutrons from the C+D reaction, E. Amaldi, D. Bocciarelli, F. Rasetti, G. C. Trabacchi—881
Of neutrons by protons, C. Kittel, G. Breit—744
Phase shift for proton-proton scattering, H. M. Thaxton, L. E. Hoisington—1194
Photoneutrons from deuterium, T. Goloborodko, A. Leipunski—891
Proton-proton and proton-neutron interactions, F. W. Brown, M. S. Plesset—841(L)
Proton-proton scattering, L. E. Hoisington, S. S. Share, G. Breit—884
Proton-proton scattering, E. Creutz—893
Of protons by protons, N. P. Heydenburg, L. R. Hafstad, M. A. Tuve—1078
Reflection of electrons by metals, L. A. MacColl—699

Secondary electrons (see **Electrons, secondary**)

Specific heat
Heat capacity at Curie point, C. C. Stephenson, J. G. Hooley—121(L)
Of monatomic liquid, W. J. Archibald—926
Of NH_3, R. F. Haupt, E. Teller—208(A)
Of Ni-Cr alloys, H. Grover, J. Hutzenlaub—212(A)

Spectra, absorption
Of AlF, G. D. Rochester—305
Of CN, J. U. White—853(A)
Of D_2O, P. E. Shearin, E. K. Plyler—845(A)
Of heavy water vapor molecule, N. Fuson, H. M. Randall, D. M. Dennison—982
Of methyl chloride at 7.4μ, A. H. Nielsen, H. H. Nielsen—274
Of NO, A. H. Nielsen, W. Gordy—781
Of NO, rotation-vibration band, R. H. Gillette, E. Eyster—1113
Of some sugars, near infra-red, E. S. Barr, C. H. Chrisman—845(A)
Water band at 4.7μ; effects of alkali halides, T. N. Gautier, D. Williams—616(L)

Spectra, atomic
Calculation of two-electron configurations, A. F. Stevenson—586
D^0p configuration of the Ni-like and Pd-like spectra, A. T. Goble—209(A)
Intensities of singlet-singlet and singlet-triplet transitions, G. W. King, J. H. Van Vleck—464
Isotope shift in Mg, J. P. Vinti—1120
Of Ne V, F. W. Paul—1067(L)
Of Ne, Paschen-Back effect, J. B. Green, J. A. Peoples, Jr.—54, 385(L)
Probabilities of forbidden lines, S. Pasternack—854(A)
Of Ag, A. G. Shenstone—209(A)
Of Th III, R. J. Lang—272
Wave functions of relativistic hydrogenic atom, L. Davis, Jr.—186
Of Y V and Zr VI, F. W. Paul, W. A. Rense—1110

Spectra, molecular (see also **Molecular structure and constants**)
Energies of pentatomic molecules, W. H. Shaffer, H. H. Nielsen, L. H. Thomas—895, 1051
Forbidden transitions in N_2, J. Kaplan—858(A)
Further resolution of NH_3 bands 10μ and 16μ, E. F. Barker, H. Y. Sheng—854(A)
Interferometer wave-lengths of lines in spectrum of H_2, L. S. Combes, R. M. Frye, N. A. Kent—678
Normal modes of long chain hydrocarbons, L. H. Thomas, S. E. Whitcomb—383(L)
Rotation temperatures of CO, M. S. McCay, H. P. Knauss, B. Archdeacon—847(A)
Temperature from nitrogen bands, O. S. Duffendack, Kuang-Tseng Chao—176
Transition of C_2, O. G. Landsverk—769

Spectroscopy, technique
Analysis of Rb in plant sap, L. A. Strait—855(A)

Stark effect
Broadening of hydrogen lines, L. Spitzer, Jr.—39

Surface tension
Temperate dependence, ridges in liquid surface, A. V. Hershey—204(L)

Thermal conductivity
In gases, I. Brody, F. de Kőrösy—217(A)
Heat transfer in atmosphere, W. M. Elsasser—855(A)
Of Zn and silocel, C. C. Bidwell—594

Thermionic emission of electrons; Emitting surfaces
Determination of work functions, G. M. Fleming, J. E. Henderson—853(A)
Dispenser cathode; cathode for gaseous discharge tubes, A. W. Hull—86
Periodic deviation from Schottky line, D. Turnbull, T. E. Phipps—663; H. M. Mott-Smith—668; R. L. E. Seifert, T. E. Phipps—652
Of surfaces of tungsten single crystal, S. T. Martin—947
Of U, W. L. Hole, R. W. Wright—785
Work function of W, J. G. Potter—216(A)

Thermodynamics
Fluctuations and entropy, E. C. Kemble—1013
Fugacity of CO_2, W. E. Deming, L. S. Deming—108
Statistical mechanics, E. C. Kemble—1146

Van der Waal forces
Potential in He, H. Margenau—1000

Vapor pressure
Of N^{14} and N^{15} ammonia, H. G. Thode—214(A)

Viscosity
Of air, J. A. Bearden—1023

Viscosity (continued)
Almost-coaxial cylinders; viscous force, D. R. Inglis—1040
Electric field; effect of, A. A. Dixon—847(A)
Structural viscosity, F. Breazeale—845(A)

Work function (see **Thermionic emission; Photoelectric effect**)

X-rays, absorption
K absorption edges of Fe to Ge, W. W. Beeman, H. Friedman—392
M_1 and M_2 edges of Pb, J. W. McGrath—765, 1068(L)
M_3 and M_4 edges of Au in pure metal and in Au-Cu alloy, J. W. McGrath—137
Resonance lines in *K* spectrum, L. G. Parratt—295

X-rays, diffraction, scattering, reflection, refraction and polarization
Diffraction pattern of calcite, F. Miller, Jr.—757
Diffraction by small crystalline particles, A. L. Patterson—972
Diffuse scattering at small angles, G. G. Harvey—247
Dispersion and atomic electron cloud distortion in Zn, E. M. McNatt—406
Fluorescing coefficient and orientation of crystal, O. J. Baltzer, G. E. M. Jauncey—289(L)
Reflections from calcite between 300° and 4.2°K, A. Dember, A. Goetz—857(A)
Scherrer formula, particle size determination, A. L. Patterson—978
Theory of diffuse scattering, G. E. M. Jauncey—644
Total scattering from crystals, G. G. Harvey—242

X-rays, emission (see also **X-rays, spectra and spectroscopy**, etc.)
Fine structure in *K* lines of Cu, S. T. Stephenson—856(A)
Intensities of lines of W and Pt, W. H. Kliever—387
K auger transitions, C. J. Burbank—142; W. Veith, P. Kirkpatrick—705(L)
Lines from double ionization of *L*-shell, R. D. Richtmyer—857(A)
Spin doublet splittings, R. F. Christy, J. M. Keller—856(A)
Theory of lines *LL-LM*, R. D. Richtmyer—146
Weak Mo*L* lines, W. Veith, P. Kirkpatrick—705(L)

X-rays, tubes, apparatus
Dental fluoroscope and shield, C. R. Fountain—844(A)

Zeeman effect
Hollow cathode source, R. A. Fisher, A. S. Fry—675
In the hyperfine structure of I, A. S. Fry, R. A. Fisher—669
Of Hg resonance radiation, E. H. Collins—48

THE AMERICAN INSTITUTE OF PHYSICS

INCORPORATED

ADMINISTRATIVE STAFF

HENRY A. BARTON, *Director*

MADELINE M. MITCHELL, *Publications Manager*

Office: 175 Fifth Avenue, New York, New York

JOURNALS

THE PHYSICAL REVIEW
REVIEWS OF MODERN PHYSICS
JOHN T. TATE, *Editor*
J. W. BUCHTA, *Assistant Editor*

JOURNAL OF APPLIED PHYSICS
ELMER HUTCHISSON, *Editor*

THE JOURNAL OF THE OPTICAL SOCIETY OF AMERICA
THE REVIEW OF SCIENTIFIC INSTRUMENTS
F. K. RICHTMYER, *Editor*

JOURNAL OF THE ACOUSTICAL SOCIETY OF AMERICA
FLOYD A. FIRESTONE, *Editor*

THE JOURNAL OF CHEMICAL PHYSICS
HAROLD C. UREY, *Editor*
JOSEPH E. MAYER, *Assistant Editor*

THE AMERICAN PHYSICS TEACHER
DUANE ROLLER, *Editor*

GOVERNING BOARD

For The American Physical Society:

JOHN T. TATE, *Chairman*
University of Minnesota

GEORGE B. PEGRAM, *Secretary*
Columbia University

KARL T. COMPTON
Massachusetts Institute of Technology

For The Optical Society of America:

E. C. CRITTENDEN
National Bureau of Standards

A. C. HARDY
Massachusetts Institute of Technology

W. B. RAYTON
Bausch & Lomb Optical Company

For The Acoustical Society of America:

FLOYD A. FIRESTONE
University of Michigan

HARVEY FLETCHER
Bell Telephone Laboratories

WALLACE WATERFALL
The Celotex Corporation

For The Society of Rheology:

WHEELER P. DAVEY
Pennsylvania State College

MELVIN MOONEY
United States Rubber Products, Inc.

R. L. PEEK, JR.
Bell Telephone Laboratories

For The American Association of Physics Teachers:

PAUL E. KLOPSTEG
Central Scientific Company

FREDERIC PALMER, JR.
Haverford College

F. K. RICHTMYER
Cornell University

The American Institute of Physics is a membership corporation of which five societies are the founding members. These five societies are the principal national societies devoted to pure and applied physics in America. Their names, and those of their representatives who form the Governing Board of the Institute, are given above. The principal work of the Institute is the publication of journals sponsored by the societies or by itself. The names and the editors of the journals are also listed above.

The broad purpose of the Institute is to represent, in all matters of wide or common interest, the five thousand or more members and subscribers associated with the Founder Societies and the journals. It aims to advance the science and profession of physics, and to promote cooperation between pure research, the applied sciences and the industries. To achieve these aims, it is greatly in need of an endowment and is empowered by law to administer grants and funds of any kind.

CONTENTS

PHYS. REV. 56 (1939) DECEMBER 15

Spin-Orbit Coupling in the Alpha-Model of Light Nuclei . . . . . D. R. INGLIS 1175

Scattering of Alpha-Particles by Nitrogen . . . . . GORDON BRUBAKER 1181

On Transition Probabilities in Double Beta-Disintegration . . . . . W. H. FURRY 1184

Phase Shift Calculations for Proton-Proton Scattering at High Energies . . . . . H. M. TRAXTON AND L. E. HOISINGTON 1194

Townsend Ionization Coefficients for Ni and Al Cathodes in an Atmosphere of Hydrogen . . . . . DONALD H. HALE 1199

Absorption of High Energy Electrons. IV . . . . . M. M. SLAWSKY AND H. R. CRANE 1203

Spin of Carbon Thirteen . . . . . C. H. TOWNES AND W. R. SMYTHE 1210

Wave Reflections from Diffuse Boundaries . . . . . C. D. THOMAS AND R. C. COLWELL 1214

On the Interpretation of Atomic Distribution Curves for Liquids . . . . . C. A. COULSON AND G. S. RUSHBROOKE 1216

Dependence of Ferromagnetic Anisotropy on the Field Strength . . . . . L. P. TARASOV 1224

Ferromagnetic Anisotropy of Iron and Iron-Rich Silicon Alloys . . . . . L. P. TARASOV 1231

Letters to the Editor:

Fast Neutron Measurements with Recoil Counters . . . . . S. A. KORFF 1241

Absorption of Mesotrons in Air and in Condensed Materials . . . . . ENRICO FERMI 1242

Helium of Mass Three as an Agent in Nuclear Reaction . . . . . WALTER H. BARKAS 1242

Use of Radioactive Elements as Tracers in Physiology . . . . . H. R. CRANE 1243

Ultrafiltration of Water . . . . . B. J. LUYET 1244

Radioactive Isotopes in Biology . . . . . LORIN J. MULLINS 1244

On Explosion Showers . . . . . GILBERT WATAGHIN 1245

Ferromagnetic Anisotropy of Low Nickel Alloys of Iron . . . . . L. P. TARASOV 1245

Author Index to Volume 56 1247

Analytic Subject Index to Volume 56 1257

Volume Table of Contents iii

LANCASTER PRESS, INC., LANCASTER, PA.

3527